THE PROTEOMICS FINGERPRINTS OF AUY922

AND 17-DMAG INDICATE COMMON MECHANISMS

OF ACTION FOR HSP90 INHIBITORS

By

SUDHAKAR VORUGANTI

Bachelor of Science in Biochemistry
Andhra University
Vishakhapatnam, Andhra Pradesh
1998

Master of Science in Biochemistry
Acharya Nagarjuna University
Guntur, Andhra Pradesh
2001

THE PROTEOMICS FINGERPRINTS OF AUY922 AND 17-DMAG INDICATE

COMMON MECHANISMS OF ACTION FOR HSP90 INHIBITORS

Dissertation Approved:

Dr. Steven D. Hartson
_____
Dissertation Adviser
Dr. Robert L. Matts
_____

Dr. Ulrich Melcher
_____

Dr. Junpeng Deng
_____

Dr. Robert Burnap
_____

Outside Committee Member

ACKNOWLEDGEMENTS

   I am thankful to everyone who helped me during all these years in my graduate school. First of all, I am extremely thankful and grateful to my graduate mentor Dr. Steven D. Hartson. He was helpful in every aspect during my graduate school and was available any time I needed his help. We had very nice and fruitful scientific discussions all these years. He was very patient and instrumental in teaching me mass spectrometry and improving my scientific writing skills. I will carry forward the skills he taught for rest of my scientific career. I am also thankful to him for providing me graduate assistantship all these years and also financially supporting a part of my ASMS expenses. I am thankful to Dr. Robert L. Matts for supporting me for the first two years of my graduate school. I was greatly inspired by his passion for science. I would also thank Dr. Matts for funding me for the mass spectrometry and microarray workshops at OSU, and providing me with antibodies needed for the experiments. I am thankful to my current and former committee members Dr. Ulrich Melcher, Dr. Junpeng Deng, Dr. Robert L. Burnap, Dr. Andrew Mort and Dr. Stacy Benson for their valuable suggestions. I am extremely thankful to Dr. Rita K. Miller for making me a part of "Izzy club", and helping me to improve my scientific and presentation skills. I am extremely thankful to Tyler Weirick and Dr. Rakesh Kaundal for helping me with bio-informatics work related to our project. I am thankful to Janet Rogers for help all these years. I also want to thank my former and current lab members and friends Jason Davenport, Liang Sun, Daniel Smith, Maurie Balch and Steven Pennington. I am thankful to undergraduate researchers Jeff LaCroix and Chelsea Rogers for assisting and helping in my work. I would also like to thank all the BMB staff for their wonderful support all these years.

       Last but not least, I am extremely thankful to my wife Swapna and my kids Sreyas and Sreehaas. Without their love, help and support I would have not made it in the graduate school. I am thankful to my mother, my brother, my in-laws and each one of my family members for their support all these years. Finally, I would like to dedicate all my work in graduate school to my late father Surya Narayana Voruganti, who passed away in 2003 after a 21 day struggle with myocardial infarction. Without his blessings this would not have been possible.

Name: SUDHAKAR VORUGANTI

Date of Degree: DECEMBER 2013

Title of Study: The proteomics fingerprints of AUY922 and 17-DMAG indicate common mechanisms of action for Hsp90 inhibitors.

Major Field: BIOCHEMISTRY AND MOLECULAR BIOLOGY

Abstract: In this work, we identified the proteomics fingerprint of the anti-cancer drug candidate AUY922 in Jurkat leukemia cells and compared AUY922's fingerprint to the proteomics fingerprints of flagship Hsp90 inhibitors 17-DMAG and radicicol. Protein expression changes were identified by a label-free mass spectrometry technique, spectrum counting using a bottom-up proteomics approach. We identified 30 protein expression changes that were conserved among all the three Hsp90 inhibitors. To further validate findings from spectrum counting assays and to identify more Hsp0 inhibitor-induced protein expression changes, we quantified AUY922-induced and 17-DMAG-induced protein expression changes by label-based Stable Isotope Labeling with Amino acids in Cell culture (SILAC) using a bottom-up proteomics approach. A total of 3000-4000 inhibitor-induced protein expression changes were quantified. After statistical validation, 260 protein expression changes were found to be conserved among both the Hsp90 inhibitors. The large conservation of protein expression changes between AUY922 and 17-DMAG suggested that both inhibitors work via a similar mechanism. The protein expression changes common to AUY922 and 17-DMAG identified in this study can be used as biomarkers to test bioactivity of AUY922 in clinical trials and can also be used to validate new Hsp90 N-terminal inhibitors. Additionally, they can be compared to the proteomic fingerprints of agents that bind to the C-terminal domain of Hsp90, to determine if both classes of inhibitors share similar mechanisms of action. I also demonstrated that the anti-proliferative effects of AUY922 could be enhanced in combinatorial treatments with protein folding antagonist L-azetadine-2-carboxylic acid (AZC). I further used the SILAC approach to determine the mechanism of combinatorial effects of AUY922 and AZC and showed that the combinatorial effects were largely due to AZC-mediated suppression of chaperone induction. Thus, findings from this study suggest approaches for enhancing AUY922's activity in clinical trials by using AUY922 in combination with agents that suppress chaperone induction.

TABLE OF CONTENTS

LIST OF TABLES

LIST OF FIGURES

CHAPTER I

Literature Review

Heat Shock Protein 90 (Hsp90)

Heat shock protein 90 (Hsp90) is arguably the most prominent of all the heat shock proteins. It is widely conserved across different domains of life (with the exception of archaea). In human beings, Hsp90 is the most abundant of all the Hsps, and constitutes about 1% of the total cellular protein. Hsp90's isoforms play distinct biological roles in different cellular compartments. Cytoplasmic Hsp90 exists in two isoforms in mammalian cells, Hsp90α and Hsp90β. Hsp90β is constitutively expressed, whereas Hsp90α is heat or stress inducible. GRP94 and TRAP are the homologs of Hsp90 in endoplasmic reticulum and mitochondria, respectively.

Structure

Hsp90 has three domains: the N-terminal domain, the middle domain, and the C-terminal domain. X-ray crystallography studies have been used to understand the biological functions of each domain. Crystal structures of complexes between yeast Hsp90 and ATP/ADP have been produced [1] . This has led to the understanding that the N-terminal domain has a pocket for ATP binding. Hsp90 inhibitors also bind to the ATP binding pocket in the N-terminal domain [2].

Hsp90's middle domain harbors two important residues: Arg 380 and Gln 384, which are essential for Hsp90 ATPase activity. The middle domain also interacts with the client proteins [3]. The N-terminal domain and the middle domain are connected to each other by a flexible linker.

The C-terminal domain is necessary for homo-dimerization. The C-terminal domain has a MEEVD sequence motif necessary for binding tetratricopeptide repeat-containing co-chaperone proteins. Several small molecule inhibitors also bind to this domain, here after called as C-terminal inhibitors [4]. Recently the C-terminal inhibitor site has been identified by protease fingerprinting, and by photo-affinity labeling followed by LC-MS/MS [5].

Hsp90 function

Hsp90 is a molecular chaperone that folds proteins. Hsp90 folds proteins by undergoing a series of conformational changes. These conformational changes are driven by ATP binding and hydrolysis and are often referred to as the Hsp90 reaction cycle. Hsp90 exists as an open dimer in its free state. When ATP binds in the N-terminal pocket, the Hsp90 dimer undergoes structural transitions and acquires a closed conformation. This conformation allows the nascent polypeptides to be folded into their native conformations. Upon ATP hydrolysis and ADP release, Hsp90 is restored back to its open conformation. In the open conformation, the folded client proteins are released from Hsp90 [6].

Hsp90 functions in co-operation with a wide variety of other chaperones and co-chaperones. All these together constitute the Hsp90 chaperone machinery [7]. Co-chaperones play important roles in regulating Hsp90's activity. A majority of the Hsp90 co-chaperones have TPR domains (examples: Hop, Chip and Tom70), and bind to the MEEVD motif in the C-terminal domain of Hsp90 [7]. Co-chaperones assist Hsp90 by regulating it's interactions with other chaperones, by stimulating or inhibiting ATPase activity, or by recruiting Hsp90 clients. Among the co-chaperones that modulate

ATPase activity of Hsp90, Aha1 and Crp6 stimulate the ATPase activity whereas Hop, Cdc37 and p23 inhibit the ATPase activity [8].

Hsp90 Clients

The proteins that depend on Hsp90 for their conformation, stability, or activity are called Hsp90 clients. To date, more than 200 proteins have been identified as Hsp90 clients, and the list is expanding. There are three major classes of Hsp90 clients: kinases, steroid hormone receptors and others that are not typically considered to be signal transduction proteins. Several steroid hormone receptors, including estrogen, androgen progesterone, and glucocorticoid receptors are known Hsp90 clients [9, 10]. A wide variety of kinases including tyrosine kinases [11] and cyclin dependent protein kinases [12, 13] are also Hsp90 clients. Telomerase [14], helicases, cytoskeletal proteins and several metabolic enzymes are other known Hsp90 clients [15]. A comprehensive list of Hsp90 client proteins can be found at http://www.picard.ch.

Hsp90 Inhibitors

Hsp90 can be inhibited by small molecule inhibitors. The benzoquinone ansamycin geldanamycin (Fig 1.1), hereafter called "GA" was the first compound identified to inhibit Hsp90. GA reverts the Src tyrosine kinase mediated oncogenic transformation of NIH 3T3 cells by binding to Hsp90 and inhibiting its function [16]. Several years later, the macrocyclic anti-fungal antibiotic radicicol (Fig 1.2) was also shown to inhibit Hsp90. Radicicol, like GA, suppresses oncogenic transformation by inhibiting the function of Hsp90 [17] . GA and radicicol act as Hsp90 inhibitors by binding to the ATP binding pocket in the N-terminal domain of Hsp90, and interfering with its ATPase cycle [18] . Thus these compounds are classified as N-terminal Hsp90 inhibitors.
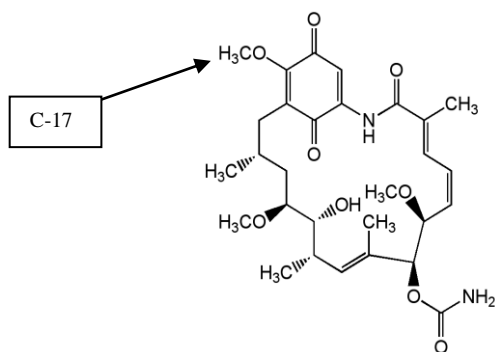
Figure 1.1 - Geldanamycin   **Figure 1.2 - Radicicol**
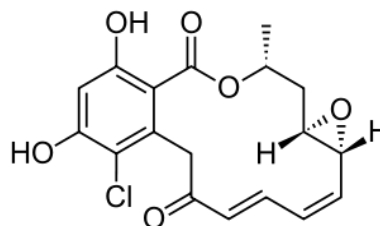
Images from Wikipedia Commons

GA showed good anti-cancer effects in cancer cell lines and animal models. But it was poorly

soluble, lacked stability and was toxic. Therefore, it was not used for clinical purposes. Instead,

derivatives of GA (17-Dimethylaminoethylamino-17-demethoxygeldanamycin, hereafter called 17-

DMAG, and 17-*N*-allylamino-17-demethoxygeldanamycin, 17-AAG) were developed. In 17-DMAG,

the C-17 methoxy group of GA was replaced by N-N-dimethylamine. Compared to GA, 17-DMAG

had better solubility and entered phase I trials. However, it was discontinued due to toxicity

(clinicaltrials.gov). Radicicol was never considered for clinical trials due to toxicity and absence of

activity in vivo [19].

Several other Hsp90 inhibitors were developed by various approaches. Currently 13 different

Hsp90 inhibitors are in clinical trials. All these inhibitors can be divided into three types depending

on similarity to geldanamycin (IPT-504), radicicol (AUY922), or an adenosine like scaffold.

AUY922

AUY922 is a small molecule Hsp90 inhibitor. AUY922 belongs to the resorcinylic isoxazole

amide class (Fig 1.3)**,** and is structurally related to radicicol by having a resorcinol moiety. AUY922

4

exhibits high affinity for Hsp90 ATP binding pocket with an IC_{50} of 21 nM. Like other Hsp90 N-terminal inhibitors, AUY922 also binds to the ATP binding pocket in the N-terminal domain of Hsp90 [20]. AUY922 depletes a wide variety of known Hsp90 clients and exerts potent anti-cancer effects in wide variety of cell lines and tumors at low nano-molar doses [21-26] . AUY922 exhibits cytostatic effects by arresting cells in G1/S or G2/M phase of the cell cycle [24]. Hence, AUY922 is considered as a promising candidate for cancer treatment. Currently, AUY922 is in Phase II clinical trials.
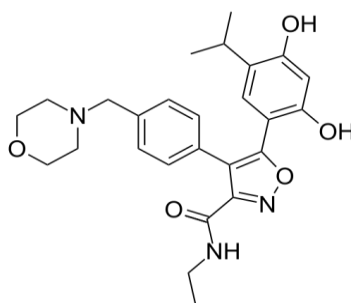
Figure 1.3 - AUY922 (Wikipedia commons)

In addition to Hsp90 N-terminal inhibitors, there are several small molecules that bind to the Hsp90 C-terminal domain. Novobiocin is a coumarin antibiotic. It was the first compound that was identified to bind to the C-terminus of Hsp90. Similar to novobiocin, the coumarin antibiotics chlorobiocin and coumermycin A1 also bind to the Hsp90 c-terminal domain. All these compounds deplete known Hsp90 clients proteins such as erbB2, Raf-1 and p53 in cultured breast cancer cells [4]. However, unlike N-terminal inhibitors, they do not up-regulate Hsp70. Cisplatin also binds to Hsp90's C-terminal domain, and inhibits its activity [27] . EGCG, a green tea ingredient, also depletes Hsp90 clients, including telomerase and several kinases [28]. Dr. Brian Blagg (Kansas University) has synthesized other structurally related C-terminal inhibitors that have anti-cancer activities in vitro [29-31]. The novobiocin and chlorobiocin binding sites in the Hsp90 C-terminal domain were identified recently [5].

Uses of Hsp90 inhibitors

The biological roles of Hsp90 have been elucidated by using Hsp90 inhibitors as tools.
Hsp90 plays important roles in cancer by supporting mutant tyrosine kinases like Src [16] and mutant
p53 [32]. These Hsp90 roles were elucidated using geldanamycin. Since then, proteins involved in the
six hallmark traits of cancer [33] including receptor tyrosine kinases (EGFR), serine threonine
kinases (Raf1 and Akt) [34], HIF1α [35] and MMP2 [36] have been identified as Hsp90 clients by
using Hsp90 inhibitors as tools.

Using Hsp90 inhibitors as tools, several Hsp90 dependent proteins have been identified [17, 37-
40] . These discoveries include steroid hormone receptors, kinases, and transcription factors.
Identifications of steroid hormone receptors, kinases and transcription factors as Hsp90 clients led to
highlight Hsp90's role in steroid signaling, signal transduction, transcription, and immune responses.
Other proteins such as Hsf1, calcineurin and nitric oxide synthase have also been identified as Hsp90
clients, thus implicating Hsp90's roles in heat shock response, calcium signaling and nitric oxide
signaling [7].

Hsp90 inhibitors are considered as promising candidates for cancer treatment. Hsp90 inhibitors
attack multiple oncogenic pathways simultaneously [41]. One model predicts that the selectively
tumoricidal activity of Hsp90 inhibitors is due high affinity confirmation of Hsp90 in cancer cells [42,
43]. However, this model has been questioned by Haystead et al. [44]. Nevertheless, the fact that
Hsp90 inhibitors accumulate at a high rate in cancer cells compared to normal cells remains [42].
Additionally, Hsp90 inhibitors result in the depletion of proteins involved in all six hallmark traits of
cancer [45]. Owing to these properties, Hsp90 inhibitors are considered to be viable candidates for
cancer treatment.

Hsp90 inhibitors are also considered for the treatment of neurodegenerative disorders.
Neurodegenerative diseases like Alzheimer's and Parkinson's are caused due to the accumulation of

toxic protein aggregates. Hsp90 inhibitors are predicted to ameliorate protein aggregates by inducing chaperones through the HSF1 mediated heat shock response [46].

Consequences of Hsp90 Inhibition

Hsp90 inhibition leads to the degradation of Hsp90-dependent client proteins. By inhibiting Hsp90 from cycling through the chaperone cycle, client protein folding is compromised, resulting in their degradation. According to one prominent model, inhibitor-bound Hsp90 recruits CHIP (carboxy-terminus of Hsp70 interacting protein), an E3 ubiquitin ligase, leading to the ubiquitylation of Hsp90 client proteins and their subsequent degradation through the proteasome [47]. Attempts to study the global effects of Hsp90 inhibitors using proteomics approaches are discussed below.

Other major consequence of Hsp90 inhibition is activation of the heat shock response (HSR). The HSR is a signaling pathway involved in regulating protein homeostasis or proteostasis during stress conditions (discussed in more detail below). Inhibition of Hsp90 by small molecule inhibitors compromises Hsp90's function. In one model, functionally compromised Hsp90 can no longer bind Hsf1 and as a result Hsf1 gets activated. Activated Hsf1 then initiates the heat shock response by acting as a transcription factor. In vitro, in an activation lysate model system, geldanamycin was reported to compromise Hsp90's function and activate Hsf1 [48]. However, this model is not universally accepted. As pointed out by Shamovsky et al. [49] : "Despite numerous studies and extensive characterization, no defined in vitro system has been developed that reproduces Hsp90-mediated repression of HSF in vitro." In transformed fibroblasts, geldanamycin treatment results in increase in the levels of Hsps and this was shown to be mediated by Hsf1 activation [50]. In primary mouse skeletal myoblasts, two distinct Hsp90 inhibitors 17-AAG and AUY922 induce the expression of Hsp70, a consequence of Hsf1 activation [51]. There are two explanations for the activation of Hsf1 by Hsp90 inhibitors. According to one explanation, Hsp90 inhibitors cause bonafide

proteotoxic stress and result in the activation of Hsf1. According to the other explanation, Hsp90 inhibitors activate Hsf1 by inhibiting Hsp90 and interfering with Hsp90 mediated repression of Hsf1.

Proteomics of Hsp90 inhibition

Prior to 2012, four different studies described the effects of Hsp90 inhibitors at the proteome level (see the 2012 review by Hartson and Matts [15]). All these studies were done utilizing mass spectrometry approaches. The effects of 17-AAG on the proteome of A2780 ovarian cancer cells were reported in 2007 using 2D gel electrophoresis followed by MALDI-TOF mass spectrometry. In this study, 42 proteins including chaperones, mini chromosome maintenance (MCM) proteins, histones and other proteins involved in post-translational modifications were found to be altered upon Hsp90 inhibition [52]. Later in the same year, proteome wide effects of GA in anaplastic large cell lymphoma cells were reported using cICAT-LC-MS/MS approach. In this study, expression of 176 proteins was found to altered by GA treatment. Proteins involved in the 26S proteasome were found to be up-regulated and proteins involved in signal transduction and protein and nucleic acid metabolism were found to be down-regulated [53]. In 2008, effects of radicicol on the ubiquitination of Hsp90 dependent proteins were reported in Hela cells using 2D gel electrophoresis followed by LS-MS/MS. This study identified several proteins involved in metabolism, gene transcription and signal transduction to be ubiquitinated upon Hsp90 inhibition, thus suggesting the Hsp90's role in regulating these processes [54]. In 2008, effects of IPI-504 on the proteome of a pancreatic cancer cell line were studied using the ITRAQ (isobaric tags for relative and absolute quantitation) technique. In this study, 20 proteins were found to be down-regulated and 40 proteins were found to be up-regulated upon Hsp90 inhibition. Proteins involved in signal transduction, transport and metabolism were found to be altered [55].

In 2011/2012, two groups reported the global proteome-wide changes induced by Hsp90 inhibitors. The first study published in late 2011, reported the global effects of 17-DMAG on the

proteome of HeLa cells using the SILAC approach. In this study, 7,000 proteins were identified and 6,000 proteins were quantified. Within the major class of proteins up-regulated were proteases and heat shock proteins and among the down-regulated were kinases and DNA damage response proteins [56]. In 2012, another landmark study reported the proteome-wide changes induced by geldanamycin in four different cancer cell lines using SILAC approach. More than 6,200 proteins were identified in all the four cell lines and 1,600 proteins showed significant changes in protein expression. This study confirmed that Hsp90 inhibition mainly results in to the up-regulation of proteins involved in the stress response and down-regulation of kinases [57].

This thesis also utilizes SILAC similar to the studies above. This work will be compared to the SILAC studies above and will be presented in detail in the discussion section of chapter III. We will also cross reference our work to the older studies.

Proteostasis

Protein homeostasis ("proteostasis") describes the concept that living cells have biological pathways that work together to preserve the biological functions of proteins under diverse growth conditions. These major signaling pathways are the heat shock response (HSR) pathway, the endoplasmic reticulum associated degradation (ERAD) pathway, the unfolded protein response (UPR) pathway, and the ubiquitin-proteasome system (UPS). These signaling pathways maintain proteostasis in distinct sub-cellular compartments. A wide variety of heat shock proteins are key components of these pathways, and help to regulate proteostasis by ensuring proper protein folding, by preventing aggregation of misfolded proteins and sending misfolded proteins for degradation [58, 59].

The Heat Shock Response (HSR)

The heat shock response (HSR) is a proteostasis signaling pathway activated upon heat stress. It protects living cells from heat stress or proteotoxic stress by inducing the expression of heat shock

proteins. Accumulation of unfolded proteins in a stressed cell prompts activation of the HSR. The HSR is regulated by heat shock factor 1 (Hsf1). Hsf1 is a transcription factor. According to one model, the activity of HSF1 is regulated by the Hsp90 chaperone complex. As per this model, Hsf11 exists in an inactive state under non-stress conditions. The Hsp90 chaperone complex binds to Hsf1 and keeps it in an inactive state. In its inactive state, Hsf1 is prevented from binding to genomic DNA. When unfolded proteins accumulate, they titrate Hsp90 from binding to Hsf1. As a result, Hsp90-bound inactive Hsf1 is released from Hsp90 and gets activated [60-62]. Activated Hsf1 then acts as a transcription factor to regulate the expression of a wide variety of genes, including Hsp genes [63]. Increased Hsp then regulates proteostasis by folding denatured proteins, by preventing aggregation of unfolded proteins, or by sending the unfolded proteins for degradation. Alternatively, Hsp90 inhibition leads to the activation of Hsf1, a topic discussed in detail in other sections of the thesis.

The unfolded protein response (UPR)

The unfolded protein response (UPR) is another major stress response pathway that is activated by the ER stress. ER is the organelle where secretory and membrane proteins are synthesized and folded into their native conformations. Protein folding in ER is mediated by ER chaperones GRP78, GRP94, calnexin and calreticulin, and Hsp47. Any compromise in protein folding in the ER (e.g. defects in glycosylation, excessive protein folding burdens caused by stress, or chaperone inhibition, or alterations in disulfide bond formation) results in ER stress.

Living cells have signaling networks to detect ER stress and respond accordingly. These signaling networks collectively control the UPR. During UPR, protein synthesis in the ER is temporarily halted and expression of the ER chaperones is increased to cope with the protein folding burdens.

The UPR is regulated by three ER transmembrane proteins. They are PKR- like endoplasmic reticulum kinase (PERK), activating transcription factor (ATF6), and inositol-requiring protein 1 (IRE1) [64]. The role of the PERK branch of the UPR is to regulate translation during accumulation

of unfolded proteins. The role of the ATF6 branch of the UPR is to up-regulate pro-survival genes in response to stress. IRE1 plays an essential role in UPR by transducing pro-survival and pro-apoptotic signals.

The activity of PERK, ATF6 and IRE1 are regulated by ER chaperone Grp78. Under normal conditions Grp78 binds to PERK, ATF6 and IRE1 and prevents them from being active. Accumulation of misfolded proteins in the ER leads to the dissociation of Grp78 from PERK, ATF6, and IRE1. Grp78 dissociates from PERK, ATF6, and IRE1 in order to bind the exposed hydrophobic residues on the unfolded proteins and to fold them back to their native conformations. Once released from Grp78, PERK, ATF6, and IRE1 become activated [64].

Endoplasmic reticulum associated degradation (ERAD)

The endoplasmic reticulum associated degradation pathway (ERAD) is a major quality control program in the endoplasmic reticulum (ER). ERAD is a response to overburden in the ER. During stress, unfolded proteins accumulate in the ER. These unfolded proteins can be refolded into their native conformations by the ER chaperones, or, they can be degraded via the ERAD pathway based on the status of "mannose trimming" [65]. Mannose trimmed proteins are subjected to degradation via the ERAD pathway. Degradation of misfolded proteins by the ERAD pathway is accomplished in three steps: (i) recognition of the misfolded proteins in the ER; (ii) transport of the misfolded proteins to the cytoplasm; and (iii) degradation of the proteins by the ubiquitin dependent proteasome system in the cytoplasm. Alternatively, an imbalance between folding capability and the protein folding burden in the ER can activate the unfolded protein response [64].

The ubiquitin proteasome system (UPS)

Ubiquitination is a protein post-translational modification by which proteins are tagged with a small protein called ubiquitin. Ubiquitination of proteins takes place in the following steps: (i) activation of

ubiquitin by an E1 ubiquitin activating enzyme; (ii) transfer of activated ubiquitin to an E2 ubiquitin conjugating enzyme, and finally, (iii) tagging of the target protein with ubiquitin (where a bond is formed between the C-terminal glycine of ubiquitin and lysine of a protein) which is mediated by the E3 ubiquitin ligases. Proteins can be ubiquitinated on a single lysine by one ubiquitin (mono-ubiquitination) or by several ubiquitins (poly-ubiquitination), or they can be ubiquitinated on several lysines (multi-ubiquitination). The ubiquitination pattern ultimately decides the fate of the substrates, with poly-ubiquitination serving as a tag for protein degradation (discussed below).

The ubiquitin proteasome system (UPS) is another mechanism for regulating proteostasis. When unfolded proteins accumulate in the cell, the UPS helps regulate homeostasis by subjecting these proteins to degradation. Protein are degraded via UPS in two steps: (i) proteins are tagged with multiple molecules of ubiquitin to form polyubiquitin chains, and; (ii) poly-ubiquitinated proteins are degraded by the 26S proteasome machinery [66].

Ubiquitinated proteins are degraded by the 26S proteasome. The 26 S proteasome is a large molecular machine made up of multiple subunits. It consists of a core complex (the 20S proteasome) which is capped on both sides by the 19S regulatory complexes. The regulatory complexes recognize and unfold the ubiquitinated proteins, and translocate them to the core of the complex for degradation. The proteolytic core complex degrades the ubiquitinated proteins [67].

Translational control of proteostasis

"Nascent polypeptide associated complex" (NAC) helps maintain proteostasis by regulating translation. NAC is a ribosome associated chaperone complex [68]. NAC folds ribosomal proteins and helps to regulate translation during normal conditions. When unfolded proteins accumulate in the cells, NAC dissociates from the ribosomes and prevents the aggregation of misfolded proteins by acting as a molecular chaperone. However when NAC is no longer associated with ribosomes,

translation is halted. Thus, NAC acts as a stress sensor, and helps to regulate translation during protein folding burdens [69].

Hsp90 inhibitors and activation of proteostasis pathways

Proteostasis pathways are activated by Hsp90 inhibitors. HSR is activated by the Hsp90 inhibitors 17-AAG and radicicol through HSF1 mediated up-regulation of Hsps [50]. Similarly, HSR is induced by another Hsp90 inhibitor AUY922 through activation of the HSF1 pathway [51]. Apart from the HSR, the UPR is also activated by Hsp90 inhibitors. IRE1 mediated UPR is activated by geldanamycin [70]. The ATF6 branch of UPR is activated by 17-AAG and radicicol [71, 72] . ER stress mediated UPR is also activated by Hsp90 inhibitors. GA and 17-AAG inhibit Grp94 (ER homologue of cytoplasmic Hsp90) and cause ER stress [73]. 17-AAG and PU-H71 induce the up-regulation of ER chaperones GRP78 and GRP94 [71, 74]. PU-H71 also generates ER stress and results in UPR in different human cancer cell lines [74].

Other agents that activate the proteostasis signaling pathways

Tunicamycin

Tunicamycin induces ER stress and activates the UPR. Tunicamycin is produced by several bacteria from the Streptomyces family. Tunicamycin inhibits N-acetyl glucosamine transferases. This compromises N-linked glycosylation of proteins in the ER. These proteins cannot be properly processed and secreted, and thus they accumulate in ER. This results in protein folding burden, and leads to the activation of the UPR signaling pathway.

Tunicamycin induces the expression of ER chaperones. In mouse models and SILAC-based quantitative analysis, TM activates the UPR by up-regulating ER chaperone Grp78 [75]. Additionally SILAC-based studies also showed that tunicamycin up-regulates other ER chaperones cyclophilins B,

DnaJ homolog subfamily B member 11, endoplasmin, hypoxia up-regulated protein 1, protein disulfide isomerase, and protein disulfide isomerase A4 [76].

Tunicamycin does not induce the expression of Hsp70. Although tunicamycin induces the expression of the ER chaperones GRP78 and GRP94, the expression of Hsp70 is unaltered by tunicamycin [77] . Since Hsp70 induction is a hallmark of HSR activation, this suggests that tunicamycin specifically activates the UPR but not the HSR. These results are consistent with previous findings that the expression of Hsp70 is not altered during the activation of the UPR by tunicamycin [77, 78] . This is an example of strict compartamentalization of the proteostasis pathways.

L-Azetadine-2-carboxylic acid (AZC)

L-Azetadine-2-carboxylic acid (AZC) is a protein folding antagonist. AZC is a plant product found in members of Ruscaceae and Fabaceae. It is an analog of proline. However, it differs from proline, in that AZC has four-membered ring instead of proline's five-membered ring. During protein synthesis, AZC can be incorporated into proteins instead of proline. This interferes with folding of those proteins [79]. As a result, unfolded proteins accumulate in the cell, thus leading to protein folding burdens.

The protein folding burdens caused by AZC leads to the activation of proteostasis signaling pathways. Although AZC's activation of proteostasis signaling pathways is not well explored, some studies suggest its role in activating these pathways. Compromise of protein folding by AZC incorporation in S. cerevesiae leads to the activation of the Hsf1-mediated HSR and results in 27-fold induction in the expression of several HSF-regulated Hsp genes [80]. In addition, AZC induces ER stress and activates UPR in human HepG2 cells as evidenced by the induction of asparagine synthetase, a marker for UPR activation [81]. AZC also activates IRE1thus triggering kinases involved in ER signaling [82].

<center>**Mass spectrometry and proteomics**</center>

Role of mass spectrometry and proteomics in systems biology

Systems biology is a discipline that deals with understanding the biology of living cells at the systems level. Systems biology gives insights on the cellular networks and their integrated roles in living cells. In order to understand how living systems work as a whole at the protein level, it is important to understand changes in protein expression under different conditions. Proteomics is a branch of systems biology that deals with studying the whole set of proteins under different conditions. Mass spectrometry is a technique used to perform large scale proteomics. With the advancement of instrumentation, separation techniques and software available to analyze the data, mass spectrometry has been a powerful tool to study systems-level changes in the expression of proteins under different conditions.

Targeted proteomics

Targeted proteomics deals with studying a selected list of proteins rather than studying all proteins in the whole sample. In targeted proteomics, specific peptides from a selected protein are monitored by the mass spectrometer. Triple quad mass spectrometers are routinely used for targeted proteomics. In the first quadrupole ions of specific mass are selected for fragmentation and in the third quadrupole, ions of specific mass are selected for detection. This process in which selected ions are monitored is called selected reaction monitoring (SRM) or multiple reaction monitoring (MRM).

Top-down and bottom-up proteomics

Proteomics experiments can be performed by two approaches: top-down or bottom-up. In top-down proteomics, mass spectrometry is performed on intact proteins. The top-down approach starts with the separation of proteins, followed by their fragmentation and measurement of the masses of the precursor ion (intact peptide before fragmentation) and the fragment ions (ions resulting from the fragmentation of the precursor ions).

<center>15</center>

In the bottom-up approach, purified proteins or complex mixture of proteins are enzymatically digested into peptides, the masses of the peptides are measured by mass spectrometry, and proteins are identified from the MS information obtained.

Principles and instrumentation of mass spectrometry

Ionization techniques

Mass spectrometers measure the masses of ionized molecules in a gas phase. The basic components of a mass spectrometer are the ion-source, the mass analyzer and the detector. For mass spectrometry analysis, molecules are ionized. Mass spectrometers work by using electric or magnetic fields to exert forces on ionized molecules. Therefore, for mass spectrometry analysis, molecules must be ionized (charged).

In proteomics, two soft ionization techniques are used to prevent fragmentation: Electrospray ionization (ESI) [83] and Matrix Assisted Laser Desorption and Ionization (MALDI) [84]. Electrospray ionization is used for ionization of the samples in liquid phase, and is thus is typically coupled to liquid chromatography (LC-MS). In MALDI, samples are embedded in a crystalline matrix, hence "off line".

Electrospray ionization works by converting the liquid carrying the analytes of interest to a fine aerosol and ionizing the molecules by solvent evaporation. To facilitate solvent evaporation and thus ionization, volatile compounds like acetonitrile are used in the solvents. Organic acids like formic acid or acetic acid are added to the solvents to increase the conductivity and reduce the size of the initial droplet. Organic acids also donate protons and facilitate the ionization process.

Mass analyzers

The mass analyzer is the heart of a mass spectrometer. Mass analyzers measure the mass-to-charge ratios (m/z) of ionized sample molecules. The key features of a mass analyzer are sensitivity (the

ability to detect low abundant molecules), resolution (ability to pack ions into tight ion packets), and accuracy (difference between the measured mass of an ionized sample molecule versus its actual mass). The accuracy of a mass analyzer depends on its resolving power. The higher the resolving power of a mass analyzer, the higher is its mass accuracy.

Different types of mass analyzers are utilized for different proteomics experiments. The most popular are quadrupole, ion-trap, Orbitrap, time-of-flight (TOF), and Fourier transform ion cyclotron (FT-MS) mass analyzers. The Quadrupole mass analyzers are made up of four cylindrical rods arranged opposite to one another. The opposing rod pairs are electrically connected and voltage is applied to the each pair of rods in alternating fashion. Varying the applied voltage filters which ions in a continuous stream hit the detector. Quadrupole mass analyzers are very fast, but have relatively low mass accuracy.

Ion-trap mass analyzers are similar to quadrupole mass analyzers, but are capped at each end with electrodes to trap ions in stable trajectories ("electrostatic bottle"). Increasing voltage in the trapping field results in the ejection of these ions through a hole, and the ions hit the detector. Ion-trap mass analyzers are different from quadrupole mass analyzers in that they fill and filter ions rather than just filtering ions. The advantages of the ion-trap mass analyzers are their robustness, sensitivity and inexpensiveness. The main limitation of ion traps is that ions smaller than $1/3^{rd}$ of the parent ion are lost during MS/MS. Another disadvantage of ion-trap mass analyzers is low mass accuracy relative to Orbitrap and TOF mass analyzers.

The Orbitrap is another mass analyzer. It was invented by Makarov [85]. The Orbitrap mass analyzer consists of a central spindle electrode and outer barrel electrode. The Orbitrap mass analyzer determines the m/z values of ions based on the frequencies of the oscillations of the orbitally trapped ions in the electric field. The main strengths of the Orbitrap mass analyzer are its high mass resolution (up to 150 000), high mass accuracy (2-5ppm), and high dynamic range (greater than 10^3) [85]. However the limitation of the Orbitrap mass analyzer is it is very slow.

TOF mass analyzers measure the m/z by measuring the time it takes for ions to reach the detector from the ion source. The advantages of TOF mass analyzers are their very high speed and accuracy.

In Fourier transform ion cyclotron (FT-MS) mass analyzers, ions are trapped in an electromagnetic field. Applying an external magnetic field makes the ions move in circular orbits. The frequency with which the ions move is called the cyclotron frequency. In FT-ICR, ion masses are obtained from their respective cyclotron frequencies. The advantages of FT-MS analyzers are their low femtomole sensitivity, high resolving power (800,000) and high mass accuracy. FT-ICR mass analyzers are good for top-down proteomics.

Tandem mass spectrometry (MS/MS)

In tandem mass spectrometry (MS/MS), the m/z measurements are done in two sectors. In the first MS sector a precursor ion of specific m/z is selected from a mixture of ions. The selected precursor ion is subsequently fragmented by collision with neutral gas to generate product ions. In the second MS sector, the m/z values of the product ions are measured. In triple quadrupole mass spectrometers, all the above steps are sequentially performed in two physical sectors which are separated in space ("tandem in space" mass spectrometry). Whereas in ion trap mass spectrometers, all the above steps are sequentially performed, but in the same physical sector of the instrument ("tandem in time" mass spectrometry).

Fragmentation techniques

In proteomics, proteins are identified based on the amino acid sequence information obtained by protein or peptide fragmentation. Depending on the site of cleavage of the peptide backbone, the ions generated are classified as a, b and c ions (if the ions contain the N-terminus of the peptide), or x, y and z ions (if the ions contain the C-terminus of the peptide). Three fragmentation techniques are commonly used for peptide fragmentation. They are the collision induced dissociation (CID), the electron capture dissociation (ECD) and the electron transfer dissociation (ETD). In the CID

fragmentation, the peptide ions are fragmented by acceleration to a high energy state and collision with molecules of a neutral gas like helium, nitrogen or argon. CID fragmentation favors the most labile bond, typically the peptide amide bond (C-N) to generate b and y ions. These can then be used for sequence determination and protein identification. In the ECD fragmentation, peptides are fragmented following capture of an electron by a multiply protonated peptide ion. The ECD fragmentation cleaves the backbone N–Cα bond and results in c and z ions. In the ETD fragmentation, peptides are fragmented in gas phase following transfer of an electron from anthracene or fluoranthene to a multiply protonated peptide ion. ETD fragmentation, similar to the ECD fragmentation cleaves the backbone N–Cα bond and yields c and z ions [86].

In top-down proteomics, ions can be fragmented by ECD or ETD fragmentation. In ECD or ETD fragmentation, fragmentation of ions is random. This helps for good sequence coverage. Additionally in ECD/ETD fragmentation, post-translational modifications are not lost. Therefore top-down proteomics is good for identifying post-translational modifications.

In bottom-up proteomics, ions can be fragmented by CID fragmentation or by HCD fragmentation. In CID and HCD fragmentation, the fragmentation is biased to weakest bonds. As a result, post translational modifications are lost. Therefore, collisional dissociation is not suited for identifying post-translational modifications. Nevertheless, the bottom-up approach is routinely used for protein identification and quantitation.

Quantitative proteomics techniques

Quantitative proteomics deals with quantitation of proteins in complex protein mixtures. Quantitative proteomics can be divided into two types: relative quantitative proteomics techniques and absolute quantitative proteomics techniques. In relative quantitative proteomics techniques, the relative abundance of proteins across two different samples is measured. There are two approaches for quantitation in relative quantitative proteomics. They are label-free and label-based. In label-free

approaches, isotope-labeled amino acids are not used, and samples from the two different experimental categories are analyzed separately. Two types of label-free approaches are used in label-free quantitation: (i) ion intensity measurement and (ii) spectrum counting. In the ion intensity approach, MS peak areas from the chromatograms of two samples are compared. Using this information, differences in relative abundance of peptides between two samples is determined. In the spectrum counting approach, the abundance of proteins in the samples is assessed by counting number of MS/MS spectra associated with peptides from each protein. An increase in the number of MS/MS spectra from a given protein indicates more abundance of that protein and vice versa.

In label-based quantitative proteomics approaches, samples from two different experimental groups are labeled with stable isotopes that share exactly the same chemical properties, but differ by mass. Isotopic labeling can be done in-vitro by chemical labeling or in-vivo by metabolic labeling. Examples of chemical labeling approaches are isotope coded affinity tags (ICAT) [87] and isobaric tags for relative and absolute quantitation (ITRAQ) [88]. ICAT labeling reagents have: (i) a reactive group that labels the thiol groups of cysteine, (ii) a linker that can be isotopically tagged and (iii) an affinity tag (biotin) which facilitates affinity purification. In ICAT, protein mixtures from two different experimental groups are tagged with light and heavy ICAT reagents, samples are mixed, digested, affinity purified, and then difference in protein expression across the experimental groups is quantified. In ITRAQ approach, peptides from different experimental samples are labeled with tags of different masses. The samples are then pooled and quantitative differences in protein expression across the groups are identified. Currently ITRAQ supports analyzing protein expression changes across 8 experimental groups (8-plex).

In the metabolic labeling approach, non-isotopic or isotopic lysine and arginine are metabolically incorporated into all proteins, (e.g. stable isotope labeling with amino acids in cell culture (SILAC)) by growing the cells in media supplemented with isotopic or non-isotopic amino acids [89]. The differentially tagged samples are then pooled, digested, chromatographically fractionated, and analyzed by mass spectrometry. In this approach, two populations of cells are grown in media

supplemented with the same components, except that one medium contains heavy isotopic amino acids and the other medium contains light isotopic amino acids. Cells grown in heavy and light media are used for studying proteins in two different conditions. For protein identification and quantitation, protein samples from both the cell populations are extracted, mixed and analyzed by mass spectrometry. Quantitation is performed by measuring the relative peak areas of heavy/light peptide pairs. SILAC offers several advantages over the label-free approaches: because different experimental samples are pooled and processed in the same way, there is less technical variability across experiments , and the time required to analyze the samples is reduced [90].

Bioinformatics tools for protein identification and quantitation

Several database search engines are available for identifying proteins from mass spectrometry data. Some commonly used search engines are SEQUEST, Mascot, OMSSA, X! Tandem and Andromeda. All these search engines work in a similar manner. They match theoretical versus experimental m/z's and generate scores for each spectrum to find peptide or protein matches. These scores represent the strength of the match between observed and predicted MS/MS spectra. Most search engines use probabilistic scoring approaches. The probabilistic approach calculates the probability that the match between experimental data and each peptide/protein sequence occurs by chance. Mascot is a proteomics search engine that uses probabilistic approach for protein identifications [91]. X! TANDEM is an open source search engine [92]. It is used as a search engine by Scaffold. Andromeda is another search engine that uses probabilistic scoring model [93]. It is used as a search engine by MaxQuant.

Scaffold is another proteomics tool. In proteomics, there is a high probability of reporting false identifications. Scaffold validates the proteins identified by other database search engines. Scaffold employs Peptide Prophet and Protein Peptide algorithms to statistically validate results obtained from the search engines. These algorithms analyze populations of search engine scores. By comparing the

results obtained from the X! Tandem and other search engines, Scaffold gives increased confidence in the proteins identified in large datasets [94]. Scaffold Q+S is new version of Scaffold for quantitative analysis of SILAC data. It performs data normalization, quantitation, and statistical analysis of SILAC output data obtained from MaxQuant (discussed below).

MaxQuant is proteomics software developed by Cox and Mann at the Max-Planck Institute. It is used for the analysis of high resolution, quantitative mass spectrometry data obtained from SILAC experiments. MaxQuant quantifies thousands of SILAC peptide pairs by using a series of algorithms for peak detection, isotope cluster detection and SILAC pair detection. To accomplish this, MaxQuant uses correlation analysis and graph theory. For peak detection and quantification, MaxQuant uses mass and intensity of the peptide peaks. In order to do this, MaxQuant fits the points in each MS scan using Gaussian curve and thus identifies the 2D peaks in each MS scan. From the 2D peaks MaxQuant then assembles 3D hills. 3D hills are generated over m/z axis. Using centroid masses, MaxQuant then estimates 3D peak volume. Using this information, MaxQuant identifies and quantifies thousands of proteins [95].

Bioinformatics programs for statistical analysis and processing of proteomics data

Perseus

Perseus is a program used for analyzing quantitative proteomics data obtained from MaxQuant. It can be used for common functions such as data normalizations, calculations (log transformations, ratios, means, medians and other common calculations) and enrichments. It can also be used for creating plots and for small range of statistical analysis. One limitation of Perseus is that its code is not open and algorithms are not well described.

CHAPTER II

Proteomics fingerprint of Hsp90 N-terminal inhibitors AUY922, 17-DMAG and radicicol using the spectrum counting approach

Introduction

Although pharmacological compounds are designed to have specificity for a particular target protein, it is highly possible that they can target other proteins. These phenomena are called off-target inhibitor effects. Targeting proteins other than the target protein may result in harmful side effects, or may prove to be beneficial in some cases. Also, structurally distinct inhibitors that are all designed to target a specific protein might have different phenotypic effects resulting from differences in their targets. Mechanisms of inhibitor action can be inferred from the phenotypic effects (reporters) that the inhibitor causes.

Several structurally distinct small molecule inhibitors bind to the Hsp90 N-terminus and inhibit its function. All these Hsp90 N-terminal binding agents lead to the indirect depletion of a wide variety of Hsp90-dependent proteins in vitro. However, in cultured cells how much of the anti-proliferative effects of these N-terminal binding agents are specifically due to Hsp90 inhibition is not well known.

We wanted to address this question by studying the proteome-wide effects of structurally distinct Hsp90 N-terminal binding agents in cultured cancer cells and comparing their proteomics fingerprints. By doing so, we would expect to see conserved inhibitors effects if all these

inhibitors inhibit cell proliferation by inhibiting Hsp90. However, if a given inhibitor acts by off target effects we would expect to see proteome alterations unique to each inhibitor.

Dr. Brain Blagg's laboratory at the University of Kansas has synthesized several small inhibitors that bind to the Hsp90 C-terminus and inhibit its function (hereafter called Hsp90 C-terminal binding agents).These C-terminal binding agents bind Hsp90 C-terminal domain in vitro. Additionally, these C-terminal binding agents exhibit anti-proliferative effects in a wide variety of cancer cell lines and deplete several known Hsp90 clients. However, proteome-wide changes induced by the C-terminal binding agents are not reported.

Long term goals of our laboratory are to validate Hsp90 C-terminal binding agents using proteomics approaches. Identifying proteomics fingerprints of Hsp90 N-terminal binding agents will allow us to compare their effects to the effects of C-terminal binding agents. This will give insights into the mechanisms of action of the two classes of inhibitors and whether their mechanisms of action are conserved. Additionally, biomarkers of Hsp90 N-terminal binding agents identified in this study can be used to validate Hsp90 N-terminal binding agents in the clinic, and will also help to characterize novel Hsp90 N-terminal binding agents.

In this study, we characterized the effects of three structurally distinct Hsp90 N-terminal inhibitors AUY922, 17-DMAG and radicicol on the proteome of Jurkat leukemia cells. We quantified changes in protein expression by spectrum counting using a bottom-up proteomics approach. We present the proteomic fingerprints of three Hsp90 N-terminal binding agents and identify a small assortment of biomarkers for Hsp90 N-terminal inhibition. We also explore the limitations of the spectrum counting technique, and thus highlight the need for using superior quantitative proteomics techniques to validate the changes identified.

Materials and Methods

Reagents

Jurkat leukemia cell line E6.1 was obtained from American Type Culture Collection. SILAC RPMI medium was purchased from Thermo Scientific (Catalog number 89984). Amino acids L-lysine-2Hcl (Catalog number 89987), L-aarginine-Hcl (Catalog number 89989) and 13C6 15N4 L-aarginine (Catalog number 89990) were purchased from Thermo Scientific. Amino acid 13C6 15N2 L-llysine (Catalog number 291-0.25) was purchased from Cambridge Isotopic Laboratories, Inc. Dialyzed fetal bovine serum (Catalog Number 89984) was purchased from Thermo Scientific. 17-DMAG, radicicol and AUY922 were obtained from LC Laboratories (Catalog Number D3440), Cayman Chemicals (Catalog Number 13089) and Selleck Chemicals (Catalog Number S1069), respectively. Hybri-Max DMSO (Catalog Number D2650) was obtained from Sigma. Inhibitors were dissolved in DMSO. L-azetadine-2-carboxylic acid (AZC) was obtained from Sigma (Catalog Number A0760) and dissolved in water. CellTiter Aqueous One Solution Cell Proliferation Assay (MTS) reagent was obtained from Promega (Catalog Number G3581). PVDF membrane was obtained from Bio-Rad. Mouse monoclonal anti-human β-actin antibodies were obtained from Sigma (Catalog number A5441). Rabbit polyclonal anti-human Poly-ADP ribose polymerase (PARP) antibodies were obtained from Cell Signaling Technology (Catalog Number 9542). Rabbit monoclonal anti-human Cdk6 (Catalog Number 3524-1), Cdk1(Catalog Number 3787-1), Dnmt1(Catalog Number 2788-1) and DDX5 antibodies (Catalog Number-5567-1) were obtained from Epitomics, goat polyclonal anti-human UNR antibodies (Catalog Number sc-79293), rabbit polyclonal anti-human MCM7 antibodies (Catalog Number sc-22782) and mouse monoclonal anti-human UHRF1 antibodies (Catalog Number sc-166898) from Santa Cruz Biotechnology Inc., rabbit polyclonal anti-human eIF4A1 antibodies from Abcam (Catalog Number ab31217). SuperSignal West Pico Chemiluminiscent substrate (Catalog Number 34077)

was purchased from Thermo Scientific. 4-20% Mini-PROTEAN TGX precast gels were purchased from Bio-Rad (Catalog number 456-1094).L-Dithiothreotol (DTT) (Catalog number 43819-1G) and Iodoacetamide (IAA) (Catalog number 16125-5G) were purchased from Sigma.

General cell culture, cell proliferation assays and inhibitors treatments

Jurkat cells were cultured in RPMI media supplemented with 10% dialyzed fetal bovine serum, 200 mM/ litre L-glutamine, light isotopic lysine (50 mg/ 500 ml) and arginine (50 mg/ 500 ml) amino acids, streptomycin (500 µg/ mL), penicillin (100 units/ mL). Cells were cultured at 37°C in a humidified 5% CO2 incubator.

For cell proliferation assays, cells were seeded in 96 well plates at a density of 10,000 cells/ 100 µl/ well. After twenty four hours, cells were treated with a dilution series of each of the inhibitors 17-DMAG (1.6, 4.9, 14.8, 44.0, 133, 400, 1200, 3600 and 10,800 nM) , radicicol (0.8, 2.3, 7, 21, 62, 185, 555, 1670 and 5000 nM) or NVP-AUY922 (1, 3.5, 11.5, 35, 100, 300 and 900 nM). For control experiments, cells were treated with DMSO (solvent in which all the three inhibitors are dissolved). Following inhibitor treatment, cells were incubated at 37°C in a CO_2 incubator. Cell viability was determined using Cell Titer Aqueous One Solution Cell Proliferation Assay(MTS) reagent from Promega (Inhibitors doses and duration are described for individual experiments). Twenty microliters of MTS reagent was added to the inhibitor treated or DMSO treated wells and the plates were incubated at 37°C in the CO_2 incubator for 4 hours. Absorbance of the 96 well plates at 490nm was recorded using Molecular Devices Versamax plate reader. All experiments were performed in three biological replicates.

For determining the IC_{50} values for Cdk6 depletion, cells were seeded in 10 mL in T-25 cm^2 flasks. After twenty four hours, cells were treated with a dilution series of each of the inhibitors17-DMAG, radicicol or AUY922 (dilution series of each inhibitors used for IC_{50} determinations are mentioned in the later sections of this chapter). For control experiments, cells

were treated with DMSO. Twenty four hours following inhibitor treatments, cells were harvested and lysates were prepared for Western blotting.

Preparation of cell lysates and determination of protein concentration

Following inhibitor treatments, cells were harvested by 5 minute centrifugation at 1700rpm. Cell pellets were washed twice with phosphate buffered saline, pH 7.4. After washing, the cell pellets were lysed with radio immuno precipitation (RIPA) lysis buffer containing 20 mM sodium phosphate, 50 mM glycerophosphate, 100 mM sodium chloride, 0.1% SDS, 2% NP40, 0.75% deoxycholate, 5 mM EDTA, 5 mM EGTA, and 2 mM sodium orthovanadate, 10 mM NaF, 0.1 mg/ml PMSF, 1 X Sigma protease inhibitor cocktail and 1mM DTT, at 4°C on a rocker. Following lysis, the lysates were clarified at 12,000 x g for 10 minutes. Protein concentrations in the lysates were determined by Bradford reagent using BSA as a standard.

Determination of IC$_{50}$ values for Cdk6 depletion

Twenty micrograms of untreated, DMSO treated, and inhibitor-treated cell lysates were boiled in SDS-PAGE buffer containing 100 mg/ ml DTT, and loaded onto an 8% polyacrylamide gel. Proteins were separated by running the gels at 25 mA. Post gel run, proteins were transferred onto a PVDF membrane and the membranes were probed with anti-Cdk6 antibodies. After incubation with secondary antibodies, the membranes were developed using standard chemiluminiscent techniques. All experiments were done in three biological replicates. IC$_{50}$ values were determined using GraphPad Prism software. Data were fit using non-linear regression analysis (least squares fit, no weighting, and no constraints). Error bars are SEM.

Sample preparation for mass spectrometry

For LC-MS/MS analysis, proteins in the cell lysates were TCA/ acetone precipitated. Resulting protein pellets were dissolved in buffered urea solution containing 8 M urea, 100 mM Tris-Hcl, pH 8.5 and reducing agent TCEP (tris (2-carboxyethyl)phosphine) at room temperature for 20 minutes and alkylated with one tenth volume of 100 mM IAA (iodoacetamide) in dark, at room temperature for 15 minutes. Samples were further reduced with one twentieth volume of 100 mM DTT in the dark at room temperature for 5 minutes. Then the samples were diluted with 100 mM Tris-Hcl, and digested with a final concentration of 4 µg/ml trypsin for overnight at 37 degrees C. Trypsin digested samples were acidified with 2 µl of 100%TFA and desalted by using C18 affinity tips (OMIX). Desalted samples were vacuum dried and stored at -80°C for subsequent LC-MS/MS analysis.

LC-MS/MS analysis

LC-MS/MS analysis was done by running samples on Thermo Fisher Scientific hybrid LTQ-Orbitrap mass spectrometer. A New Objective PV-550 nanoelectrospray ion source was used for electrospray ionization. An Eksigent NanoLC-2D liquid chromatography system was used for separation of the peptides. Peptides were first trapped on a 2.5 cm pre-column with a vented column configuration (5-µm Magic C18 AQ). Trapping was done at high flow rates and was used to remove residual salts in the sample. Salts were disposed through waste and only peptides were allowed to flow though the analytical column. Trapped peptides were then separated on a 75 µm ID 15-cm fused silica column (5-µm Magic C18 AQ) terminated with an integral fused silica emitter. Peptides were eluted by using a 2.5-28% ACN/0.1% formic acid gradient over 116 min at a flow rate of 300 nL/min. Each biological sample was run on LTQ-Orbitrap in four technical replicates.

Eluted peptide samples were ionized by nanospray. Instrument was operated in a data dependent scanning mode. Data dependent scanning mode allows for an automated choice for selecting specific ions for further MS/MS analysis. Full scan MS spectra for ions 360-1400 m/z were acquired in the Orbitrap with a nominal resolution of 60,000 FWHM. Full range lock-mass FT-MS scan was enabled for real time calibration and for high accuracy measurements. The six most abundant peptides (top six) were selected for further fragmentation in the ion trap by using CID (collision induced dissociation) fragmentation. For MS/MS analysis, only intense ions (with ion-intensity counts greater than 8,000) were chosen. To save instrument time and duty cycle only mono-isotopic precursors were selected for MS/MS analysis. Parent ions with unassigned charges were not chosen for further MS/MS analysis because the m/z values cannot be determined for these ions. Ions previously identified as contaminants and ions already selected for MS/MS analysis (dynamic exclusion at 150% of the observed chromatographic peak width) were also not chosen for further MS/MS analysis.

Data analysis

MS spectra from the parent ions and MS/MS spectra (tandem spectrum) of the resulting daughter fragments were acquired and stored. Extract_msn_.exe utility from Bioworks 3.3.1 was used to extract the tandem mass spectra by converting the raw files into peak list files. Extracted MS/MS spectra were searched against a database which has tandem spectra of all known human proteins generated by in-silico digestion. Tandem mass spectra were searched against IPI.HUMAN.v3.87 database (91,464 protein entries) using Mascot (Matrix Science, London, UK; version 2.2.04) and X! Tandem (The GPM, thegpm.org; version 2007.0.1.01.1) with the assumption that trypsin was the enzyme used for in-silico digestion of the human proteins. Parameters used for Mascot and X! Tandem search were: fragment ion mass tolerance of 0.60 Da (i.e. the difference between observed mass and theoretical mass should be 0.6 Da) and parent ion

tolerance of 5.0 PPM, variable modifications specified were S-carbamoylmethylcysteine cyclization, n-Formylation of the N-terminus, acetylation of the N-terminus and iodoacetamide derivative of cysteine (telling the program there could be mass difference due to these modifications).

Criteria used for protein identification

Scaffold version 3.6.5 (Proteome Software) was used to validate peptide and protein identifications using Scaffold's Peptide prophet and protein prophet algorithms and high mass accuracy scoring option. Protein identifications were based on 99% protein probability, 2 minimum peptides, and 50% minimum peptide identification probability. Proteins that shared similar peptides but could not be differentiated based on MS/MS analysis alone were grouped to satisfy the principles of parsimony (i.e. reporting the minimum set of protein sequences that adequately account for all observed peptides). Databases searches also included searches against decoy database (database with reverse sequences) to estimate the incorrect protein identifications, i.e. false discovery rates (FDR).

The spectrum counting approach was used for quantitative analysis of changes in protein expression. Analysis was done by normalizing the data. Normalization was done assuming unequal sample load and/or variations in the sample processing. Scaffold's normalization works by multiplying some fractional amount across samples so that the total spectra are same within each category and also across categories. Statistical analysis was done by using Student's T-test.

Results

   Before characterizing AUY922's effects on the Jurkat cell proteome, we wanted to first establish the concentrations of AUY922 that inhibited 50% of the proliferation of Jurkat cultures (IC_{50}). To accomplish this, we treated Jurkat cultures with the indicated doses of AUY922 and measured the effects on cell proliferation. Results showed that AUY922 caused anti-proliferative effects starting from 3.5 nM to 11.5 nM, inhibiting the proliferation of 25% of the cells. Beyond 35 nM doses, AUY922 completely inhibited the proliferation of Jurkat cultures. At the 35 nM - 900 nM dose range, cells maintained densities that were used during seeding. Therefore it was concluded that AUY922 exhibits cytostatic rather than cytotoxic effects. We also identified that AUY922 inhibits the proliferation of Jurkat cultures at low nano-molar doses, with calculated IC_{50}'s of 10.27 nM, 7.2 nM and 8.6 nM after 24 hours, 48 hours and 72 hour respectively (Fig 2.1). This suggested that AUY922's effects were stronger at 48 and 72 hours. Our results were consistent with previous reports that AUY922 inhibits the proliferation of several cancer cell lines at low nano-molar doses [26, 96, 97] and exhibits cytostatic effects [24].

   Before characterizing the effects of Hsp90 inhibitors on Jurkat proteome, we wanted to identify a strong Hsp90 dependent reporter protein that can be best used to identify appropriate Hsp90 inhibitor concentrations. Previous reports [98, 99] , and unpublished results from our lab, showed Cdk6 to be rapidly depleted and easily detectable upon Hsp90 inhibition. Therefore, we chose to test if Cdk6 is a sensitive reporter of Hsp90 inhibition. To accomplish this, we treated Jurkat cultures with classic Hsp90 inhibitor 17-DMAG and assayed the inhibitors' effects on Cdk6 depletion**.** Results showed the rapid depletion of Cdk6 after 8 hour treatment with 150 nM 17-DMAG (Fig 2.2). Thus, we concluded that Cdk6 was sensitive marker for Hsp90 inhibition.

Figure 2.1: Effects of AUY922 on Jurkat cell proliferation.

Jurkat cultures were incubated for 24, 48 or 72 hours with indicated concentrations of AUY922 and cell proliferation was measured as described in methods. Each data point represents % proliferation relative to control. Error bars are the SEM (N=3). For the curve fits shown, the R^2 values were 0.8957, 0.9801 and 0.9966 for 24, 48 or 72 hour respectively.
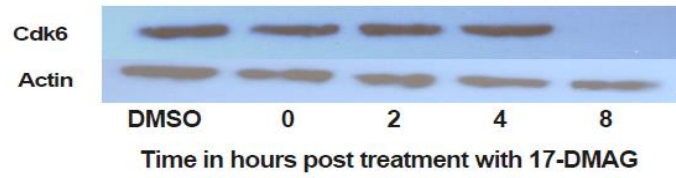
Figure 2.2: Time course of Cdk6 depletion upon treatment with 150 nM 17-DMAG.

Jurkat cultures were treated with 150 nM 17-DMAG and after 0, 2, 4 or 8 hours of treatment,

Cdk6 levels were assayed by Western blotting. Actin was used as a lane loading control.

After establishing Cdk6 as a sensitive reporter for Hsp90 inhibition, Cdk6 was used as a marker to identify the appropriate concentration of AUY922 that depletes Hsp90 dependent client proteins in cultured Jurkat cells. To accomplish this, Jurkat cells were treated for 24 hours with the indicated doses of AUY922 and assayed the inhibitor's effects on Cdk6 levels. Results demonstrated a dose-dependent depletion of Cdk6 by AUY922 as shown in Figure 2.3A. Thus, we concluded that AUY922 lead to the depletion of Cdk6 with a calculated IC_{50} of 11 nM as shown in Figure 2.3B. For AUY922, the IC50 doses for Cdk6 depletion (11 nM) closely matched with the IC-50 doses for cell proliferation (10 nM). Our results were also consistent with previous reports showing Cdk6 depletion by AUY922 at 10 nM concentration in human gastric cancer cell line NCI-N87 [25].

To characterize the effects of AUY922 and other Hsp90 inhibitors on the Jurkat proteome, we first wanted to treat Jurkat cultures with appropriate doses of AUY922, but without grossly compromising cell viability. Thus, PARP cleavage was used as a marker for apoptosis. During apoptosis PARP is cleaved by caspases to yield two fragments of molecular weights 89 kDa and 24 kDa [100, 101]. Therefore, Jurkat cultures were treated for 24 hours with the indicated doses of AUY922, and the inhibitor's impacts on PARP cleavage were assessed. Results showed that at doses ranging from 1- 16 nM, AUY922 had negligible effects on PARP cleavage. At higher doses, AUY922 induced some PARP cleavage (Fig 2.4). Therefore, we conclude that the effects of AUY922 were largely sub-apoptotic at doses ranging below 1- 128 nM.

Before comparing AUY922's effects on the Jurkat proteome to the effects caused by other Hsp90 inhibitors 17-DMAG and radicicol, we wanted to identify the appropriate doses of DMAG and radicicol for cell proliferation. We accomplished this, using the same approaches as described for AUY922 in the above sections. Results showed that 17-DMAG, similar to AUY922, exhibited cytostatic effects at high doses but had a less steep dose response curve compared to AUY922. However, radicicol unlike AUY922 and 17-DMAG, exhibited cytotoxic rather than

A.
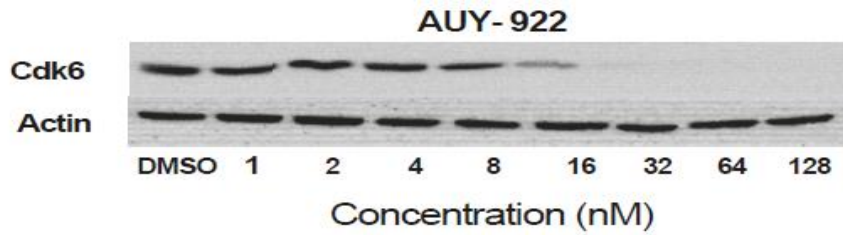
B.
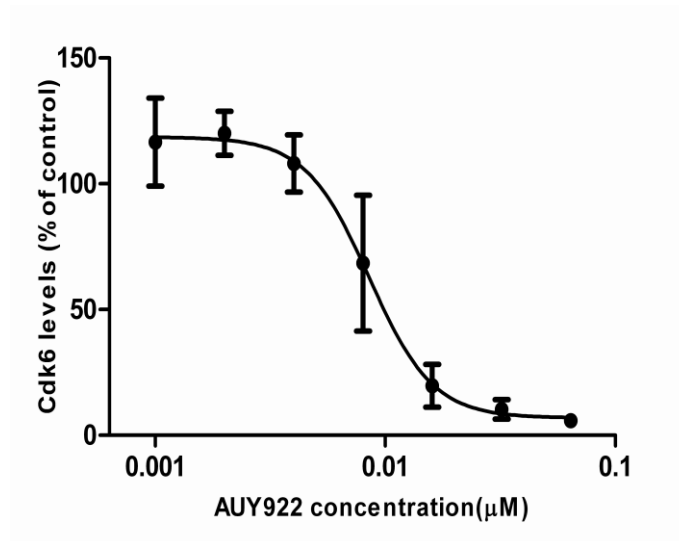
Figure 2.3: Dose-dependent depletion of Hsp90 dependent client protein Cdk6 by

AUY922.

Panel A: Jurkat cultures were incubated for 24 hours with indicated concentrations of AUY922

and Cdk6 depletion was assessed by western blotting. Actin was used as a lane-loading control.

Panel B: IC_{50} values for Cdk6 depletion were estimated by performing densitometry on

independent biological experiments (N=3). Data were curve-fitted as described in methods. The

R^2 value was 0.8570.
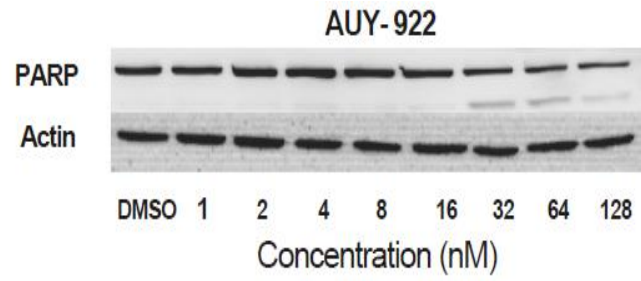
Figure 2.4: Apoptotic effects of AUY922 as assessed by PARP cleavage.

Jurkat cultures were treated for 24 hours with the indicated doses of AUY922. After 24 hours,

PARP cleavage was assessed by western blotting. Actin served as a lane-loading control.

cytostatic effects and the dose response curve was less steep compared to AUY922 and 17-DMAG (Fig 2.5, Panel B). 17-DMAG and radicicol inhibit the proliferation of Jurkat cells with IC_{50} values as shown in the Table 2.1 below. Therefore, we conclude that both 17-DMAG and radicicol inhibit the proliferation of Jurkat cultures, but with less potency compared to AUY922.

Similarly, we determined the IC_{50} values for 17-DMAG and radicicol for Cdk6 depletion as described for AUY922 in the above sections. Results showed a dose-dependent depletion of Cdk6 by both inhibitors (Fig 2.6, Panel A & Fig 2.7, Panel A), with calculated IC_{50} values of 30 nM for 17-DMAG (Fig 2.6, Panel B) and 60 nM for radicicol (Fig 2.7, Panel B).
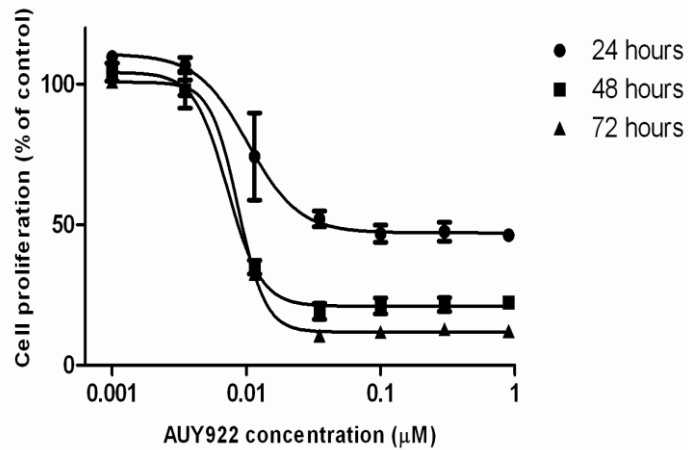
A.
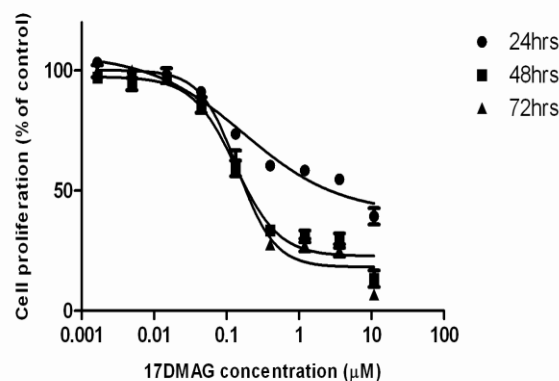
B.
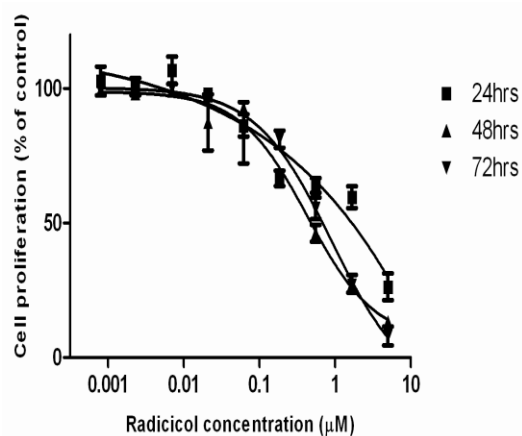
Figure 2.5: Effects of 17-DMAG (5a) and radicicol (5b) on Jurkat cell proliferation.
Jurkat cultures were incubated for 24, 48 or 72 hours with the indicated concentrations of
17-DMAG (Panel A) and radicicol (Panel B), after which cell proliferation was measured
as described in methods. Each data point represents proliferation relative to control. Error
bars are the SEM (N=3). For the curve fits shown, the R^2 values for 17-DMAG were
0.9575, 0.9685 and 0.9690 for 24, 48 and 72 hours respectively, and the R^2 values for
radicicol were 0.9031, 0.9566 and 0.9560 for 24, 48 and 72 hours, respectively.

Table 2.1: IC$_{50}$ values for cell proliferation for AUY922, 17-DMAG and radicicol.

	AUY-922	17-DMAG	Radicicol
IC-50 values	24 hours- 11.2 ± 4.47 nM 48 hours- 7.44 ± 1.67nM 72 hours- 8.77 ± 1.24 nM	24 hours- 211 ± 120 nM 48 hours- 138 ± 37.2 nM 72 hours- 146 ± 35.3 nM	24 hours - 922 ± 388 nM 48 hours - 504 ± 261 nM 72 hours - 1320 ± 967 nM

A.

17-DMAG

| Cdk6 |
| Actin |

DMSO 1.6 4.8 14 44 133 400 1200 3600 10800

Concentration (nM)

B.

Cdk6 levels (% of control) vs 17-DMAG concentration (μM)
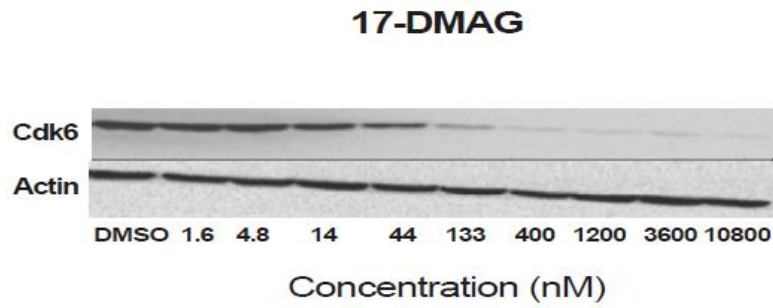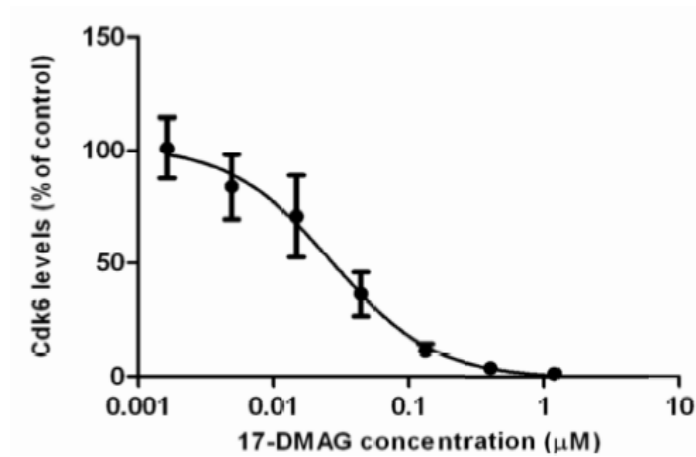
Figure 2.6: Dose-dependent depletion of the Hsp90 dependent client protein Cdk6 by

17-DMAG.

Panel A: Representative western blot of Cdk6 depletion as described in Figure 2.3. Panel B:

Densitometry analysis of Cdk6 depletion from three biological replicates. R^2 value was 0.8552.

A.
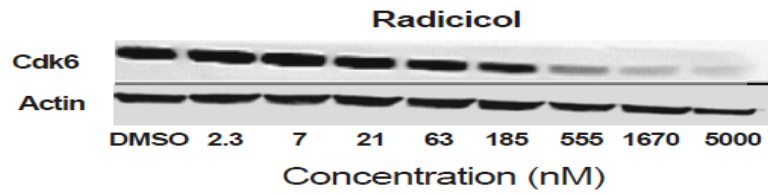
B.
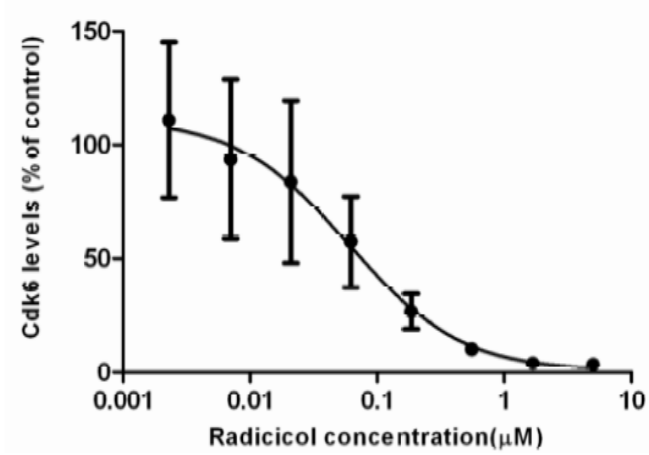
Figure 2.7: Dose dependent depletion of Hsp90 dependent client protein Cdk6 by radicicol.

Panel A: Representative western blot of Cdk6 depletion as described in Figure 2. 3. Panel B: Densitometry analysis of Cdk6 depletion from three biological replicates. R^2 value was 0.6116.

Apoptotic effects of 17-DMAG and radicicol were assessed in the same way as described for AUY922 (Fig 2.8, Panels A & B respectively). Results indicated that the effects of 17-DMAG were largely sub-apoptotic at doses ranging from 1- 133 nM, and the effects of radicicol were largely sub-apoptotic at doses ranging from 1-185 nM. Doses above the mentioned concentrations for both inhibitors begin to show PARP cleavage indicating that those doses induce cell death.

After characterizing dose-curve responses of all the three Hsp90 inhibitors in Jurkat cells, we chose to study their effects on the Jurkat proteome by using 5-7x the IC_{50} doses for Cdk6 depletion. Before doing so, I wanted to test the effects of these dosages on cell viability. To accomplish this, Jurkat cultures were treated for 24 hours with 75 nM AUY922, 150 nM 17-DMAG and 300 nM radicicol. Then cell viability was determined by the Trypan blue dye exclusion assay. Results showed that more than 80% of the cells were viable after treatment with the indicated doses of all three inhibitors (Fig 2.9). Thus we concluded that the 5-7x doses of the three inhibitors did not grossly compromise cell viability.

After confirming that these doses did not grossly affect cell viability, we treated Jurkat cultures for 24 hours with these doses of each inhibitor to study their effects on Jurkat proteome. After treatment, cellular proteins were analyzed using the "bottom-up" proteomics approach as described in Methods.

A.
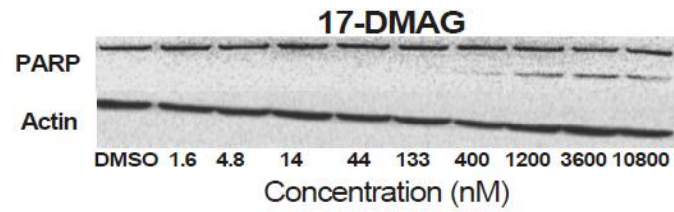
B.
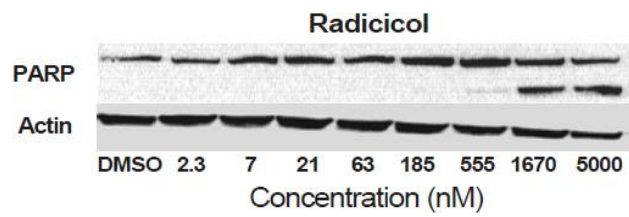
Figures 2.8: Apoptotic effects of 17-DMAG and radicicol as assessed by PARP cleavage.

Panel A: Representative western blot for 17-DMAG. Panel B: Representative western blot for radicicol. Apoptotic effects were assessed as described in Figure 2.4.
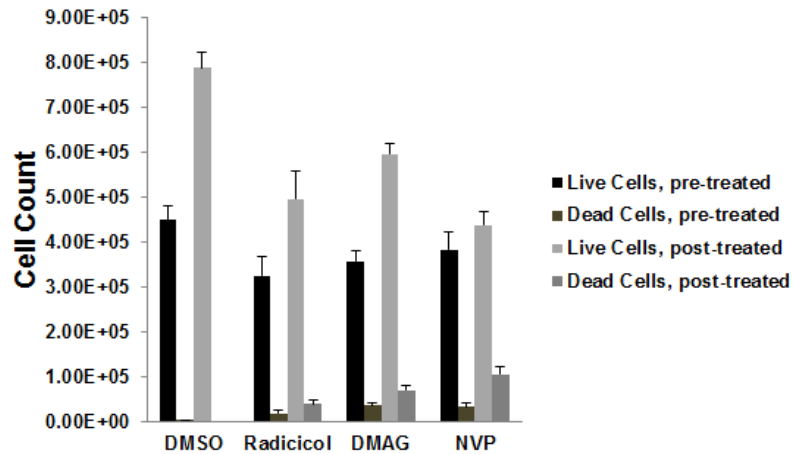
Figure 2.9: Effects of 5-7x IC$_{50}$ doses of AUY922, 17-DMAG and radicicol on Jurkat

cell viability as assessed by Trypan blue counting.

Cells were incubated for 24 hours with 5-7x IC$_{50}$ concentrations of AUY922, radicicol or 17-DMAG. Live and dead cell counts were performed before and after inhibitor treatments. Results shown were from three individual biological replicates.

Using the protein identification criteria as described in Methods, 931 proteins were identified in cells treated with AUY (FDR of 0.5%), 921 proteins were identified in cells treated with DMAG (FDR of 0.5%) and, 900 proteins were identified in cells treated with radicicol (FDR of 0.4%). Inhibitor-induced changes in protein expression were analyzed by the spectrum counting technique. Upon statistical analysis, 9.7% of the total proteins identified were found to be significantly altered by AUY922 (P< 0.05), 8.9% of the total proteins identified were found to be altered by 17-DMAG (P<0.05) and 7.6% of the total proteins identified were found to be altered by radicicol (P<0.05) (Supplemental excel sheet 1). Among the significant changes in protein expression across the 9 experiments (3 inhibitors x 3 biological replicates), 178 proteins showed altered expression. Among these 178 proteins, 92 proteins (51.6%) were found to be down-regulated and 85 proteins (47.6%) were found to be up-regulated.

A wide variety of proteins involved in various biological processes were found to be altered in amount by all three inhibitors. Among the proteins up-regulated were heat shock protein family proteins (large Hsps, small Hsps and chaperonins), Hsp90 co-chaperones, transport proteins, RNA processing proteins (especially hnRNPs), tRNA synthetases (glycyl and tyrosyl), a few metabolic enzymes (phosphoglycerate dehydrogenase and phosphoserine aminotransferase) and proteins involved in ubiquitination and protein turnover. Among the list of down-regulated proteins were kinases, helicases, ribosomal proteins, DNA damage/repair proteins, MCM proteins and a few metabolic enzymes.

Among the significant changes in protein expression across the 9 experiments (3 inhibitors x 3 biological replicates), 17.4% of the protein expression changes were common to all three inhibitors, 23.6% changes were common to at least 2 inhibitors and 44% changes were unique to each inhibitor (Fig 2.10). A summary of protein expression changes common to all three inhibitors (Supplemental Table-2.2), at least two inhibitors and (Supplemental Table-2.3) to one inhibitor (Supplemental Table-2.4) is provided.
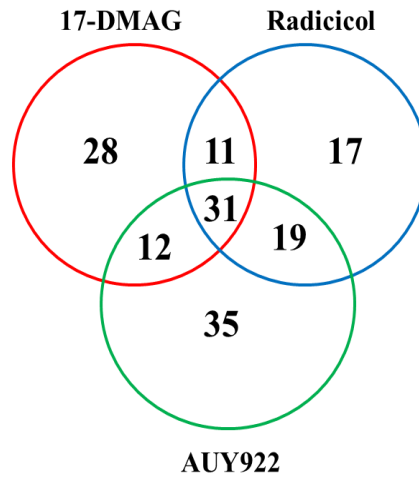
Figure 2.10: Venn diagram representing protein alterations common and unique to AUY922, 17-DMAG and radicicol.

Proteins expression changes observed with all three inhibitors, or with just two inhibitors, showed consistency in expression patterns. Among the list of proteins, proteins down-regulated by one inhibitor were down-regulated by the other two inhibitors and proteins up-regulated by one inhibitor were up-regulated by the other two inhibitors. Similarly proteins changes common to any two inhibitors followed the same trend (with just three exceptions - RPL13A, RAN and HNRPDL).

From the inhibitor-induced changes identified from LS-MS/MS experiments, seven proteins were chosen for confirmation by Western blotting. All of the seven selected proteins were depleted by the inhibitors in a dose-dependent manner (Fig 2.11).
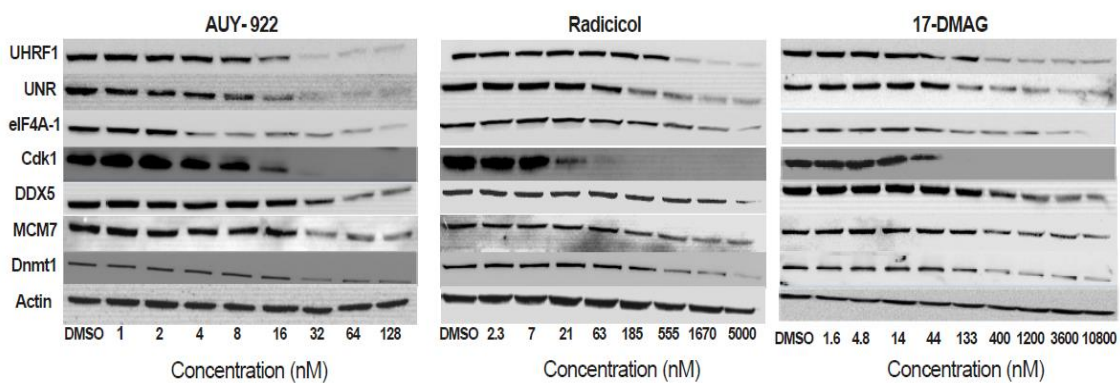
Figure 2.11: Western blotting to confirm inhibitor induced changes in protein

expression identified from LC-MS/MS experiments.

Jurkat cultures were treated for 24 hours with various concentrations of indicated inhibitors.

Changes in each protein's expression were analyzed by Western blotting. Actin served as a lane-

loading control.

Discussion

In this study, the effects of the new Hsp90 inhibitor AUY922 on Jurkat proteome were determined using a label-free LC-MS/MS approach. The effects were also compared to those caused by flagship Hsp90 inhibitors 17-DMAG and radicicol. For this comparison, equi-potent doses of the each inhibitor were used. Appropriate doses of all three inhibitors were identified based on their IC_{50} doses for depletion of a known Hsp90 client protein Cdk6 (Fig 2.3a, 2.6a & 2.7a). The IC_{50} doses for Cdk6 depletion for AUY922, 17-DMAG and radicicol were 12 nM, 27 nM and 60 nM respectively. Of the three drugs, AUY922 was the most potent.

For proteomics assays, 5x to 7x the IC_{50} concentrations of each inhibitor were used. It was also confirmed that these 5-7X doses were largely sub-apoptotic, based on their effects on cell viability (Fig 2.9) and PARP cleavage (Fig 2.4, 2.8a &2.8b). Decision to work with these doses (75 nM AUY922, 150 nM 17-DMAG and 300 nM radicicol) sets this work apart from two recently published SILAC-based Hsp90 inhibition studies [56, 57] , wherein high micro-molar doses of Hsp90 inhibitors (50 μM 17-DMAG and 10 μM GA respectively) were used. These high doses of Hsp90 inhibitors cause death of 50% of the cells. Therefore, many of the responses that Sharma et al., and Wu et al., observed could be due to the cellular response to apoptosis.

All of the three inhibitors generated conserved proteomics fingerprints (Fig 2.10). This indicates a conserved mechanism of action, namely Hsp90 inhibition. The most robust, conserved responses seen in the proteome were a set of 31 protein expression changes that included induction of chaperones Hsp90 alpha, Hsp70, Hsp105, Serpin H1, Spectrin, DnaJ and the T-complex proteins, and depletion of Hsp90 clients such as EEF2, Dnmt1, DDX5, CAD protein, and the kinases Cdk1, Cdk6. Moreover, these conserved changes showed consistency in expression pattern: proteins up-regulated by one inhibitor were found to be up-regulated by the other two inhibitors. Similarly, proteins down-regulated by one inhibitor were found to be down-regulated by the other two inhibitors. This identification of conservation of proteomics

fingerprints across three distinct Hsp90 inhibitors strongly validates our mass spectrometry assays of Hsp90 inhibition.

The proteome-wide changes induced by AUY922, 17-DMAG, and radicicol were consistent with the two known hallmarks of Hsp90 inhibition. Traditional Western blotting techniques have demonstrated : (i) the induction of a small number of chaperones, especially Hsp70 and (ii) the depletion of proteins known to be Hsp90-dependent [41] . In this study, all three inhibitors induce a wide variety of chaperones, suggesting the activation of Hsf1 [102]. Additionally, all three inhibitors deplete several known Hsp90-client proteins. Demonstrating that all three inhibitors display traditional hallmarks of Hsp90 inhibition using mass spectrometry assays supports the validity of our mass spectrometry assays.

Other observations validate the results from this work. Seven of the protein expression changes that were identified by mass spectrometry assays were confirmed using western blotting, (Fig 2.11). Not only these inhibitor-induced changes were confirmed, but they were also shown to be dose-dependent (Fig 2.11). Additionally, most of the proteins identified as inhibitor-responsive in this study have been previously reported to be interact physically or functionally with Hsp90 [15] . Many of the inhibitor responses that were observed in leukemia cells have also been observed in other cancer cell lines treated with Hsp90 inhibitors [56, 57] . All these arguments support the validity of the results obtained from mass spectrometry assays.

While the above findings indicate the power of mass spectrometry to study Hsp90 inhibitor-induced changes in protein expression, the technique had certain limitations. Apart from the conserved changes in protein expression mentioned above, some changes in protein expression were statistically significant in cells treated with two inhibitor treatments, but not in cells treated with the third inhibitor (Fig 2.10). For instance, the expression changes for 12 proteins were statistically significant in cells treated with AUY922 and 17-DMAG, but not in cells treated with

radicicol. Similarly, expression changes for 19 proteins were statistically significant in cells treated with AUY922 and radicicol, but not in cells treated with 17-DMAG (Fig 2.10). Moreover, there were 11 proteins whose expression changes were statistically significant in cells treated with 17-DMAG and radicicol, but not in cells treated with AUY922.

We offer for the protein expression changes observed in cells treated with two inhibitors, but not identified as statistically significant in cells treated with the third inhibitor: (i) The protein expression not identified as significant in only one out of the three assays might be a real change, but did not survive the statistical analysis (false negatives, or "type-II errors"), (ii) the protein expression changes identified in cells treated with two inhibitors might not be real changes, but appeared as significant none the less (false positives, or "type-I errors") or, (iii) the assays might be detecting true, inhibitor-specific changes. Our favorite explanation is that the third drug is also altering the expression of these outlier proteins, but they are not being identified as statistically significant, due to the weakness of the spectrum counting assays. Thus, we believe that these changes fail to survive statistical tests and are thus misinterpreted as false negatives in cells treated with the third inhibitor.

Similarly, some changes in protein expression appeared unique to cells treated with one of the inhibitors, but not for cells treated with the other two inhibitors. Specifically, 35 protein expression changes were unique to cells treated with AUY922, 28 protein expression changes were unique to cells treated with 17-DMAG and 17 protein expression changes were unique to cells treated with radicicol. We offer similar possible explanations for these apparent inhibitor-specific effects: (i) The inhibitor-specific protein expression changes might not be real (false positives) or, (ii) the expression of these proteins might have been significantly altered in cells treated with the other two inhibitors, but did not survive the statistical tests (false negatives). Again, these assays might be detecting real changes, specific to a single Hsp90 inhibitor. These changes could be a combination of type I and type II errors.

Deeper bio-informatics analysis of this data was not performed. It was not well justified to do deeper bioinformatics and make big conclusions about the processes altered by these Hsp90 inhibitors based on the few conserved changes that were identified in this study.

These data raise several other interesting questions. Are there really only 31 conserved protein responses to Hsp90 inhibitors? Does this shortlist of 31 proteins adequately represent the proteomics fingerprint of Hsp90 inhibition? Do any of the inhibitors have true drug specific effects?

Given the nature of the spectrum counting technique, a stronger quantitative proteomics technique is required to address the questions raised above. In Chapter IV, these questions will be addressed using stable isotope labeling with amino acids in cell culture (SILAC) -proteomics approach.

CHAPTER III

Evaluation of the raw SILAC data and choice of a statistical test for validating

drug-induced changes in protein expression

Introduction

Before performing a deeper analysis of SILAC data, there was a need to assess the quality of

the raw data generated from MaxQuant searches to identify potential defects in the data and to

assess reproducibility across the biological replicates. It was also important to choose appropriate

statistical tests to validate changes in protein expression caused by the Hsp90 inhibitors. Thus, in

this chapter, the quality of raw SILAC data from the proteomes of Jurkat cells treated with 75 nM

AUY922 (AUY922 dataset) were analyzed. Similarly, the quality of the raw SILAC data from the

proteomes of Jurkat cells treated with 150 nM 17-DMAG (17-DMAG dataset) were also

analyzed. The quality of raw SILAC data from this study were also compared to the quality of the

raw SILAC data from two recently published papers describing the proteome-wide effects of two

other Hsp90 inhibitors. Subsequently, these SILAC data were analyzed using various statistical

tests. Results from these comparisons will guide the choice of statistical tests that will be used to

analyze AUY922 and 17-DMAG SILAC data.

<center>**Materials and Methods**</center>

Materials

96-well TARGA C18 macrospin plates were purchased from Nest group (Catalog number SNS SS18R)

General cell culture and inhibitor treatments

To prepare SILAC "light" fractions, Jurkat cells were cultured in SILAC RPMI media containing 10% dialyzed FBS and supplemented with light isotopic lysine ($C_6H_{14}N_2O_2$) and arginine ($C_6H_{14}N_4O_2$) amino acids. For preparing "heavy" SILAC fractions, Jurkat cells were cultured in SILAC RPMI media supplemented with heavy isotopic lysine ($13C_6H_{14}\ 15N_2O_2$) and arginine ($13C_6H_{14}\ 15N_4O_2$) amino acids. Conditions for culturing cells were otherwise the same as described in Chapter II.   To assess the impacts of Hsp90 inhibitors on the Jurkat proteome, cells growing in SILAC light media were treated with DMSO, while cells growing in SILAC heavy media were treated either with 75 nM AUY922 or 150 nM 17-DMAG. After 24 hour incubation cells were harvested and lysed as described in Chapter II. Protein concentrations in the lysates were estimated by Bradford assays.

Sample preparation for mass spectrometry

Fifty micrograms of untreated (light) Jurkat lysate were mixed with fifty micrograms of inhibitors-treated (heavy) lysate. Samples were then precipitated with TCA/acetone using the protocol described in Chapter II. Protein pellets were resolubilized in 2x SDS sample buffer, and proteins were reduced by 10 mM DTT and alkylated with 50 mM IAA. Proteins were then fractionated on precast mini-gradient gels (4-20% Bio-Rad). Each lane was excised with a razor blade to produce ten fractions. Gel bands in each fraction were sliced into small pieces. Slices were then washed with 25 mM ammonium bicarbonate / 50% acetonitrile and dehydrated with

<center>54</center>

ACN. Gel slices were briefly air dried, then rehydrated with 25 mM ammonium bicarbonate containing 8 μg/ml trypsin. Digestion was performed overnight at 37° C. Peptides in each fraction were then extracted with 60 μl of 0.5% TFA. Salts in the peptide samples were cleaned using Nest group's TARGA C18 96 well plates. Peptides were vacuum dried and analyzed by LC-MS/MS.

LC-MS/MS analysis

LC-MS/MS analysis was performed on a Thermo Fisher Scientific hybrid LTQ-Orbitrap XL mass spectrometer. A New Objective PV-550 nanoelectrospray ion source was used for electrospray ionization. An Eksigent 1-D UPLC system was used to separate the peptides. Peptides were first trapped on a trapping column in a vented column configuration (5 cm of 3 μm Magic C18 AQ). Trapped peptides were then separated on a 75 μm ID 40-cm fused silica column (3-μm Magic C18 AQ), terminated with an integral fused silica emitter. Peptides were eluted by using a 0-37% ACN/0.1% formic acid gradient over 220 min at a flow rate of 250 nL/min.

Eluted peptides were analyzed using a data dependent scanning mode, automatically selecting specific ions for MS/MS analysis. The full scan MS spectra for ions 360-1400 m/z were acquired in the Orbitrap sector, providing a nominal resolution of 60,000 FWHM. Lock-mass was enabled for internal calibration on the polysiloxane $[C_{12}H_{37}0_6]^{+1}$ ion (m/z 445.1200). For MS/MS, the six most abundant peptides were selected for further fragmentation in the ion trap by the CID (collision induced dissociation). For MS/MS analysis, only ions with intensities greater than 8,000 were chosen. To optimize the instrument duty cycle, only mono-isotopic precursors were selected for MS/MS. Parent ions with unassigned charges were not chosen for further MS/MS analysis (because their m/z values cannot be determined). Ions previously identified as contaminants, and ions already selected for MS/MS analysis (using dynamic exclusion at 150% of the observed chromatographic peak width), were also excluded from further MS/MS analysis.
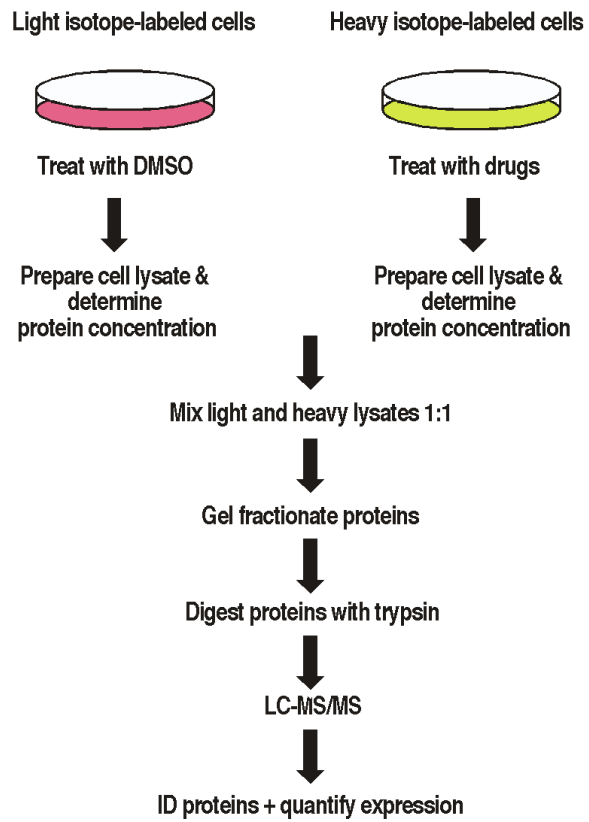
Figure 3.1: Summary of experimental design (SILAC)

Data analysis

Raw LC-MS/MS data were processed using MaxQuant (Version 1.3.0.5). The Andromeda search engine was used for database searches. Database searches were done against Uniprot_human database (Released on 2013_03) containing 87,656 sequences. Additionally database searches included known contaminants as well as reverse protein sequences. Searches also included hypothetical peptides with variable modifications oxidation (M), acetyl (protein N-term), carbamidomethyl (C), Gln to pyro-Glu and Glu to pyro-Glu. Trypsin was specified as the digestion enzyme allowing up to two missed cleavages. Minimum peptide length for identification was set to 7 amino acids. Search thresholds utilized a peptide and protein false discovery rate (FDR) of 0.01. Fragment ion mass tolerance was set to 0.5 Da. MaxQuant determines the parent ion mass tolerance on the basis of mass accuracy achieved and hence was not specified.

Data normalization

Data in each biological replicate were normalized using a global normalization approach. Treated (Heavy, H) and untreated samples (Light, L) are hereafter referred to as separate channels. Normalization for each channel was done separately. The normalization factor for each protein in each channel of each biological replicate was calculated by dividing the raw intensity of that protein in that channel of that bio-rep by average raw intensity of that protein across all of the bio-reps.

 (**Normalization factor for a protein (X) in L or H channel** = Raw intensity of X in L or H channel in a bio-rep / average intensity of X in L or H channels in all 5 bio-reps).

Using the normalization factors for all in each L/H channel of a bioreps, an average normalization factor for whole L/H channel in that bio-rep was obtained by averaging the normalization factors of all the proteins in that bio-rep.

(**Normalization factor for each bio-rep** = Median of normalization factors of all proteins in that bio-rep).

This generated an average normalized factor for each H/L biorep. Subsequently the intensities of each protein in that bio-rep were normalized by dividing their raw intensities by the channel-specific normalization factor.

Statistical analysis

The distribution of the heavy and light populations was identified using the Shapiro-Wilk test using the code in the R-program. Variances across the light and heavy populations were determined using the F-distribution function in Microsoft Excel. Student's T-tests were performed using functions in Microsoft Excel. One sample T-tests were performed using software package Perseus. Benjamini-Hochberg (B-H) FDR correction [103] of the one sample T-test p-values were performed using the code in R . Storey FDR [104] correction of the one sample T-test p-values were performed using the code in the R-program.

Results

Evaluation of raw SILAC data from Jurkat cells treated with Hsp90 inhibitor AUY922

Reproducibility across five biological replicates

In order to assess the reproducibility of our SILAC data, we compared data from all of our five biological replicates of Jurkat cells treated with AUY922 (AUY922 is an Hsp90 inhibitor). For each of the proteins quantified, ratios of protein expression in treated cells (H) vs. control cells (L) (Heavy/Light ratios) from one biological replicate were log2 transformed, and plotted against the protein expression changes observed for each of the other 4 biological replicates (Fig 3.2). Each of the individual scatterplots can be divided into four quadrants through its $\log_2$ equals zero values (no change in expression) on both the X and Y axes. Proteins (dots) represented in the lower left-hand quadrant indicate proteins down-regulated in both the biological replicates. Proteins (dots) represented in the upper right hand quadrant indicate proteins up-regulated in both the biological replicates. Proteins (dots) represented in the other two quadrants indicate proteins up-regulated in one biological replicate, but down-regulated in the other biological replicate. The majority of the proteins were distributed in the lower left quadrant and the upper right quadrant in all the scatterplots, and there were very few proteins in the lower right hand quadrant and in the upper left hand quadrant. This indicated that down-regulation and up-regulation were consistent across the biological replicates. That is, there were relatively few proteins that appeared to be up-
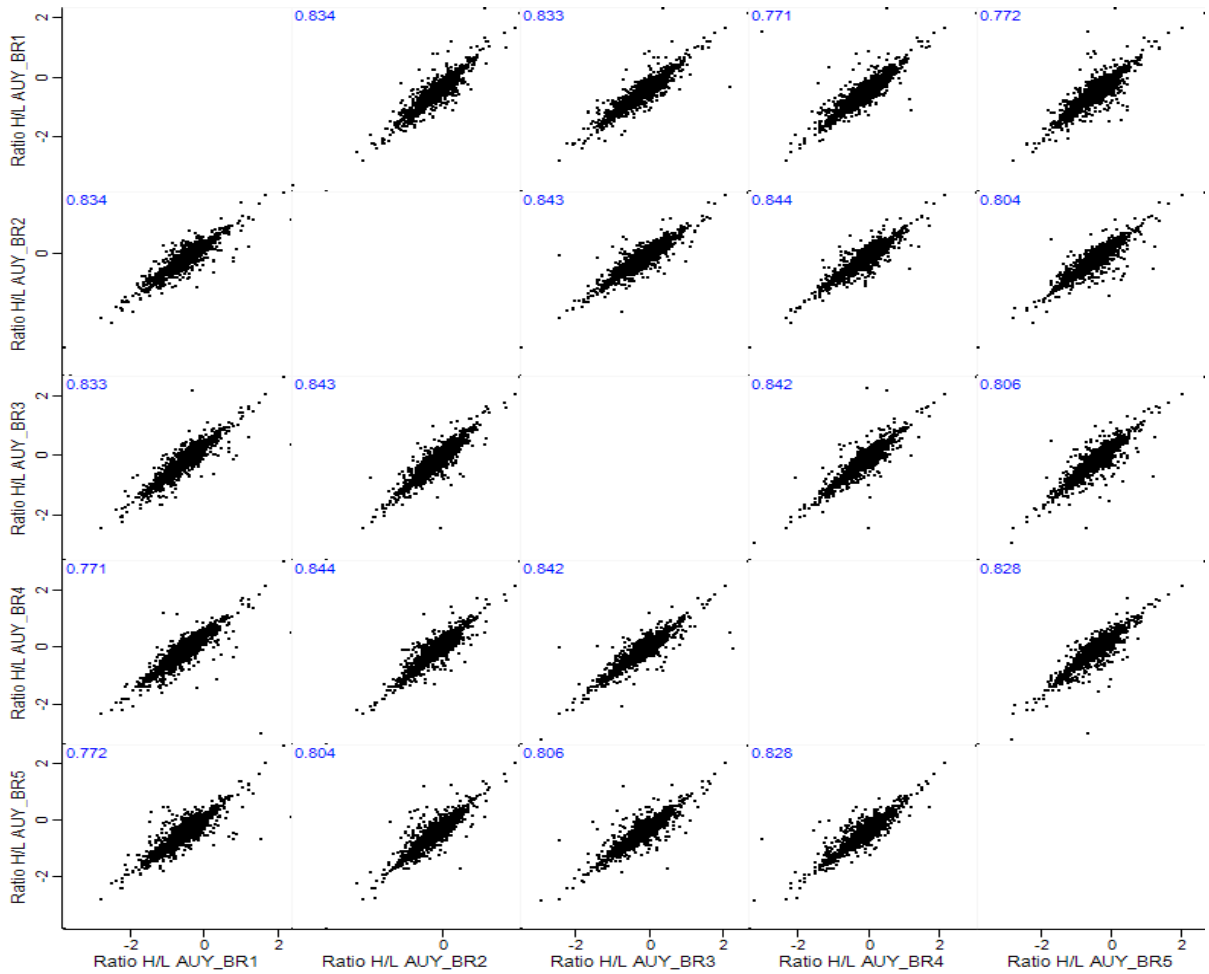
Figure 3.2: Reproducibility across biological replicates in AUY922.

Each dot represents protein expression changes (Log$_2$ ratio H/L) from one biological replicate analyzed against protein expression changes from each of the other 4 biological replicates. The X-axis and the Y-axis represent fold changes in protein expression. AUY denotes cells treated with AUY922, and BR denotes the individual biological replicate.

regulated in one bio-rep but down-regulated in the other bio-reps. The degree of agreement between biological replicates is indicated by coefficient of variance (R^2, calculated using a linear fit), which is presented on the top left corner of each scatterplot. The R^2 values for the comparisons across different biological replicates ranged from 0.771 to 0.844. The strength of the R^2 values across different comparisons indicated good experimental reproducibility. Based on the distributions of proteins on the scatterplots, and the generally strong R^2 values, we concluded that our assays were highly reproducible across the five biological replicates.

In order to further assess the quality of our data, we similarly analyzed the raw data (Fig 3.3) from Sharma et al. [56] characterizing the proteomes of HeLa cells treated with 50 μM geldanamycin. Their R^2 values ranged from 0.54 to 0.701. Additionally, their data showed more outliers (points that deviate from best fit line) than those observed in our data (c.f. Fig 3.2 vs. Fig 3.3). Based on the comparison of their R^2 values to our R^2 values, our reproducibility across our five biological replicates was as good/better compared to data from Sharma et al. However, it should be noted that the number of proteins they assayed (7,056 proteins) was much higher compared to our assays (3,146 proteins). This would make their outliers more visible, when visually compared to our data (c.f. Fig 3.2 vs. Fig 3.3).

Data normalization

For SILAC analysis, heavy-labeled and light-labeled samples should be mixed ideally in an equal mass to mass ratio. Here, it will referred to as channel-level normalization. Similarly, artifactual differences in the intensities of heavy and light ions caused by errors in sample-level mixing will be referred to as imperfect channel-level normalization.

There are two possible sources for imperfect channel-level normalization. The first source could be imperfect protein quantification of the individual light and heavy lysates (e.g., imperfect
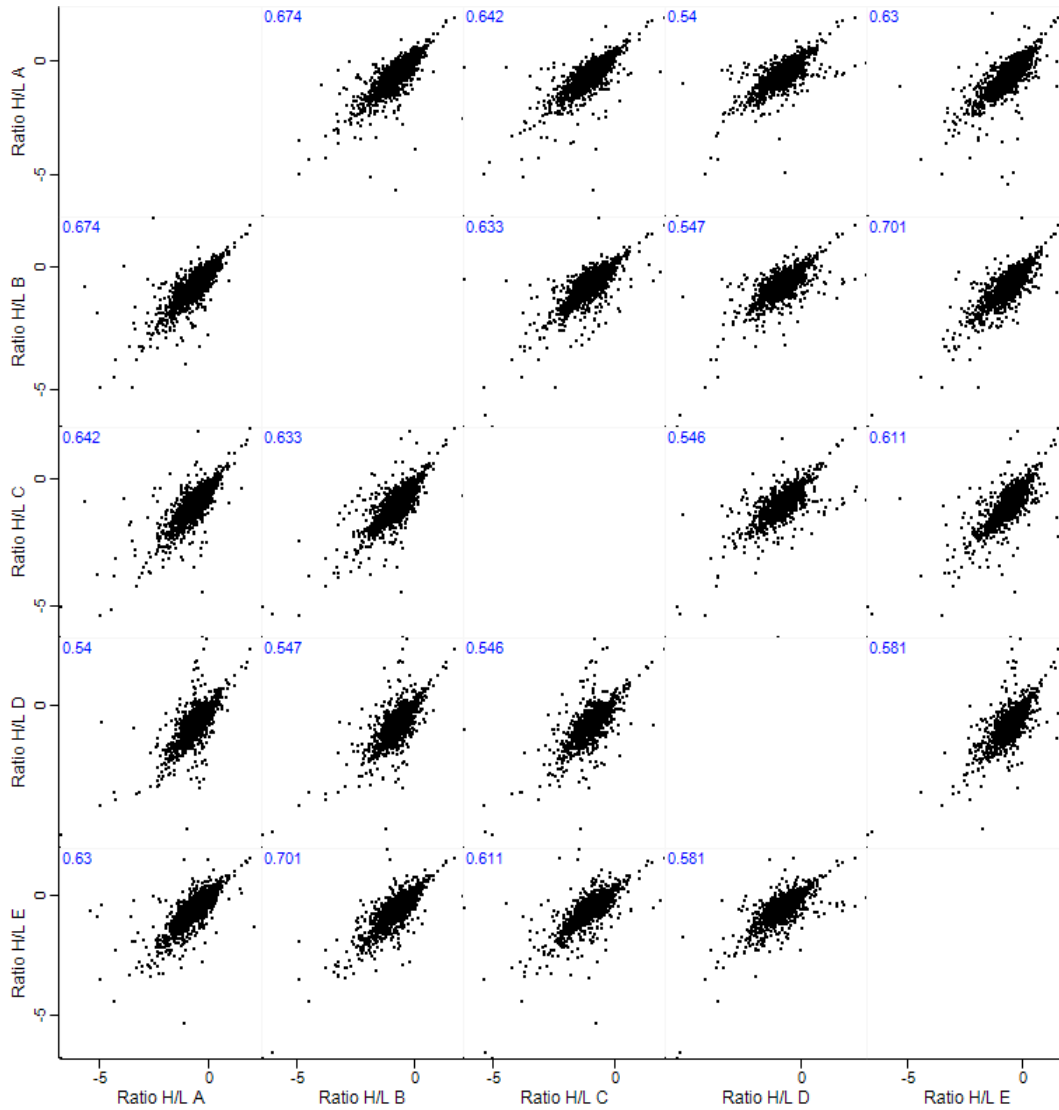
Figure 3.3: Reproducibility across biological replicates in data from Sharma et al. [56].

Reproducibility of data from Sharma et al. [56], was assessed by comparing protein expression changes as described for Figure 3.1.

Bradford assays). A second source could be imperfect pipetting of the light and heavy lysates during mixing.

A different source of artifactual variability in SILAC data is potential changes in ionization efficiency as the spray tip ages, and/or aging of the instrument's electron multipliers. This is relevant, because our SILAC datasets were run 24 hrs. / day, 7 days / week, for 60 days. Thus, either or both of these sources can distort the comparison of raw peptide ion intensities across different biological replicates.

Therefore it is important to assess potential normalization defects prior to statistical analysis of the data. To do this, we $\log_2$ transformed each "protein raw intensity" (values calculated by MaxQuant, representing individual protein abundances) in each channel (H or L) across the five biological replicates, and plotted the distributions of these values as histograms. We also transformed the raw H/L ratios, and similarly plotted their distributions. To compare the reproducibility among the five biological replicates, we overlaid histograms of all 5 bioreps (Fig 3.4).

For the raw intensities, this overlay did not reveal major issues. However, a similar analysis of ratios showed that there were normalization problems between biological replicates. H/L ratios from biological replicates 2, 3 and 4 were very similar (Fig 3.4). In contrast, biological replicates 1 and 5 showed lower H/L ratios (Fig 3.4). Based on these observations, we concluded that there were channel-level normalization defects across the five biological replicates, and we concluded that our data needed to be normalized.

A.

B.

C.
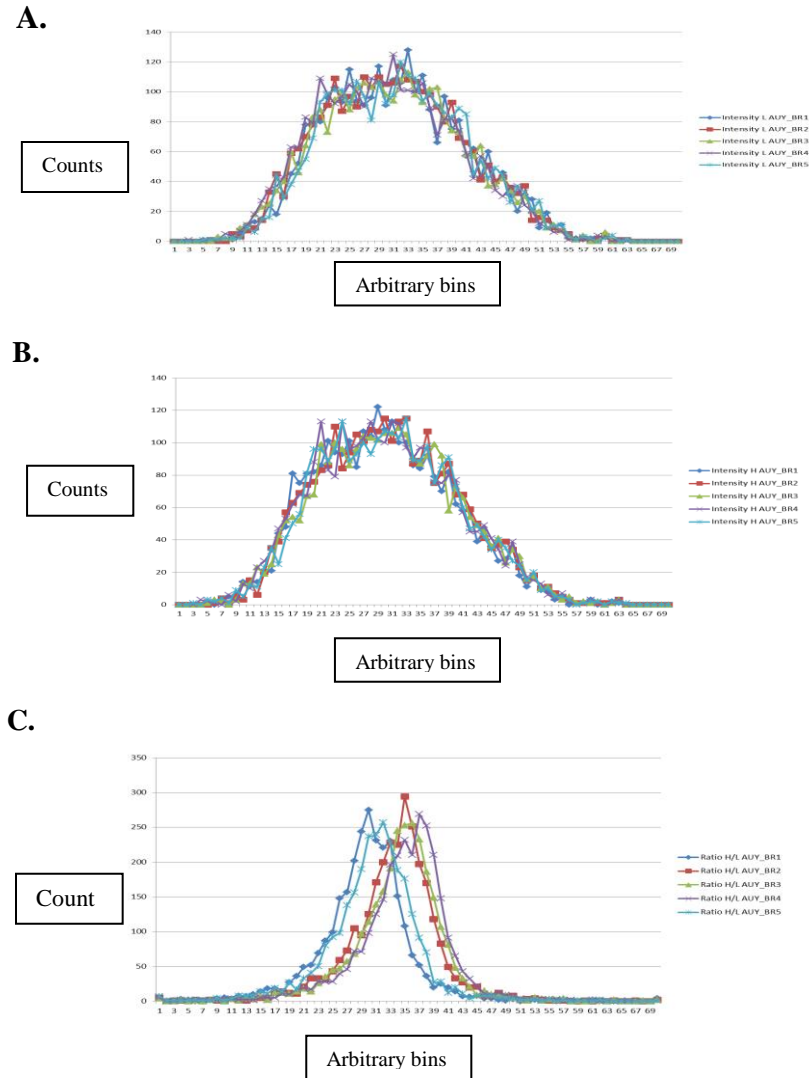
Figure 3.4: Assessment of the quality of raw intensities and raw ratios in AUY922 data.

The frequencies of raw light and heavy protein intensities (Panels A & B, respectively), and raw

H/L ratios (Panel C) from the 5 bio-reps were plotted as distributions (histograms). The X-axis

represents arbitrary binning of proteins based on intensity. The Y-axis represents the respective

bins. Resulting distributions from the 5 bio-reps were overlaid to assess reproducibility.

We extended our examination of the quality of the raw data by plotting each protein's raw H/L ratio versus its raw protein intensity (Fig 3.5). In biological replicates 2, 3 and 4, the majority of the proteins on the graph were nearly centered on $\log_2 0$ on the X-axis (Fig 3.5, panels B, C, D), indicating good normalization of the treated and control samples. In contrast, in biological replicates 1 and 5 the majority of the proteins showed a larger offset from the $\log_2 0$ on the X-axis (Fig 3.5, panels A & F). These observations reinforced our conclusion that the biological replicates 2, 3 and 4 were well normalized at the channel level, but that the biological replicates 1 and 5 were imperfectly normalized.

Because there were normalization defects across the five biological replicates, we performed a global normalization of the protein intensities in the control and treated samples. To accomplish this, we normalized each protein's raw intensity using the normalization approach described in the Materials and Methods section for this chapter. After normalization, the reproducibility across the five biological replicates was enhanced, as evident by a more uniform distribution of H/L ratios among bioreps (Fig 3.6C). Thus, our normalization strategy successfully minimized variability across the five biological replicates (c.f. Fig 3.6C vs. Fig 3.4C).

Biological replicate 1   Biological replicate 2   Biological replicate 3

Biological replicate 4   Biological replicate 5
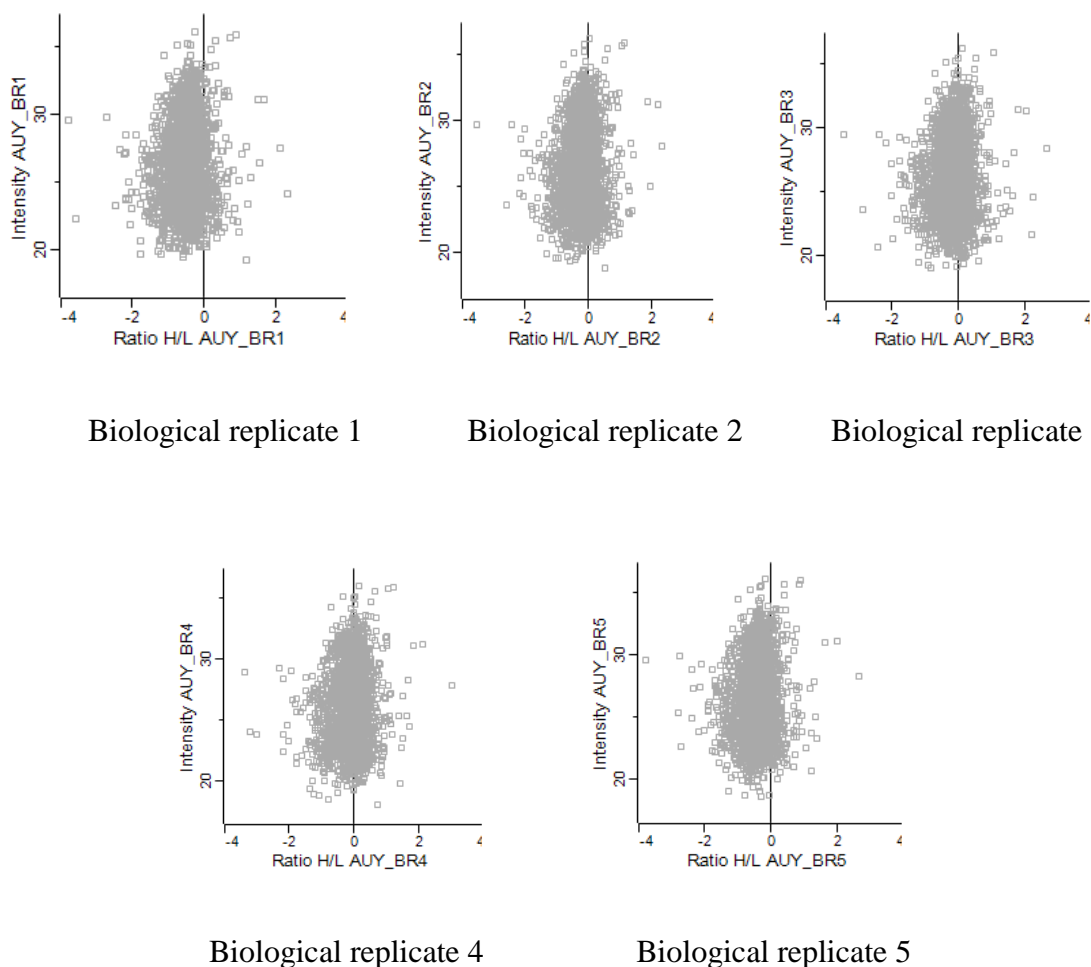
Figure 3.5: AUY922 raw data before normalization –Ratio versus intensity plots

Protein expression changes (log$_2$ ratio H/L) from each biological replicate were plotted against the protein abundance to assess normalization defects. The X-axis represents the protein expression and is expressed in log2 scale. The Y-axis represents the protein abundance. Each spot on the scatterplot represents an individual protein.

A.

B.

C.
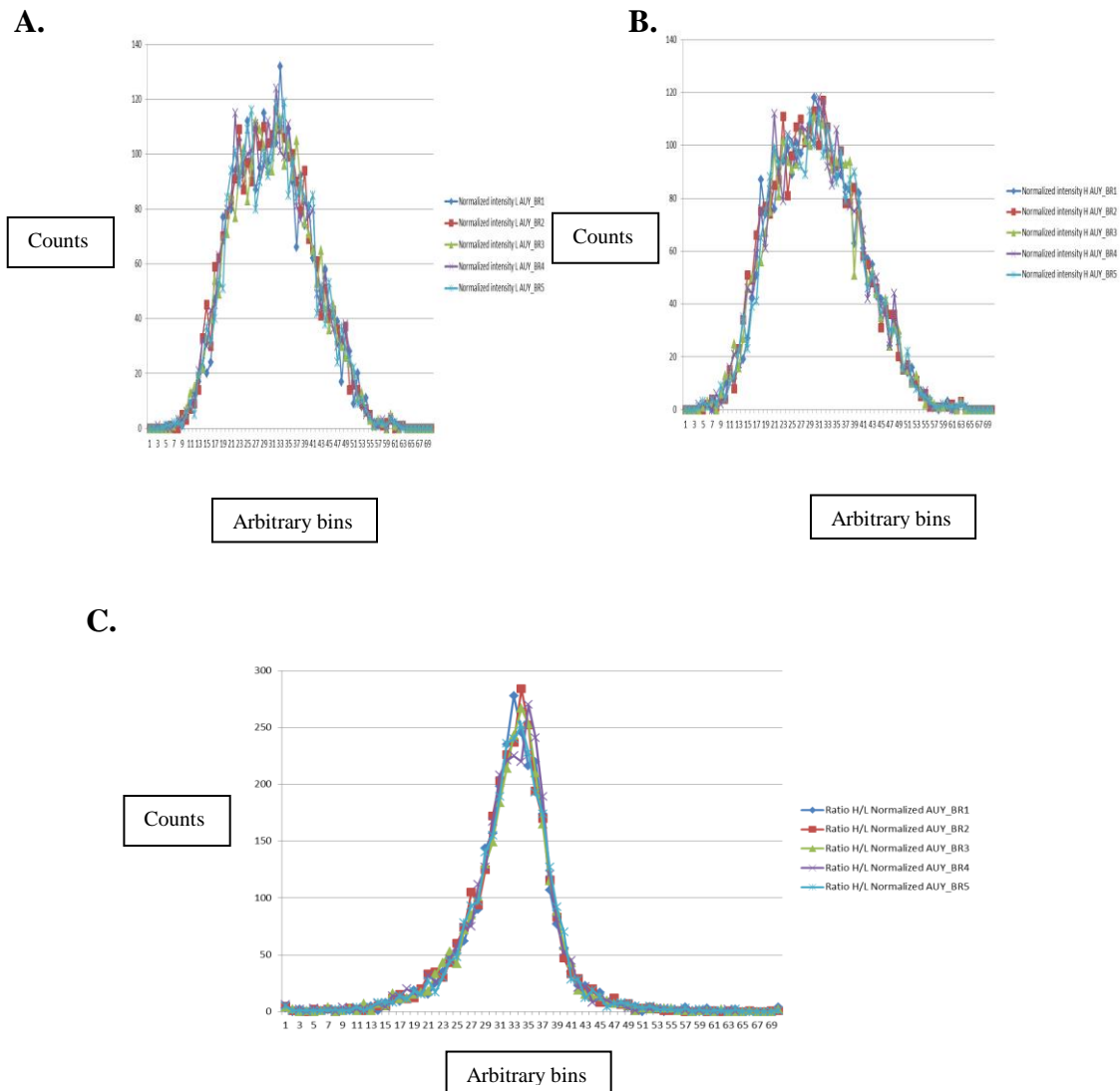
Figure 3.6: Global normalization minimized reproducibility issues across the five biological replicates in AUY922.

Normalized light and heavy intensities (Panels A & B), or normalized ratios (Panel C), from the five biological replicates were plotted as described for Figure 3.4.

We extended our analysis by visualizing the effects of normalization using ratio versus intensity plots. The log-transformed normalized H/L ratios vs. intensities from all the five biological replicates were reproducibly oriented with regards on the $\log_2$ of the X-axis (Fig 3.7). This visualization confirmed that our normalization strategy minimized variability across the five biological replicates (c.f. Fig 3.7 vs. Fig 3.5).

Does normalization affect the data quality?

To assess if our normalization strategy compromised the H/L ratios, we compared distributions of H/L ratios before and after normalization. To do this, we averaged the raw H/L ratios and normalized H/L ratios from 5 biological replicates and plotted these distributions as a histogram. Mean histogram of H/L population distribution before normalization and after normalization were nearly identical (c.f. 3.8A vs. 3.8B). This indicated that the normalization did not grossly distort the protein expression ratios. In contrast, comparison of the individual raw vs. normalized histograms showed the correction of channel level mis-normalization (Fig 3.9).

Biological replicate 1   Biological replicate 2   Biological replicate 3

Biological replicate 4   Biological replicate 5
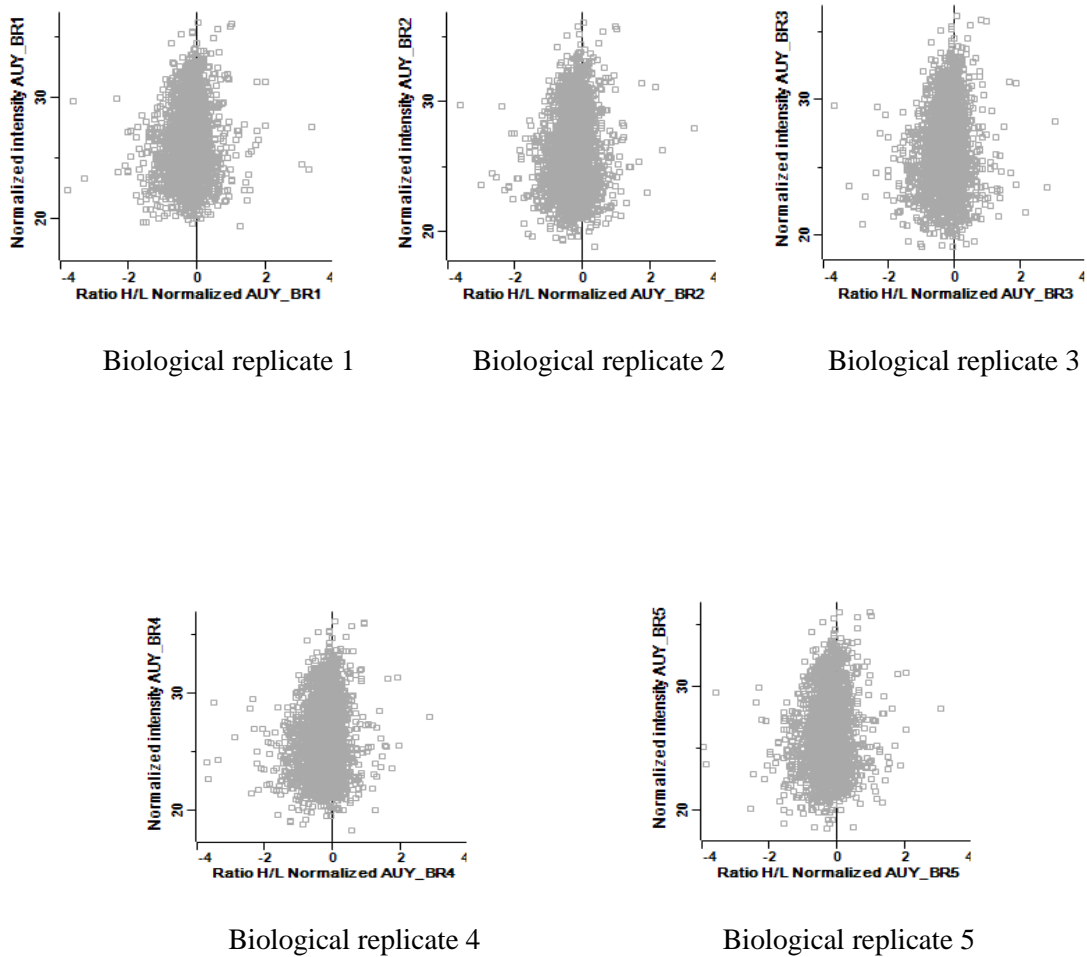
Figure 3.7: AUY922 raw data after normalization –Ratio versus intensity plots.

Protein expression changes (log_2 ratio H/L) from each biological replicate were plotted as described in Figure 3.5.

A.　　　　　　　　　　　　　　　　**B.**
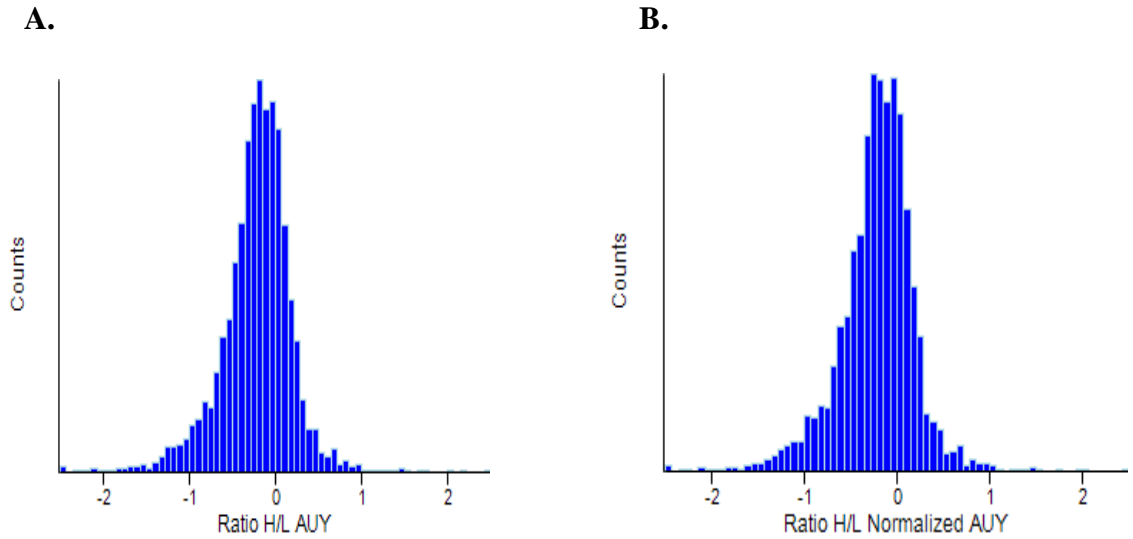
Figure 3.8: Histograms of average protein expression of all five biological replicates in AUY922 before and after normalization.

Log 2 of the ratios of H/L intensities from all the five biological replicates were averaged and plotted as histograms before (Panel A) and after normalization (Panel B). The X-axis represents binning of proteins based on abundance. The Y-axis represents the number of proteins in each bin.
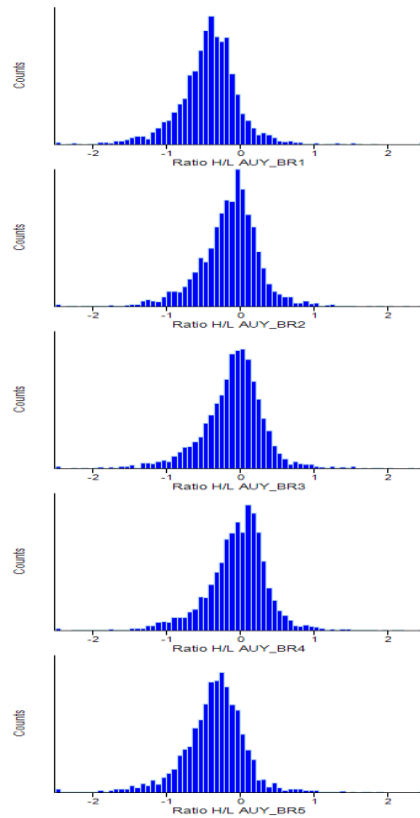
A.   **B.**
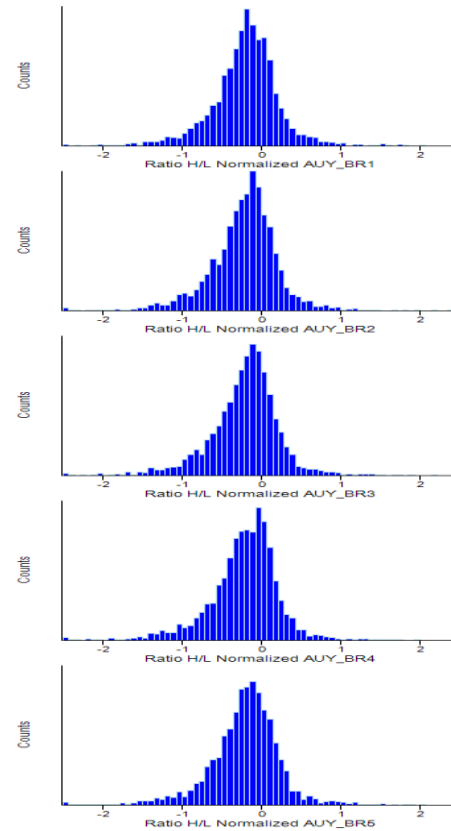
Figure 3.9: Histograms of protein expression from individual biological replicates in AUY922 before and after normalization.

Protein intensities from control and treated samples of AUY922 dataset were normalized using global normalization approach as described in the text. Protein expression across the five biological replicates were plotted before (Panel A) and after normalization (Panel B) as described in Figure 3.8.

Results from Western blotting assays in our spectrum counting work consistently showed that actin expression was unaltered even after treating cells with a high dose of Hsp90 inhibitors (Fig 2.11, Chapter II). Therefore, we assessed the expression (H/L ratios) of actin and other house-keeping genes before and after normalization (Table 3.1). Results showed that average H/L ratios for house-keeping genes before and after normalization were almost identical indicating that our normalization did not distort the data (consistent with Fig 3.8). Moreover, the average normalization factor values across the biological replicates were all nearly the same after normalization indicating that our normalization minimized variability across the biological replicates (consistent with Fig 3.6c).

Comparison of our data with two recently published SILAC based studies on Hsp90 inhibition.

Two recent publications utilized SILAC approaches to report the effects of Hsp90 inhibitors on cellular proteomes. The publication from Sharma et al. [56] reported proteome-wide changes in HeLa cells treated with 50 μM 17-DMAG [56]. The publication from Wu et al [57] , reported the effects of 5 μM to 10 μM geldanamycin on the proteomes of MDAMB231, K562, Colon205 and Cal27 cell lines [57].

We compared our data to the raw SILAC data from these two studies. To accomplish this, we plotted histograms representing the raw protein expression ratios from the 5 biological replicates of HeLa cells treated with 17-DMAG [56] and from the 3 biological replicates of MDAMB231 and Colon205 cells treated with geldanamycin [57]. The data from Sharma et al. showed protein expression ratios centered below the zero ordinate of log2 on the X-axis, with minor

Table 3.1: H/L ratios of house-keeping proteins across five biological replicates in

AUY922 before and after normalization

The H/L ratios of house-keeping genes from all five bioreps were calculated and tabulated before and after global normalization. Additionally, the average ratios before and after normalization, and the average normalizer ratios were also tabulated.

Protein names	Ratio H/L BR1		Ratio H/L BR2		Ratio H/L BR3		Ratio H/L BR4		Ratio H/L BR5		Average of 5 BRs	
	Before	After	Before	After	Before	After	Before	After	Before	After	Before	After
Actin, alpha	0.89	1.04	1.04	0.99	1.13	1.03	1.16	1.03	0.95	1.05	1.03	1.03
Actin, cytoplasmic 2	0.89	1.04	1.07	1.00	1.13	1.05	1.17	1.04	0.96	1.06	1.04	1.04
Tubulin alpha-1A chain	0.87	1.02	1.04	1.00	1.03	0.95	1.19	1.06	0.91	1.00	1.01	1.01
Tubulin alpha-1C chain	0.80	0.93	0.94	0.89	0.99	0.91	1.05	0.94	0.90	1.00	0.94	0.93
Tubulin beta chain	0.77	0.90	0.95	0.90	1.02	0.94	1.04	0.92	0.81	0.90	0.92	0.91
Tubulin beta-4A chain	0.86	1.00	0.92	0.87	0.95	0.88	0.92	0.82	0.80	0.88	0.89	0.89
Tubulin beta-4B chain	0.78	0.91	0.98	0.93	1.01	0.93	1.06	0.94	0.85	0.94	0.94	0.93
Tubulin beta-8 chain	0.76	0.89	0.93	0.88	0.98	0.90	1.02	0.91	0.82	0.91	0.90	0.90
Average normalized ratio	0.83	0.97	0.98	0.93	1.03	0.95	1.08	0.96	0.88	0.97		

normalization defects apparent across their biological replicates. Their normalization defects were similar to those observed in our data (c.f. Fig 3.10 vs. Fig 3.9). Based on these observations, we concluded that their normalization defects were comparable to those that we experienced. We also concluded that the majority of their proteome was down-regulated upon Hsp90 inhibition, similar to the down-regulation apparent in our data.

In contrast, raw data of Wu et al. representing the proteomes of MDAMB231 cells treated with 5 µM geldanamycin appeared perfectly reproducible across the three biological replicates (Fig 3.10, Panel B). Their raw H/L ratios were greater than 0, but not less than 0 implying up-regulation of majority of the proteome (Fig 3.10, Panel B). Despite raw ratios from cells treated with MDAMB231 implying up-regulation, after variance stabilization normalization (VSN), Wu et al. concluded that there were more down-regulated proteins (247 proteins) than the up-regulated proteins (232 proteins). By analyzing MDAMB231 dataset from Wu et al. and noting a discrepancy from their conclusion that more proteins are down-regulated versus their actual raw data indicating up-regulation, we felt that the quality of their raw data was weaker than our raw data. Both our raw data and statistical analysis of the data, agreed with each other, by indicating down-regulation of the proteome.

However, their raw data from their Colon205 cells treated with 10 µM geldanamycin were very different across the biological replicates (Fig 3.10, Panel C). Moreover, in their Colon 205 raw data, one biorep implied up-regulation whereas the other two implied down-regulation (Fig 3.10, Panel C), whereas our raw data had consistent down-regulation across all five bioreps (Fig 3.9, Panel A). I note that their sample level normalization was done by mixing treated and untreated cells directly, rather than lysates. Moreover, at 10 µM dose of geldanamycin 50% of their cells were dead (Supplementary Figure S1 from Wu et al. [57]). This raises questions about their normalization at the cell level, rather than the protein level. Thus, based on these comparisons we concluded that our raw data was better than the data from Wu et al.

74

A. **B.** **C.**
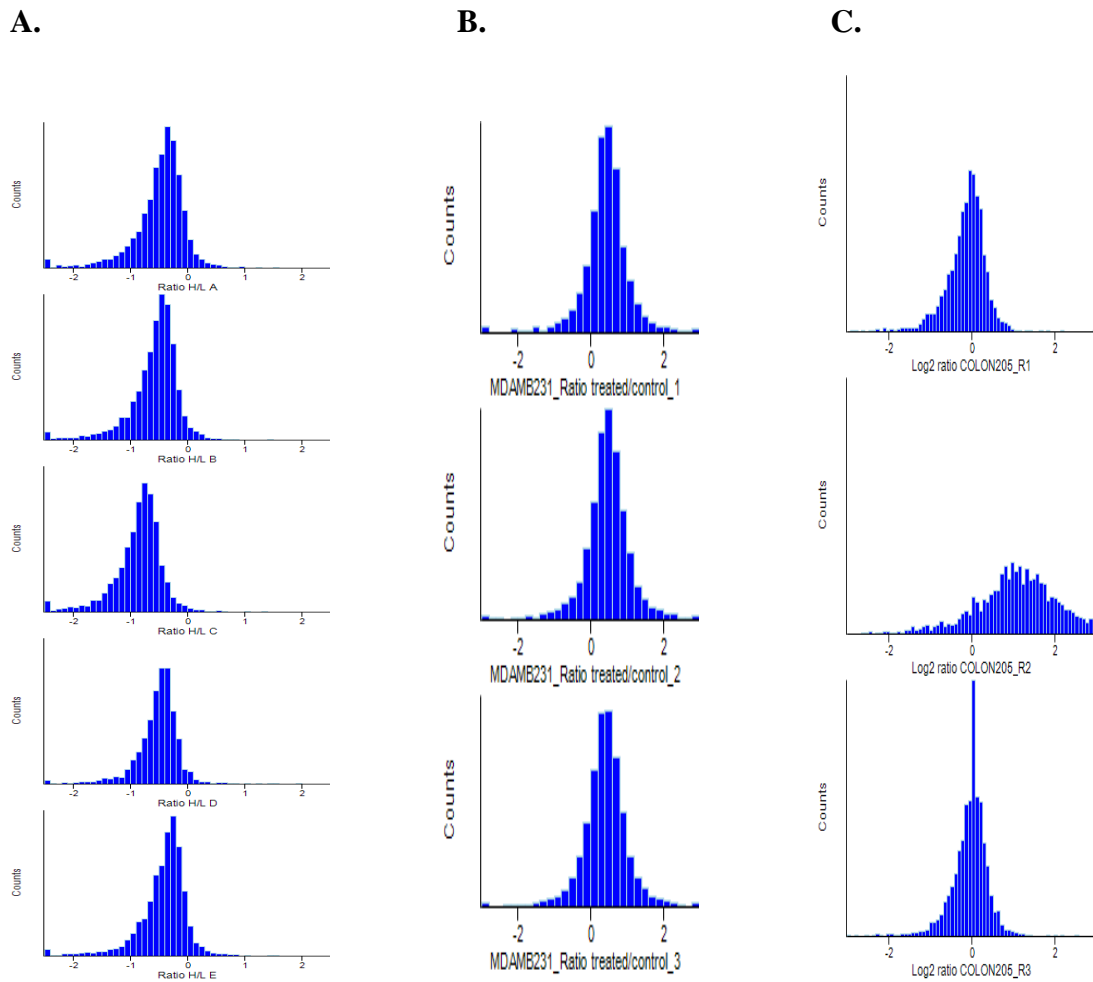
Figure 3.10: Assessment of the quality of raw data from Sharma et al. and Wu et al.

H/L protein expression ratios from references [56] (Panel 10A) & [57] (Panel 10B & 10C) were plotted as histograms as described in Figure 3.8.

Analysis of our raw data from cells treated with 150 nM 17-DMAG

In preceding sections, we discussed the analysis of raw data from cells treated with AUY922, and compared that data to data from other studies. Here, we similarly analyze our SILAC dataset from cells treated with a second Hsp90 inhibitor namely, 17-DMAG (Fig 3.11, 3.12 and 3.13). Results showed a good degree of reproducibility across the five biological replicates (Fig 3.11), evident by R^2 values ranging from 0.791 – 0.835 and by the clustering of the data in upper right hand quadrant or lower left hand quadrant of scatterplots of protein intensities among experiments (Fig 3.11).

Additionally, our data from cells treated with 17-DMAG reinforced our conclusions that a large portion of the proteome was down-regulated in cells treated with Hsp90 inhibitors (Fig 3. 16). Minor normalization problems (Fig 3.12 & 3.13) prompted us to normalize the data using the same approach as described for proteomes isolated from cells treated with AUY922. As we described for AUY922 dataset, this normalization minimized the variation and enhanced reproducibility across the five biological replicates (Fig 3.14, 3.15 & 3.16), but without distorting mean expression ratios (Fig 3.17).
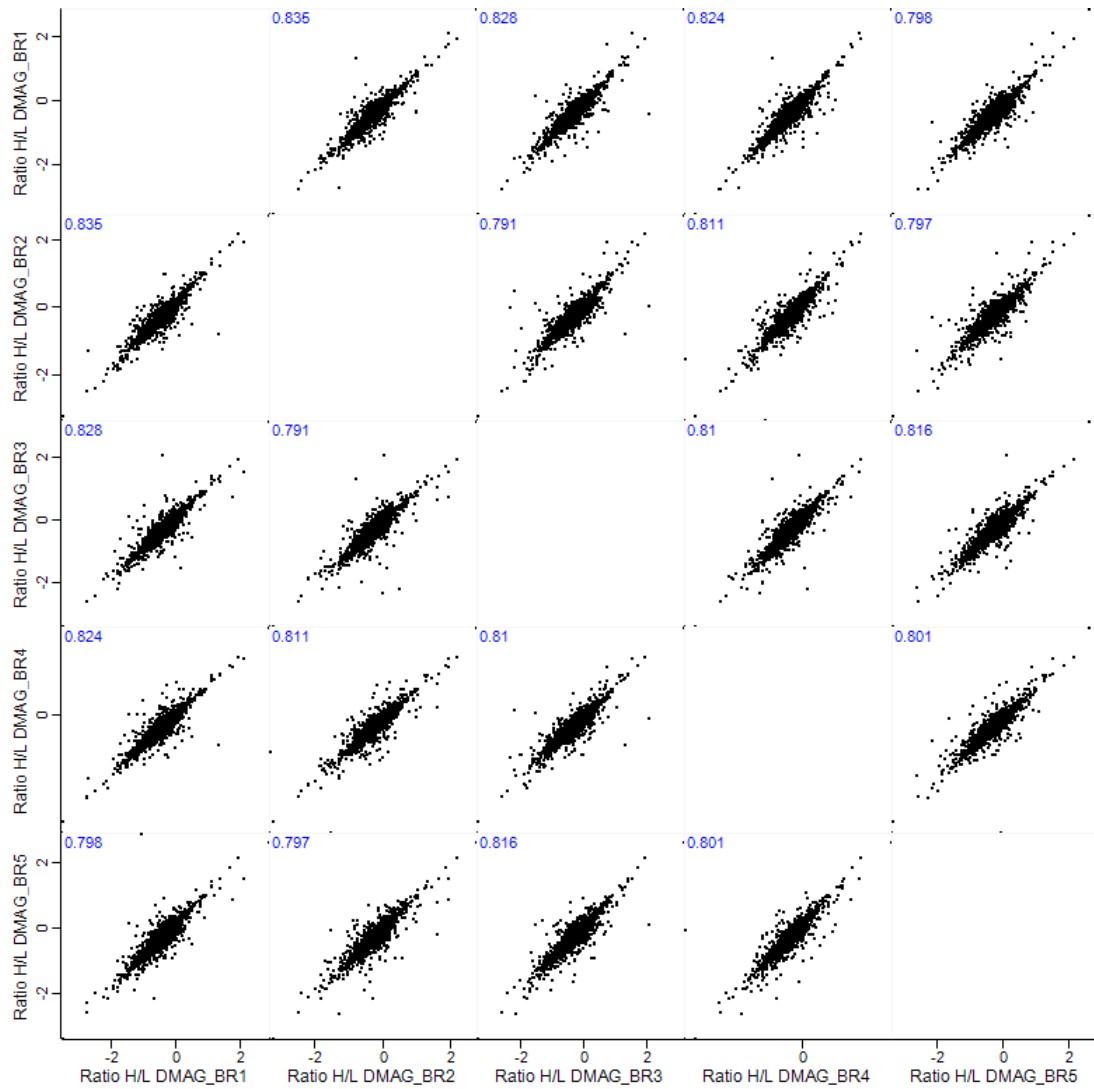
Figure 3.11: Reproducibility across biological replicates in cells treated with 17-DMAG.

Protein expression changes (Log$_2$ ratio H/L) were plotted across the five biological replicates as described in Figure 3.2.
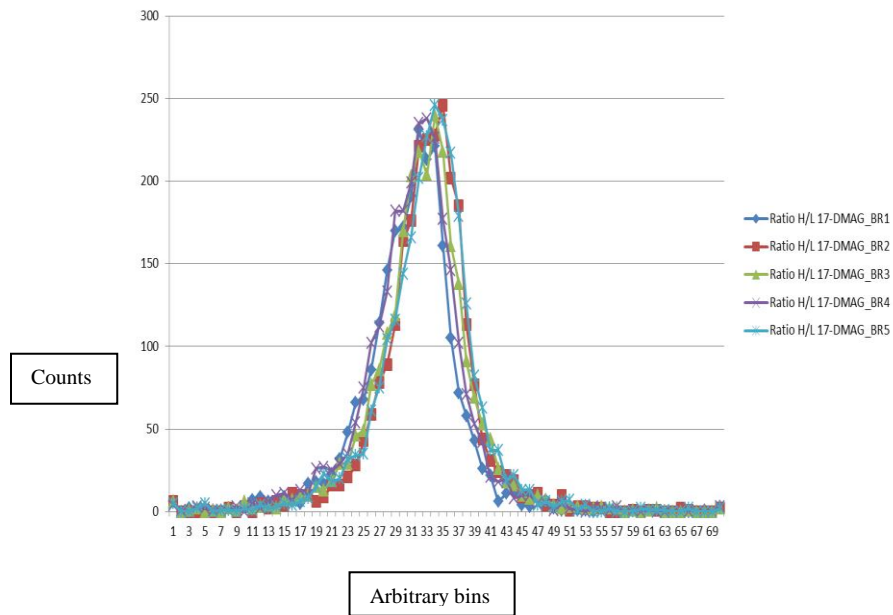
Figure 3.12: Assessment of the raw ratios in cells treated with 17-DMAG.

The frequencies of raw ratios from the 5 biological replicates were plotted as histograms as described in Figure 3.4.

Biological replicate 1 · Biological replicate 2 · Biological replicate 3

Biological replicate 4 · Biological replicate 5
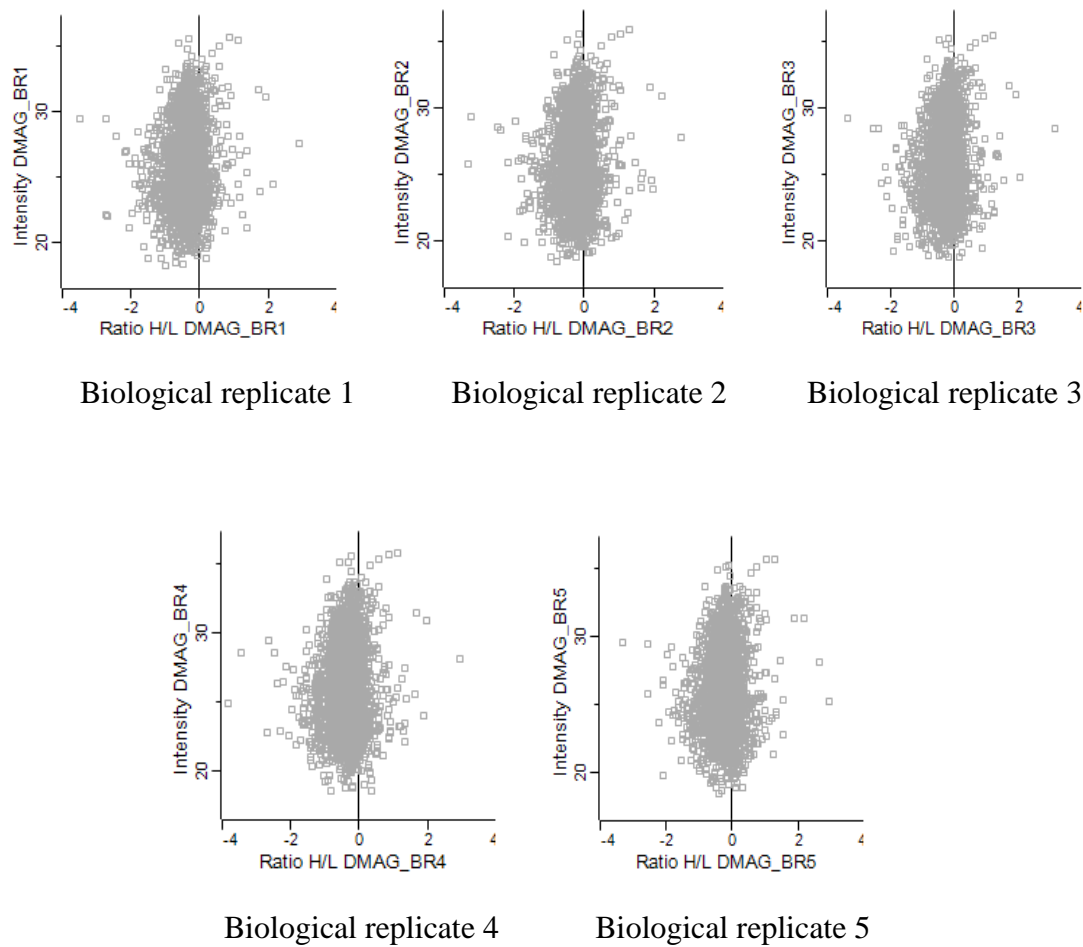
Figures 3.13: 17-DMAG raw data before normalization.

Protein expression changes (log$_2$ ratio H/L) from each biological replicate were plotted against the protein abundance to assess for normalization defects as described in Figure 3.5.
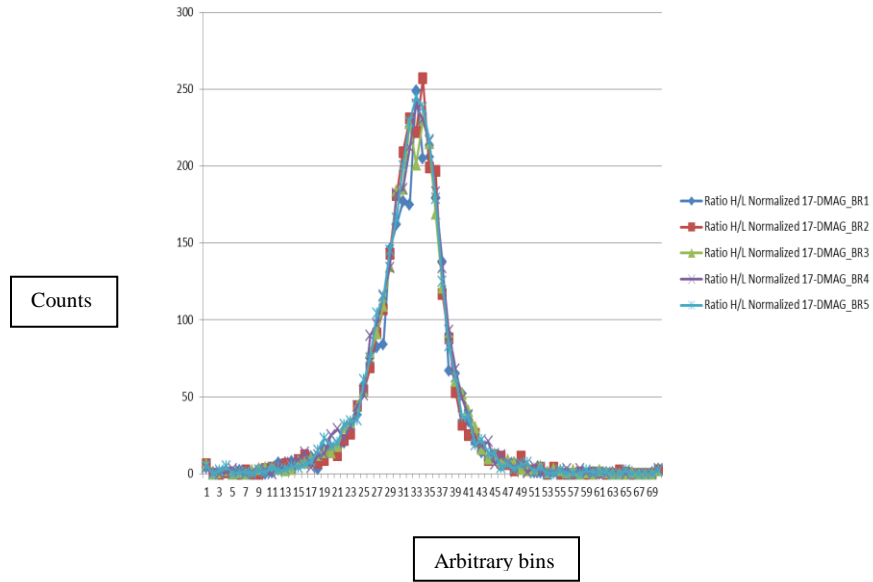
Figure 3.14: Global normalization minimized reproducibility issues across the five biological replicates in 17-DMAG.

Normalized ratios from the five biological replicates were plotted as described in Figure 3.6.
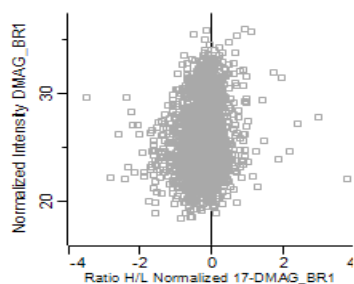
Biological replicate 1
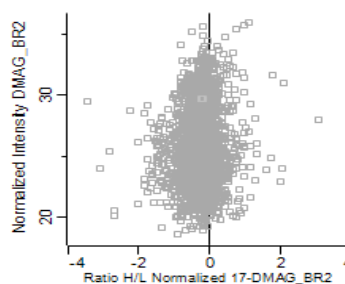
Biological replicate 2
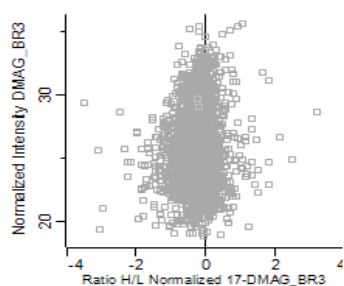
Biological replicate 3
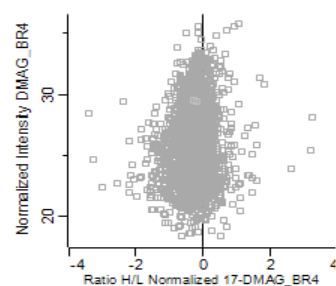
Biological replicate 4
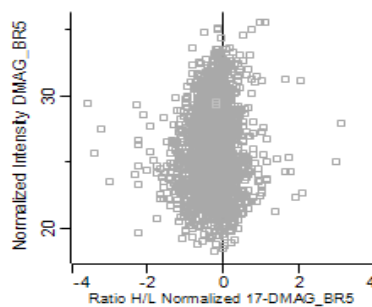
Biological replicate 5

Figure 3.15: 17-DMAG data after normalization –Ratio versus intensity plots.

Protein expression changes ($\log_2$ ratio H/L) from each biological replicate were plotted as described in Figure 3.7.
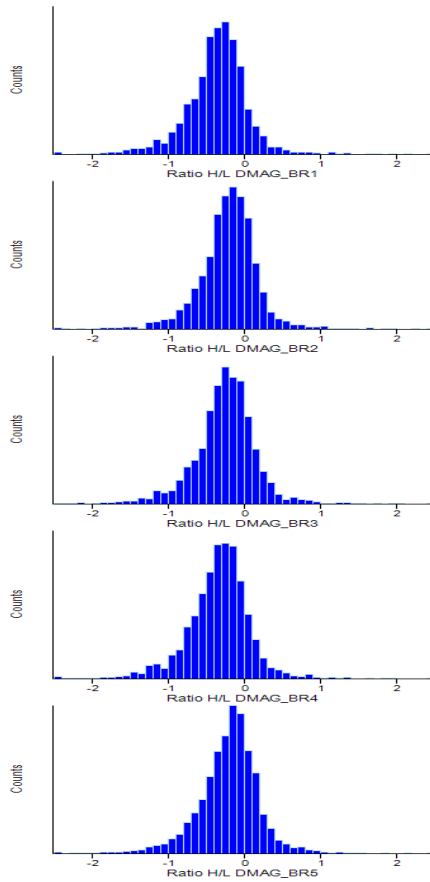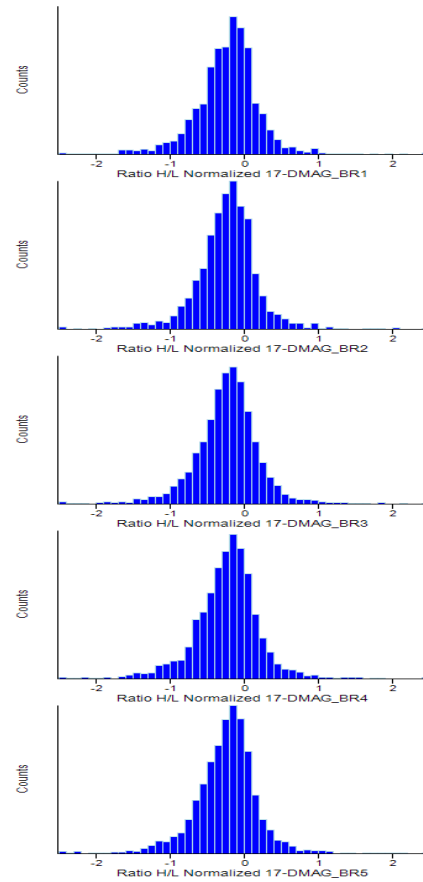
Figure 3.16: Histograms of protein expression from individual biological replicates in 17-DMAG before and after normalization.

Protein intensities from control and treated samples of 17-DMAG dataset were normalized using global normalization approach as described in the text. Protein expression across the five biological replicates were plotted before (Panel A) and after normalization (Panel B) as described in Figure 3.9.
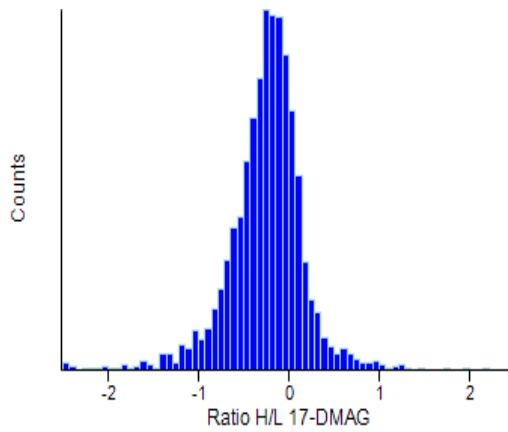
A.   **B.**
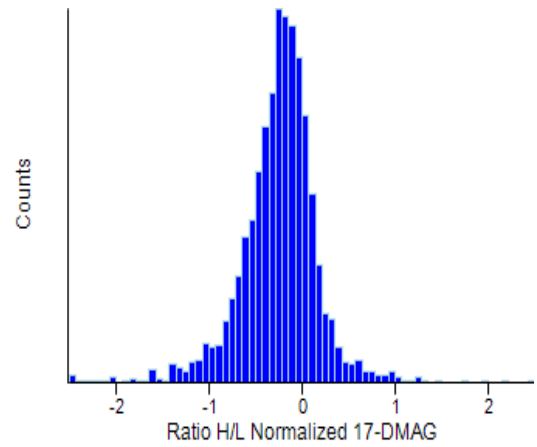
Figure 3.17: Histograms of average protein expression of all five biological replicates in 17-DMAG before and after normalization.

Ratios of H/L intensities from all the five biological replicates were averaged and plotted as histograms before (Panel A) and after normalization (Panel B). The X-axis represents binning of proteins based on intensity. The Y-axis represents the number of proteins in each bin.

Assessment of the population distribution of protein intensities in our AUY922 dataset

To decide which statistical tests were most appropriate for our data, we first determined whether our data followed a normal distribution**.** To do this, we pooled all protein intensities from all 5 bio-reps, and applied the Shapiro-Wilk test to determine if the data followed normal distribution. Results showed that the p-values for our dataset were greater than the chosen alpha level (Light Stat: 0.89, Light p-value: 0.19 Heavy Stat: 0.85, Heavy p-value: 0.19). This indicated that our data followed a normal distribution. This normal distribution was also evident in visual representation of the data populations (Fig 3.18). Thus, we concluded that Student's T-test might be an appropriate choice to validate significant changes in protein expression among treated versus un-treated cells.

To perform a Student's T-test, we had to decide whether to use statements of equal variance vs. un-equal variance between protein intensities from 5 treated samples and 5 untreated samples. Thus, we analyzed treated and control populations using the F-distribution function in Microsoft Excel. Results showed that the F-ratio was higher than the critical F-value (FINV) at the 90% confidence interval (Table 3.2).Thus, we concluded with 90% confidence that the two populations did not have equal variances. Thus, we concluded that T-test, two-sided (since we do not know the direction of the change), with unequal variance would be appropriate test for identifying significant drug-induced changes in protein expression.

After identifying Student's T-test as an appropriate test, this test was used to analyze AUY 922 data (two sided with statements of unequal variance). Very few protein changes out of the total proteins altered were identified as significant using this test (13%). Applying the B-H FDR

A.
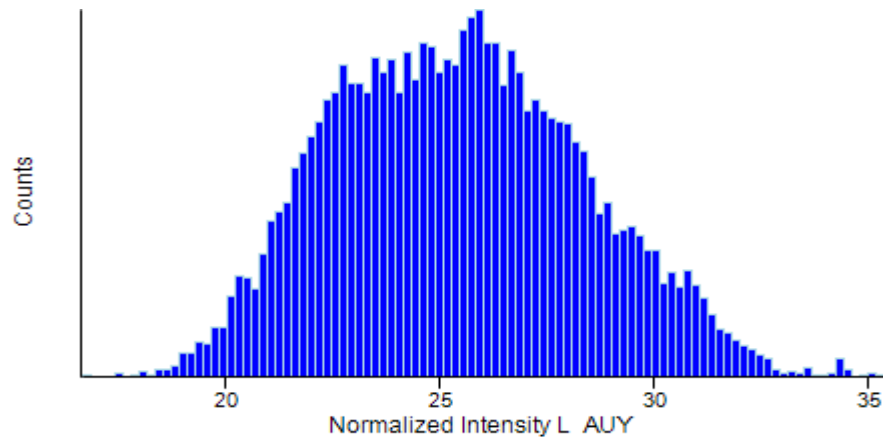
B.
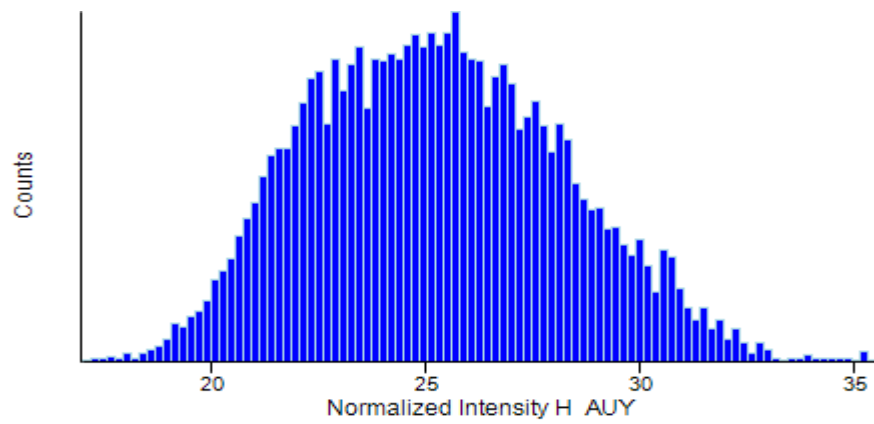
Figure 3.18: Assessment of the distribution of light and heavy intensities in AUY922.

The populations of light intensities and heavy intensities were plotted as histograms to assess the distribution (Panel A & B respectively). The X-axis represents binning of proteins based on their intensities and the Y-axis represents the number of proteins in the each bin.

Table 3.2: F-distribution test to determine if treated versus control populations have equal or unequal variance in AUY92 data.

	Light (Control)	Heavy (Treated)
VARP (Variance of the population)	1.96E+18	2.84E+18
Total count	15370	15370
F ratio (VARP Heavy/VARP Light)	1.444877023	
Confidence	90%	
Significance	10%	
FINV =(Confidence, Total count heavy-1,Total count light-1)	0.979536857	

Variance for the light and the heavy populations in AUY922 were calculated using VARP (variance of the population) function. Ratio was calculated by dividing VARP Heavy by VARP light. The critical F value was calculated using FINV function.

correction the number of significant proteins reduced this to 3%. Adding a third filter to require

1.5 fold change further reduced the number of significant changes down to 2%.

Similarly we analyzed raw data from Wu et al. representing MDAMB231 cells treated with 5

μM geldanamycin [57]. After Student's T-test and B-H FDR correction, very few proteins from

the total proteins were identified as significant. Furthermore, with B-H FDR correction and the

1.5 fold threshold, none of the proteins were identified as significantly altered in their data (Table

3.3).

In contrast, my analysis of each protein's average expression ratio in treated versus un-treated

cells suggested that the majority of the cellular proteome was down-regulated upon Hsp90

inhibition (Fig 3.7, 3.8 & 3.9). In 5/5 experiments, the majority of the protein ratios

(treated/untreated) were represented on the left side of the log2 scale, as opposed to being

distributed uniformly on the left and right sides of the log2 scale. (Fig 3.8A & 3.8B).This

indicated that much of the proteome was being reproducibly down-regulated upon Hsp90

inhibition. This contrasts with the results from Student's T test above, where only 2% of the

proteome changes were identified as significant. This suggested that Student's T-test with B-H

FDR correction and 1.5 fold change criteria probably understate the significant changes in protein

expression caused by drug treatment. Thus, we concluded that Student's T-test is not an

appropriate test for reporting significant drug-induced changes in protein expression.

In order to assess other statistical methods that might be used to validate changes in protein

expression, we assessed our data, data from Sharma et al. [56], and the data from Wu et al. [57]

using the one sample T-test used by Sharma et al. [56]. However, Sharma et al. did not describe

their statistical analysis in their publication [56] . Therefore, we de-constructed their statistical

analysis. For this, we analyzed their normalized H/L ratios from all the five biological replicates

using the "One sample T-test" function embedded in their software package Perseus. Their

Table 3.3: Comparison of the effects of statistical tests on 3 Hsp90 inhibited proteomes

Statistical analyses were performed as described in the text.

Test	Variation of the test	Datasets- % of proteins responding to Hsp90 inhibition			
		Our AUY922 dataset (5 bio-reps)-in-house normalized	Wu et.al (MDAMB431)		Sharma et.al MaxQuant normalized data
			Un-normalized	Normalized (by our method)	
One sample T-test embedded in Perseus software package (T-test of ratios) used by Sharma et.al	T-test p values (p<0.05)	54%	43%	44%	41%
	With BH FDR correction(FDR < 0.05)	52%	25 %	24%	30%
	BH correction plus 1.5 fold cutoff	13%	15%	14%	14%
	With Storey FDR correction (FDR < 0.05)	50%	ND	24%	30%
	Storey FDR correction plus 1.5 fold cutoff	12%	ND	14%	14%
Standard T-test (Two tails Unequal variance)	T-test p values (p<0.05)	13%	ND	5%	Not done because raw intensities were not available
	With BH FDR correction (FDR<0.05)	3%	ND	Zero	
	BH correction plus 1.5 fold cutoff	2%			

treated/untreated ratios were presumably normalized by MaxQuant during peptide peak detection, capture and collection into protein intensities. Using this test, we identified 2,861 changes in protein expression in their dataset with T-test p values < 0.05 (out of the 7,028 total proteins assayed). However, their final list of up-regulated and down-regulated proteins contained only 2,107 proteins whose expression was altered. In order to reconcile these two numbers, we applied the B-H FDR correction embedded in their software package Perseus (B-H = 0.05 FDR) to their T-test p values. This correction invalidated proteins with a t-test p value ≤ 0.015. This allowed us to exactly duplicate their list of significantly altered proteins and their p values (Fig 3.19).

Using this approach, we analyzed normalized data from Wu et al. (MDAMB231 cells treated with 5 μM geldanamycin using the one sample T-test used by Sharma et al. Using this test, 43% of the total proteins altered were identified as significant. The number of significantly altered proteins reduced to a 24% by applying a B-H FDR correction.

Applying 1.5 fold threshold along with B-H FDR correction further reduced the number of significant proteins to 14% (Table 3.4). Thus, we concluded that the number of proteins identified as significantly altered in data from Wu et al. were reduced to similar extent relative to data from Sharma et al.

Subsequently we analyzed our normalized AUY922 data using the one sample t-test. We identified 57% of the total proteins as being significantly altered. The B-H FDR corrections further reduced the number of significantly altered proteins to 51%. Applying 1.5 fold threshold further reduced the number of significantly altered to 12%. Thus, we concluded that the number of significantly altered proteins in our AUY922 dataset was reduced to by applying both B-H FDR correction and 1.5 fold threshold and that this reduction was similar to the reduction observed in data from Sharma et al. and Wu et al.
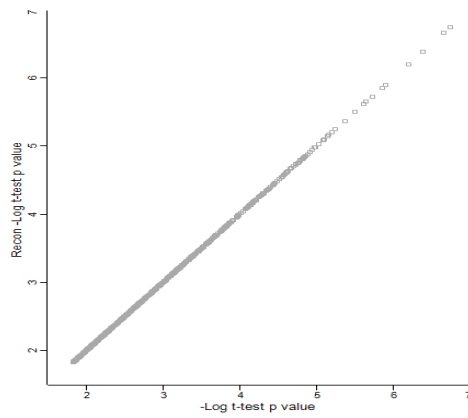
A.   **B.**
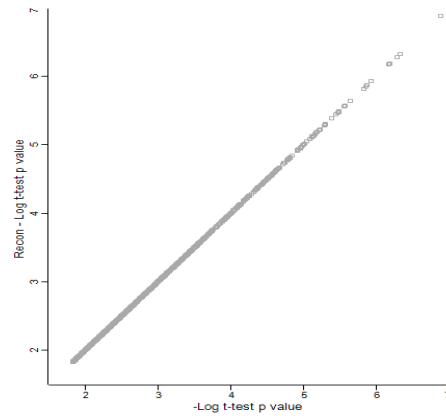
Figure 3.19: Comparison of deconstructed data from Sharma et al. to their actual data.

Statistical analysis from Sharma et al. was de-constructed using one sample T test embedded in their software package Perseus, and results were compared by plotting the –log (p values) from published data of Sharma et al. versus my de-constructed –log (p values). Panel A: Comparison of p values for significantly up-regulated proteins and Panel B: Comparison of p values for significantly down-regulated proteins.

The B-H FDR test is a test for multiple corrections. It is designed to validate only a few significant differences in a large dataset. However, when there are many significant differences in a large dataset, the Storey FDR test is a more appropriate test. Similar to B-H FDR test, Storey FDR test is a false discovery correction test that validates larger p-values than the B-H FDR test. This helps to validate more positives in datasets that have large numbers of differences.

Our AUY922 dataset suggested that the majority of the proteome was down- regulated by Hsp90 inhibition. Similarly, we had many proteins with significant one sample T test p values. Thus, the Storey FDR test was more appropriate than the BH- FDR test for our data. Therefore, we applied the Storey FDR to the p values from our T-test and identified 10% more proteins as significantly altered, than those we identified using B-H FDR correction. After applying 1.5 fold threshold, the number of proteins identified as significantly altered reduced to 14%, thus suggesting that 1.5 fold threshold is very rigorous and eliminates more than half of the proteins. Thus, we identify a short list of protein expression changes with high confidence.

We similarly re-analyzed normalized data from Sharma et al and Wu et al. using a Storey FDR correction and 1.5-fold threshold (Results shown in Table 3.1). The number of proteins identified as having significant alterations in protein expression using B-H FDR test and Storey FDR test were the same for the data from Sharma et al. Similarly, in data from Wu et al, Storey and B-H FDR tests identified the same number of proteins with significant alterations in protein expression. Applying an additional 1.5 fold threshold to both the datasets (Sharma and Wu) reduced the total number of proteins with significant changes in protein expression to about 14%.

Thus, we concluded that one sample T-test with Storey FDR correction and 1.5 fold change threshold criterion is an appropriate approach to report highly confident changes in protein expression from our data showing large drug-induced changes in the proteome.

Discussion

In summary, analyzing our raw SILAC data representing the proteomes of Jurkat cells treated with AUY922, we noted minor normalization problems across the 5 biological replicates (Fig 3.4 & 3.5). By comparing the quality of our raw data to the raw SILAC data of other cell lines treated with Hsp90 inhibitors we concluded that our raw data were as good as data from Matthias Mann's lab [56] , (c.f. Fig 3.2 vs. Fig 3.3), and perhaps superior to the data from David Kuster's lab [57], (c.f. Fig 3.2 vs. Fig 3.10B & 3.10C).

To address our minor normalization defects, we developed a global normalization strategy. Our strategy minimizes variation across the biological replicates (Fig 3.6 & 3.7), but does not distort the data (Fig 3.8 & 3.9).

We demonstrate that while the Student's T-test might be appropriate for validating our data, we show that the one sample T test used by Manns'group is more appropriate test for identifying significant changes in protein expression (c.f. Table 3.3 vs. Fig 3.8 & 3.9).

Therefore our final choice was to include a 1.5 fold change threshold criterion but with the Storey FDR correction of one sample T-test to generate a short-list of proteins in which we have high confidence, rather than reporting a larger list of changes which we are not confident. We will go on to use these criteria to analyze 5 other SILAC datasets collected in subsequent experiments in this study.

CHAPTER IV

**The proteomics fingerprints of AUY922 and 17-DMAG are largely similar in Jurkat
leukemia cells, indicating common mechanisms of action for Hsp90 inhibitors.**

Introduction

In Chapter II, we quantified the changes in protein expression induced by anti-cancer drug

candidate, AUY922 in Jurkat leukemia cells using the spectrum counting approach. We compared

AUY922-induced changes to the expression changes induced by classical Hsp90 inhibitors 17-

DMAG and radicicol. Using this approach, we identified around 180 proteins showing significant

changes in expression. Although we identified 31 protein expression changes that were common

to all three inhibitors, we also identified changes that were not universal. Thus, we were faced

with questions about which of these changes were real.

To address these questions, and also to identify more protein expression changes induced by

Hsp90 inhibitors, a better quantitative proteomics approach was needed. In this chapter, the stable

isotope labeling with amino acids in cell culture (SILAC) approach was used to compare the

proteomic fingerprints of AUY922 and 17-DMAG. Results from this study were anticipated to

validate findings from our spectrum assays. It was also anticipated that SILAC would allow

identifying more inhibitor-induced protein expression changes so that a stronger and deeper

proteomics fingerprint of Hsp90 inhibition could be established. The proteins thus identified in this study would serve as candidate biomarkers for Hsp90 N-terminal inhibitors. Identification of the proteomics fingerprint of Hsp90 C-terminal inhibitors is one of the long term goals of our laboratory. Therefore the proteomics fingerprint of Hsp90 N-terminal inhibitors identified in this study could be compared to the fingerprint of Hsp90 C-terminal inhibitors. This would give insights into the mechanism of action of both classes of inhibitors and would reveal if they have similar or different mechanisms of action.

Materials and Methods

All the materials and methods and statistical testing used in this study were the same as described in Chapter III. A summary of the experimental design was described in Chapter III. In order to identify the significant alterations in protein expression, normalized H/L ratios were validated by one sample T-test, with multiple tests correction using the Storey FDR test. The final list of proteins with significant alterations in expression consisted of proteins with greater than 1.5 fold changes in expression and Storey FDR values less than 0.05.

Drug treatments and LC-MS/MS analysis

Jurkat cultures adapted to SILAC heavy media were treated for 24 hours with 75nM or 150nM of AUY922 or 17-DMAG respectively. These doses represent 5-7X IC_{50} doses for Cdk6 depletion (See Fig 2.3 & 2.6 from Chapter II). As controls, Jurkat cultures adapted to SILAC light media were treated with DMSO. All the experiments were performed in five biological replicates. Protein in the cell lysates from drug-treated and control samples were quantified, mixed in a 1:1 ratio (50 ug of treated lysate + 50 ug of untreated lysate), precipitated with TCA/acetone and fractionated by SDS-PAGE. Following fractionation, samples were trypsinolyzed and processed as described in the Materials and Methods section of Chapter III. Resulting trypsinolytic peptides

were analyzed by LC-MS/MS analysis using a Thermo LTQ-Orbitrap XL mass spectrometer. Protein identification and quantification was performed using MaxQuant (v 1.3.0.5).

GO analysis

Proteins with significant changes in expression were categorized for biological process, molecular function and cellular component using the DAVID bioinformatics program [105]. To gain insights into the functional categories represented, functionally related GO terms were grouped using web server REVIGO [106] with the following default settings : Allowed similarity- medium (0.7), number associated to GO categories are – p-values, database with GO term sizes –whole Uniprot, semantic similarity measure to use -SimRel. For REVIGO analysis only GO terms whose BH- corrected p values were less than < 0.05 were used.

Results

In this study, impacts that two distinct Hsp90 inhibitors, namely AUY922 and 17-DMAG, have on the proteome of Jurkat leukemia cells were assessed using a SILAC approach. To identify how reproducible the biological replicates in the AUY922 dataset were, we compared the total number of proteins identified in all the 5 biological replicates. Results indicated that majority of the proteins identified (2,400) were observed in all the 5 biological replicates (Fig 4.1). Thus, we concluded that there was a high degree of reproducibility across the 5 biological replicates in AUY922 dataset. Similarly, we compared the reproducibility across the 5 biological replicates in 17-DMAG dataset using the same approach as described for AUY922. Results indicated that similar to AUY922, 17-DMAG dataset also displayed a high degree of reproducibility with majority of the proteins identified (2193) being observed across the 5 biological replicates (Fig 4.1).

To identify how similar the AUY922 and 17-DMAG datasets were, we compared the total number of proteins identified across the 5 biological replicates in both the datasets. Results showed that the size of both the datasets were similar as indicated by the total number of proteins identified in all the 5 biological replicates (Fig 4.1). Thus, we concluded that both the datasets were highly similar to each other in terms of the number of proteins identified.

Prior to determining how conserved the protein expression changes between AUY 922 or 17-DMAG treated Jurkat proteomes were, changes in protein expression induced by the drugs were validated using one sample T-test. Results showed that the one sample T-test yielded nearly a similar number of protein expression changes with $p < 0.05$ in both AUY922 and 17-DMAG datasets and suggested that 50% of the proteome was being altered by both drugs (Fig 4.2A). Thus, we concluded that the one sample T-test had similar effects on both AUY922 and 17-DMAG datasets, and that the changes in protein expression induced by both drugs were highly
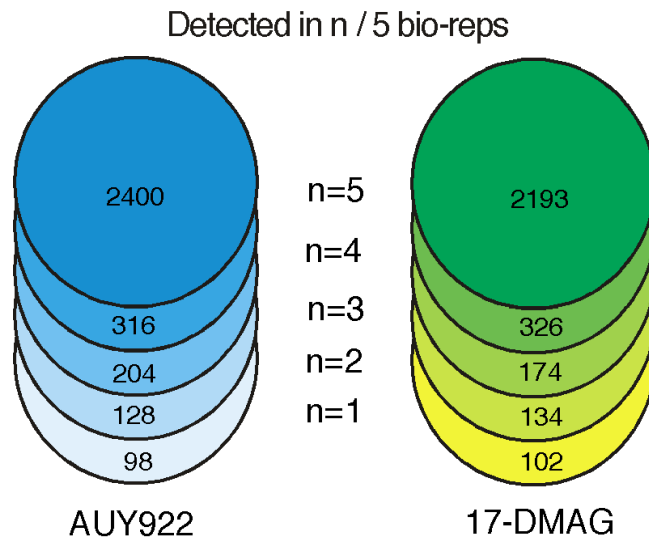
Figure 4.1: Total number of proteins detected across biological replicates in the proteomes of Jurkat cultures treated with AUY922 and DMAG.

The total number of proteins detected across the five biological replicates in the proteomes of Jurkat cultures treated with AUY922 and 17-DMAG are represented. N represents the number of biological replicates. The N = 5 circle represents the number of proteins identified in 5/5 experiments. The N = 4 crescent represents the difference between the number of proteins identified in 5/5 experiments vs. the number of proteins identified in 4/5 experiments (and so on for N = 3, N = 2, N = 1).

similar. This was highly consistent with our raw data that suggested that the majority of the proteome was being down-regulated upon Hsp90 inhibition (Fig 3.7 and 3.18, chapter III).

   To minimize reporting false positive changes in protein expression and to avoid missing any true changes, we then performed multiple test correction of the T-test p-values from both AUY922 and 17-DMAG datasets using the Storey FDR test setting the FDR < 0.05. This slightly reduced the total number of protein expression changes identified as significantly altered in both AUY922 and 17-DMAG datasets (c.f. Fig 4.2A vs. Fig 4.2B). After this Storey FDR correction, 59% of the total identified proteins showed significant changes in expression that were common between both drugs (Fig 4.2B). The large degree of overlap in the number of significantly altered proteins among the two drugs reinforced our conclusion that their effects were largely similar.

   In order to report only the protein expression changes which we had high confidence in, we applied a 1.5-fold change criterion in conjunction with the Storey FDR correction. Among the total proteins with expression changes $\geq$ 1.5-fold in both the drugs, 49% of them were the same between both drugs (Fig 4.2C). We then compiled the total number of proteins that pass both criteria (Storey corrected values < 0.05 and fold change $\geq$ 1.5) in both the AUY922 and 17-DMAG datasets. Applying these two criteria greatly reduced the number of proteins identified as significantly altered in both AUY922 and 17-DMAG datasets (Fig 4.2D). Of both the criteria, 1.5-fold change criteria were more stringent and resulted in invalidating the majority of the protein expression changes. We concluded that applying both criteria to validate changes in protein expression was very rigorous and eliminated several proteins from being reported as significantly altered. Thus, these criteria allowed us to report only high confidence changes in protein expression.
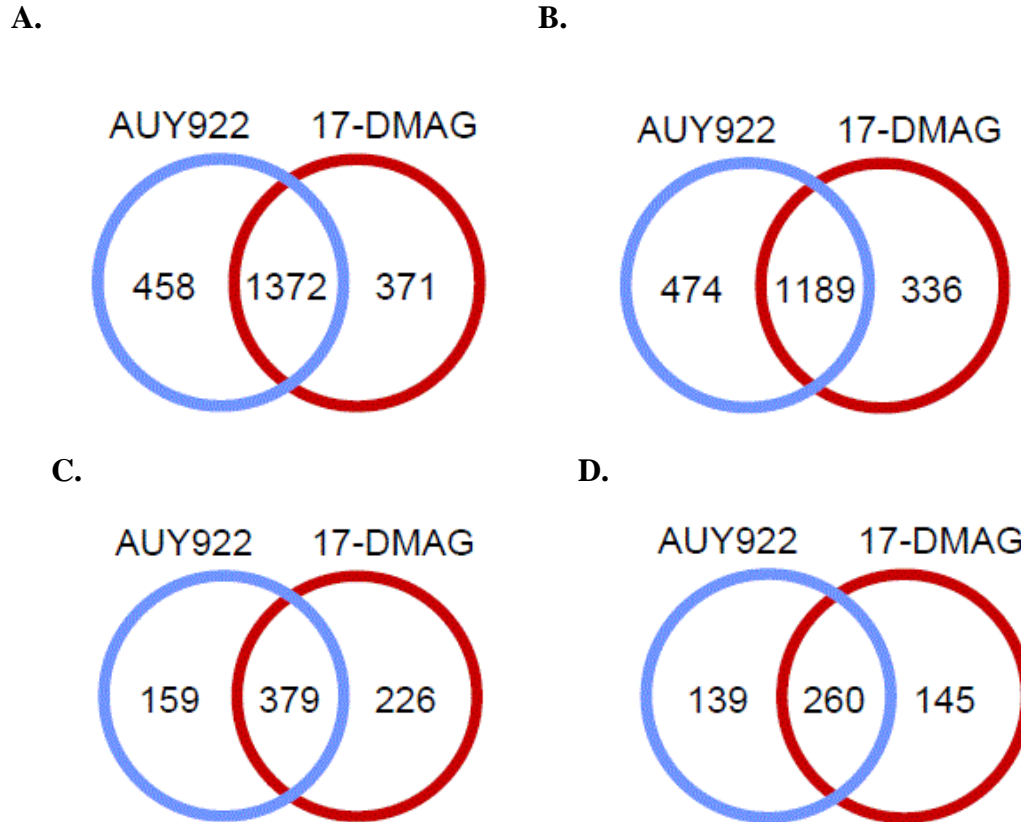
Figure 4.2: Venn analysis of the effects of statistical criteria on evaluating protein expression changes in Jurkat cultures treated with AUY922 vs. 17-DMAG.

Statistical analysis was performed as described in text. Panel A: Total number of proteins with one-sample T-test p values < 0.05. Panel B: Total number of proteins with Storey FDR corrected p-value thresholds of< 0.05. Panel C: Total number of proteins with changes in expression ≥ 1.5 fold. Panel D: Total number of proteins with changes in expression equal to or greater than 1.5 fold, and having Storey FDR corrected p-value thresholds of< 0.05.

Failure to see selective enrichment of proteins in the unions between the drugs after each statistical step suggested that there could be many protein expression changes that were drug-specific but did not pass the statistical criteria for both the drugs. Therefore, subjecting the data to all the statistical tests may have resulted in discarding true protein expression changes. However, our raw data suggested that the majority of the proteome is being altered by both inhibitors. Nevertheless, we decided to use the more stringent criteria in order to report only high confidence changes in protein expression.

We next assessed consistency in the direction of the protein expression changes for the proteins that pass both criteria in both AUY922 and 17-DMAG datasets. Direction here refers to up-regulated or down-regulated. To accomplish this, we divided the proteins showing significant alterations in expression from both datasets into up-regulated and down-regulated proteins, and then compared the AUY922 and 17-DMAG datasets to look for consistency in expression patterns (Fig 4.3). Among the proteins that were identified as significantly altered, the majority were down-regulated, as opposed to being up-regulated. This was consistent with our raw histograms that indicated that the majority of the proteome is down-regulated by Hsp90 inhibition (Fig 3.7 & 3.18, Chapter III). Among 476 proteins down-regulated by either AUY922 or 17-DMAG, 48% of the responses were common to both inhibitors. Among the 69 proteins up-regulated by either inhibitor, 46% of the responses were common to both inhibitors (Fig 4.3). Thus, we concluded that Hsp90 inhibition leads to more down-regulation than up-regulation. Moreover, the direction of the changes was highly similar among drugs, with the majority of the proteins down-regulated in the proteome of one drug treated cells also being down-regulated in the proteome of cells treated with the other drug. This was also the case for up-regulated proteins. This commonality gives high confidence in the validity of protein expression changes that we identified.
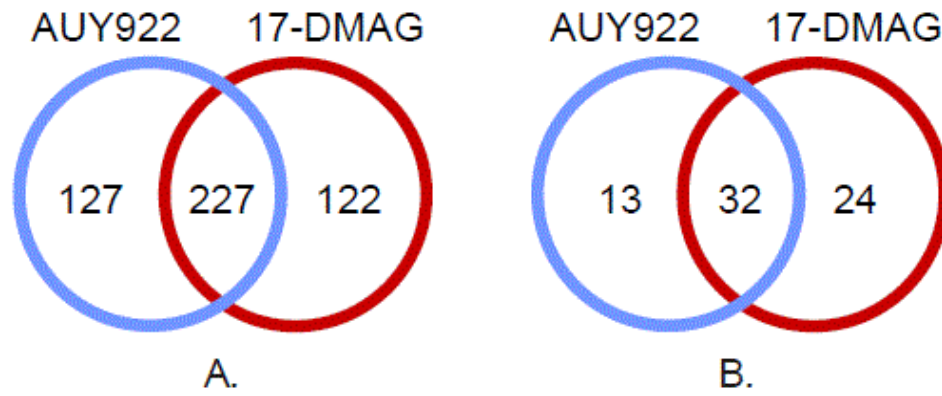
Figure 4.3: Comparison of down-regulated and up-regulated proteins expression changes in Jurkat cells treated with AUY922 and 17-DMAG

Panel A: Total number of proteins down-regulated by AUY922 and/or 17-DMAG. Panel B:

Total number of proteins up-regulated by AUY922 and/or 17-DMAG.

In order to visualize the direction and magnitude of the changes induced by AUY922 and 17-DMAG, the magnitude of changes induced by AUY922 were plotted versus the magnitude of changers induced by 17-DMAG. The majority of the protein changes (both significant and non-significant) were well centered on the diagonal of this plot generating an R^2 value of 0.681 (Fig 4.4). This suggested that the protein expression patterns were similar in the Jurkat cells treated with either drug. Moreover, in both AUY922 and 17-DMAG datasets, the majority of the significant changes (crosses) were distributed in the lower left hand quadrant of the scatterplot (Fig 4.4), suggesting that the majority of the proteins were being down-regulated by both inhibitors.

There were some significant changes in the upper right hand quadrant in both the datasets, indicating proteins that were up-regulated by both the inhibitors. In contrast, there were very few changes that were distributed in the lower right hand quadrant and the upper left hand quadrant in both the datasets. This suggested that there were very few proteins that were up-regulated by one inhibitor but down-regulated by the other inhibitor, and vice versa. In summary, these results suggested that: (i) that the inhibitors generated similar effects; and (iii) both the inhibitors cause more down-regulation of the proteome than up-regulation.
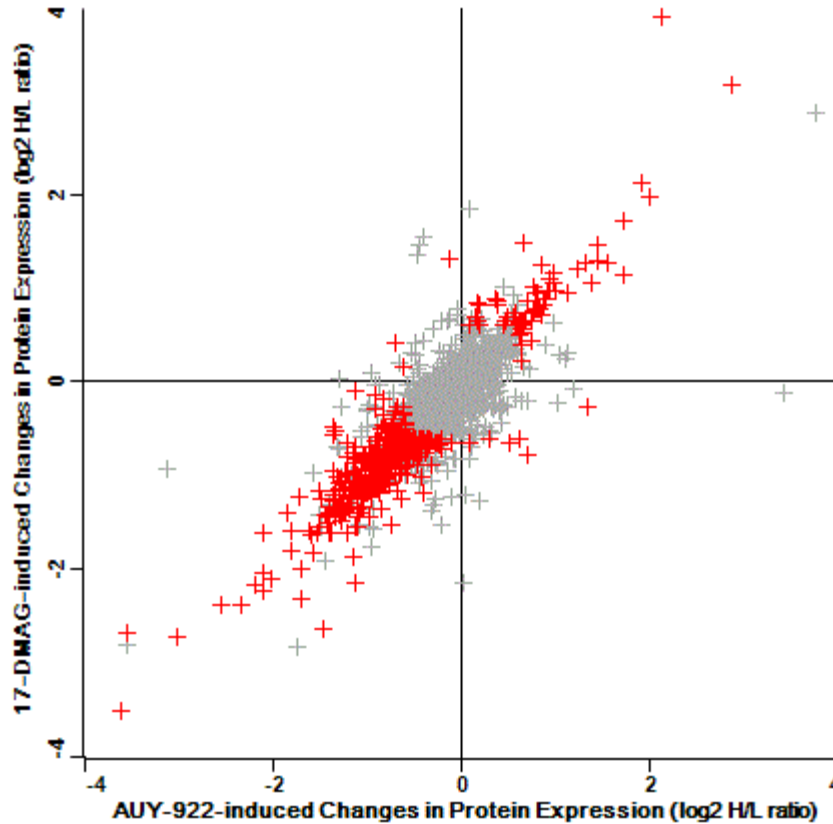
Figure 4.4: Comparison of changes in protein expression induced by AUY922, 17-DMAG and both AUY922 & 17-DMAG.

The X-axis represents the log2 values of H/L ratios for individual proteins in the proteomes of Jurkat cultures treated with AUY922. The Y-axis represents the log2 values of H/L ratios for individual proteins in the proteomes of Jurkat cultures treated with 17-DMAG. The red crosses represent the union of AUY922-induced changes & 17-DMAG-induced changes. The grey crosses represent the proteins that did not pass both the Storey FDR values < 0.05 and fold change criteria in either drug.

To further visualize the inhibitor-specific effects we again plotted the magnitude of changes induced by AUY922 versus the magnitude of changes induced by 17-DMAG, but highlighted the significant changes induced by AUY922 only (Fig 4.5A). Similarly we plotted 17-DMAG induced changes only (Fig 4.5B). Both the plots were largely indistinguishable suggesting that the drugs largely shared similar effects. However, there were some changes that appeared to have significant alterations in protein expression unique to each drug but failed to survive the rigorous statistical tests. This suggested that although the expression changes of these proteins are similar between both inhibitors, rigorous statistical tests invalidate them from being detected in both. We also plotted the changes induced by both inhibitors (Fig 4.5C). The total number of protein changes that are common between both drugs is reduced (c.f. Fig 4.5A, 4.5B vs. 4.5C). This reinforced our opinion that the rigorous statistical tests eliminated many proteins with altered protein expression.

We similarly plotted changes induced by AUY922 versus 17-DMAG after removing all the proteins that were not significantly altered by either inhibitor (Fig 4.6A to 4.6C) or that were not altered by both inhibitors (Fig 4.7). Eliminating those proteins that were not significantly altered improved the R^2 values from 0.681 to 0.838. Eliminating proteins that were not altered by both the drugs improved the R^2 values from 0.838 to 0.95.

A.
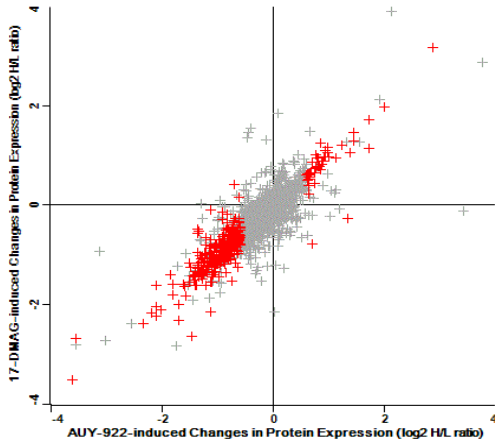
B.
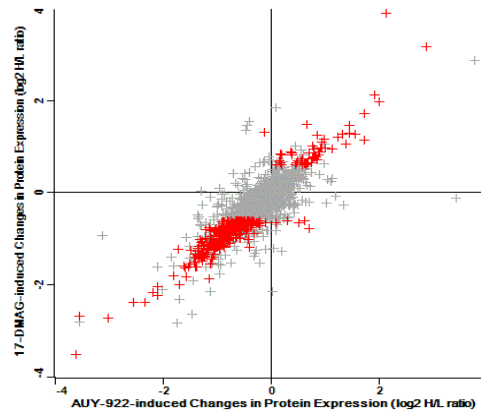
C.
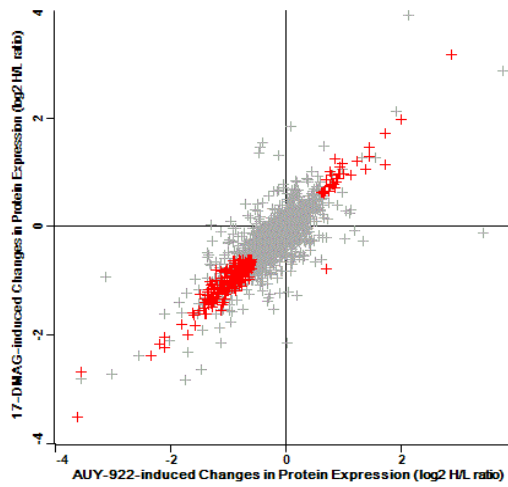
Figure 4.5: Comparison of the changes in protein expression caused by either AUY922 or 17-DMAG or both.

Analysis as described for Figure 4.4. ***A:*** Red crosses are those proteins that are significant in AUY922 only. ***B:*** Red crosses are the proteins that are significant in 17-DMAG only. **C:** Red crosses are those proteins that are significant in both AUY922 and 17-DMAG.

A.

B.

C.
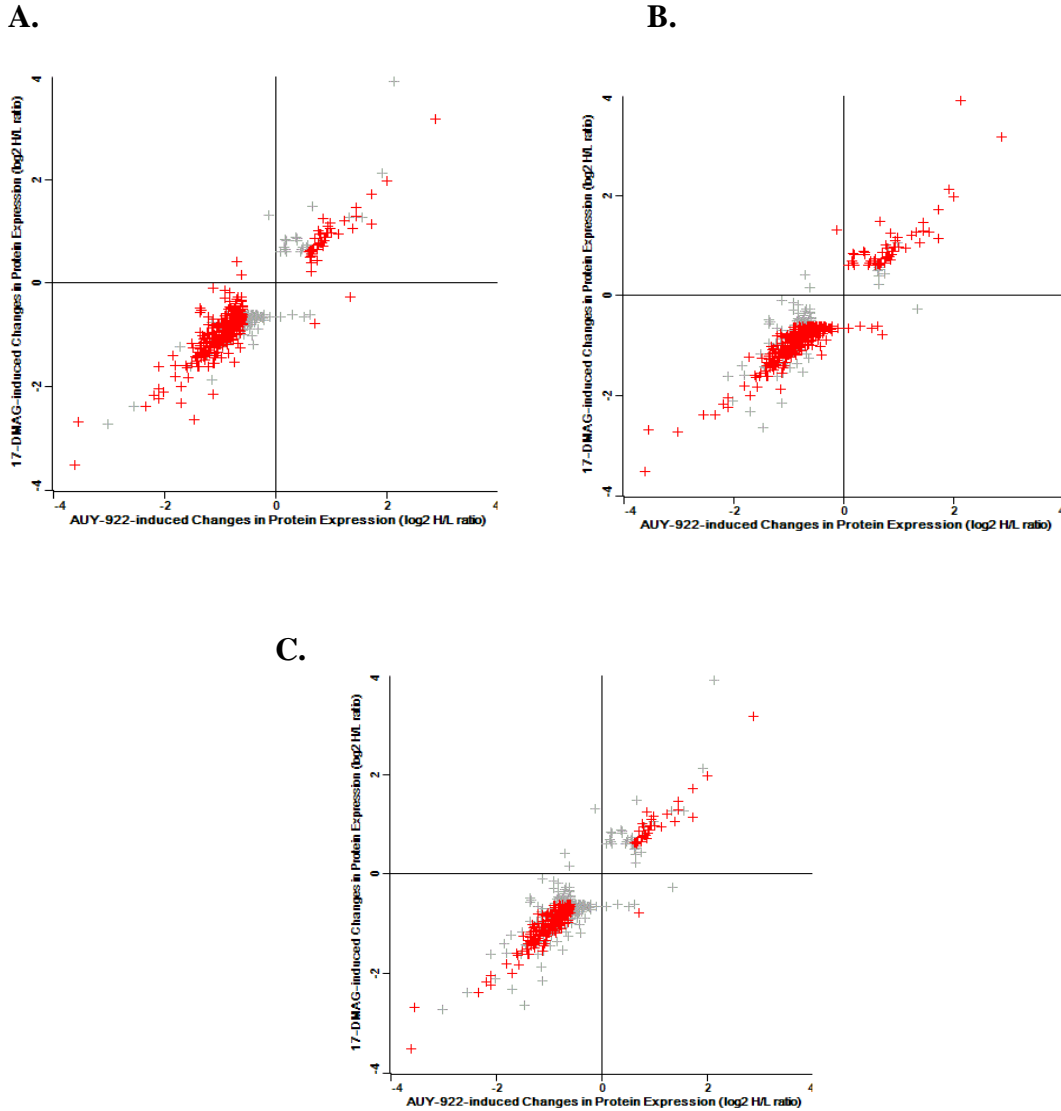
Figure 4.6: Comparison of the changes in protein expression caused by AUY922 vs. 17-DMAG after deleting proteins not significant in either or both drugs.

Analysis as described for Figure 4.4. *A:* Red crosses represent AUY922 induced changes. *B:* Red crosses represent 17-DMAG induced changes. *C:* Red crosses represent changes common to both AUY922 and 17-DMAG.
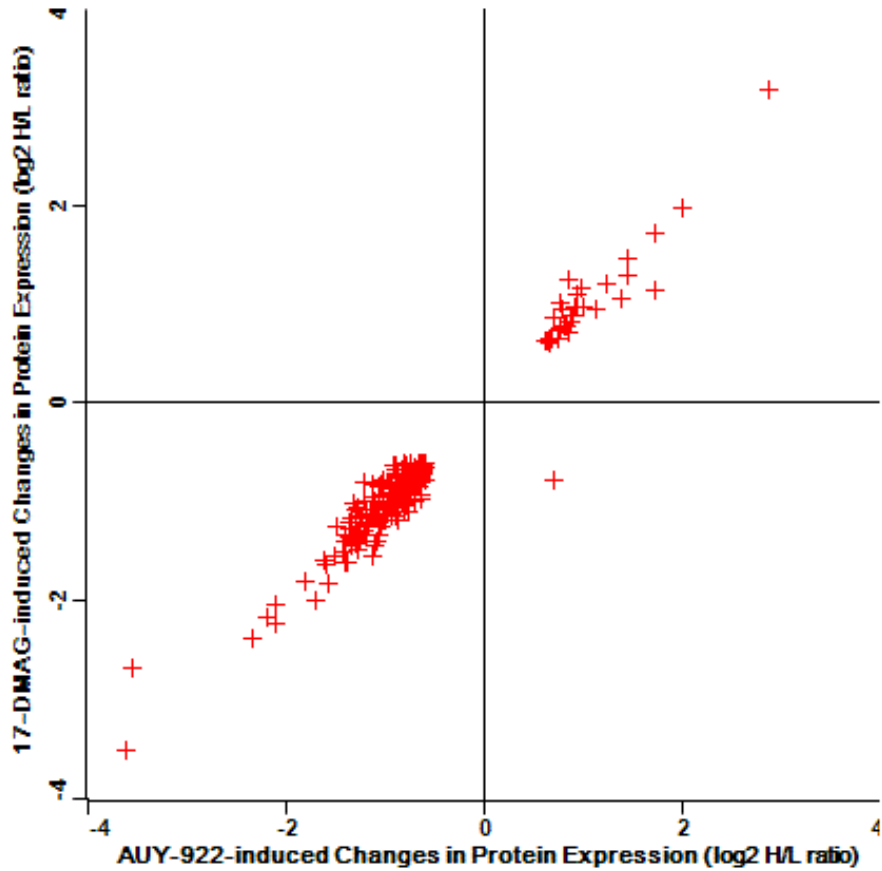
Figure 4.7: Comparison of the changes in protein expression caused by AUY922 & 17-DMAG only

Analysis as described for Figure 4.4. These plots were constructed after removing those proteins that did not pass both criteria in either AUY922 or 17-DMAG or both. Red crosses are drug-induced changes common to both AUY922 and with 17-DMAG.

Eliminating proteins whose expression changes were not significant improved the R^2 fits. This suggested that there was high degree of agreement between these proteins altered by both the inhibitors, thus indicating that the two inhibitors share common effects. Results also showed that the total number of proteins that pass both criteria in both drugs is smaller than the total number of proteins that pass both criteria in individual drugs (Fig 4.6B, 4.6C vs. Fig 4.6D and 4.7). Thus, we concluded that criteria we used for reporting the proteins with significant alterations in protein expression were very stringent and eliminate many drug-specific changes in protein expression.

Comparison of the number of proteins identified in 5 bioreps versus 3 bioreps

To test the effects of the number of biological replicates on our ability to validate protein expression changes, we identified the total number of significant protein expression changes in 3 biological replicate datasets and compared them to the total number of changes identified in 5 biological datasets by using both ≥ 1.5 fold change and Storey FDR corrected p-value thresholds of < 0.05. The total number of changes identified in 3 biological replicate datasets were almost 45% less than those identified in 5 biological replicate datasets for both AUY922 and 17-DMAG datasets (Table 4.1).

Table 4.1: Number of significant protein expression changes identified in 5 biological replicate datasets versus 3 biological replicate datasets

Number of biological replicates (N)	Number of significant protein expression changes identified in AUY922 treated cells	Number of significant protein expression changes identified in 17-DMAG treated cells	Number of significant protein expression changes common to both drugs
N =5	399	405	260
N =3	209	252	158
% Difference	47.7%	37.8%	39%

These results indicated that using more biological replicates in SILAC experiments allows for the identification of a higher number of significant protein expression changes. The total number of protein expression changes we identified in 5 biological replicate datasets were nearly 50% higher than the number of protein expression changes identified in 3 biological replicate datasets in both AUY922 and 17-DMAG datasets. Thus we concluded that, more the number of biological replicates, the greater the power to identify more expression changes and thus more discovery.

GO analysis

To gain insights into the biological processes affected by the AUY922 and 17-DMAG, we performed gene ontology (GO) analysis of the proteins that passed both criteria (Storey FDR corrected p-value thresholds of< 0.05, and ≥ 1.5 fold change) for each drug. Only the GO terms whose B-H corrected values < 0.05 were considered. Both AUY922 and 17-DMAG affected a wide variety of functional categories (Tables 4.2 & 4.3). Several processes were down-regulated by both AUY922 and 17-DMAG (Table 4.2).Similarly up-regulated categories were also common between both the inhibitors (Table 4.3). Indistinguishable GO profiles of AUY922 and 17-DMAG suggested that the inhibitors have similar mechanism of action in cultured cells.

Table 4.2: Major functional categories down-regulated by either AUY922 or 17-DMAG.

GO Term	Function	BH corrected values AUY922	BH corrected values 17-DMAG
GO:0004672	Protein kinase activity	5.0E-12	2.2E-10
GO:0005524	ATP binding	3.6E-10	1.5E-07
GO:0032559	Adenyl ribonucleotide binding	6E-10	2.3E-07
GO:0004674	Protein serine/threonine kinase activity	4.3E-09	3E-06
GO:0030554	Adenyl nucleotide binding	9E-09	1.95E-06
GO:0001882	Nucleoside binding	8.2E9	7.5E7
GO:0001883	Purine nucleoside binding	2.3E8	1.9E6
GO:0032553	Ribonucleotide binding	8.2E8	1.1E5
GO:0032555	Purine ribonucleotide binding	8.2E8	1.1E5
GO:0006468	Protein amino acid phosphorylation	5.4E9	3.2E7
GO:0017076	Purine nucleotide binding	7.1E7	6E5
GO:0022403	Cell cycle phase	9.1E8	10E9
GO:0004693	Cyclin-dependent protein kinase activity	5.4E6	7.1E5
GO:0016310	Phosphorylation	4.9E7	2.1E5
GO:0005694	Chromosome	1.8E8	2E6
GO:0051301	Cell division	7.2E7	4.9E7
GO:0044427	Chromosomal part	1.1E6	2.1E6
GO:0004386	Helicase activity	4.2E5	5.71E4
GO:0007049	Cell cycle	5.4E6	1.6E7
GO:0006796	Phosphate metabolic process	7.1E6	6.8E5
GO:0006793	Phosphorus metabolic process	7.1E6	6.8E5
GO:0005654	Nucleoplasm	1.9E5	1.4E5
GO:0007067	Mitosis	2.2E5	1.9E4
GO:0000280	Nuclear division	2.2e5	1.6E4

GO:0000279	M phase	2E5	1.3E5
GO:0031981	Nuclear lumen	7E5	4.7E6
GO:0000087	M phase of mitotic cell cycle	3.3E5	2.6E4
GO:0048285	Organelle fission	4E5	3.1E4
GO:0000166	Nucleotide binding	2.3E4	-
GO:0022402	Cell cycle process	1.3E4	8.2E6
GO:0000278	Mitotic cell cycle	1.4E4	6.6E5
GO:0000775	Chromosome, centromeric region	4.2E4	0.002
GO:0003677	DNA binding	8.1E4	-
GO:0006259	DNA metabolic process	2.8E4	-
GO:0005657	Replication fork	9.3E4	-
GO:0005643	Nuclear pore	8E4	8.3E4
GO:0051329	Interphase of mitotic cell cycle	3.9E4	1.9E4
GO:0051325	Interphase	3.9E4	1.9E4
GO:0000776	Kinetochore	0.002	-
GO:0000793	Condensed chromosome	-	3.3E5
GO:0000779	Condensed chromosome, centromeric region	-	9.2E4
GO:0000777	Condensed chromosome kinetochore	-	6.4E4
GO:0044451	Nucleoplasm part	-	9E4
GO:0000796	Condensin complex	-	0.001
GO:0046930	Pore complex	-	0.002

Table 4.3: Major functional categories up-regulated by either AUY922 or 17-DMAG.

GO Term	Function	BH corrected values AUY922	BH corrected values 17-DMAG
GO:0006986	response to unfolded protein	2.4E9	1.4E11
GO:0051789	response to protein stimulus	5.3E9	4.1E11
GO:0051082	unfolded protein binding	3.5E5	1.5E7
GO:0010033	response to organic substance	8.2E5	1.8E5
GO:0006457	protein folding	-	7.1E6

Discussion

In this study, we use the SILAC approach to compare the proteome-wide changes induced by two structurally distinct Hsp90 inhibitors, AUY922 and 17-DMAG, in Jurkat leukemia cells. AUY922 and 17-DMAG generated conserved proteomics fingerprints with 1190 protein expression changes regulated by both the inhibitors. Moreover, nearly all proteins up-regulated by one inhibitor were up-regulated by the other inhibitor, and proteins down-regulated by one inhibitor were down-regulated by the other inhibitor (with one exception (discussed below)). These similar effects indicate a common mechanism of action.

The classic cellular responses of Hsp90 inhibition are the degradation of Hsp90-dependent client proteins and the induction of chaperones. In our SILAC assays, both AUY922 and 17-DMAG down-regulated several known Hsp90 clients (kinases, helicases and transcription factors). Both the inhibitors up-regulated several members of heat shock protein family. Display of classic hallmarks of Hsp90 inhibition by both AUY922 and 17-DMAG in our SILAC data strongly validate our mass spectrometry assays.

Hsp90 inhibition leads to more down-regulation of the proteome, rather than up-regulation. This was evident in both AUY922 and 17-DMAG raw data (Chapter III, Fig 3.8a & 3.9a, and Fig 3.18a & 3.19a) and after statistical analysis (Fig 4.3). This is also consistent with two recent published SILAC studies of Hsp90 inhibition [56, 57].

Our results are consistent with previous reports that Hsp90-inhibition mainly down-regulates kinases [56, 57] . Both AUY922 and 17-DMAG altered the expression of 30 kinases involved in different biological processes. Among the kinases with altered expression, almost all of them (except Tyrosine-protein kinase Blk) were down-regulated by both the inhibitors. Tyrosine-protein kinase Blk was up-regulated by both AUY922 and 17-DMAG. Thus, the down-regulation of several kinases by both the inhibitors strongly validates our mass spectrometry assays.

114

We report several candidate biomarkers for Hsp90 inhibition in leukemia cells by identifying highly confident protein expression changes common to both AUY922 and 17-DMAG. AUY922 is a drug candidate currently in Phase II clinical trials for the treatment of a wide variety of cancers. Thus, these candidate biomarkers can be used to validate the biological activity of AUY922 in clinical trials. However, whether the changes we observe in cultured cancer cells are preserved in vivo needs to be determined.

Additionally, these candidate biomarkers can also be used to validate novel Hsp90 inhibitors. Long term goals of our laboratory are to determine whether Hsp90 C-terminal binding agents inhibit Hsp90 in vitro in cultured cancer cells. Thus, these biomarkers can be compared to the fingerprint of C-terminal binding agents and can be used determine if both classes of inhibitors have similar of different mechanisms of action.

Our results confirm that MaxQuant is a very reliable proteomics software for analyzing SILAC data. The expression changes we identified using MaxQuant were highly similar between both Hsp90 inhibitors. Moreover, they were also previously identified in our lab using the label-free proteomics techniques of spectrum counting. Thus, all these validations give us high confidence in the quality of the outcome provided by MaxQuant.

However, we did encounter that MaxQuant has certain limitations. It was difficult to compare MaxQuant outputs from two different drug treatment experiments, since MaxQuant provides slightly different lists of identifiers to the proteins in the two experiments searched in two different MaxQuant runs. In the output, MaxQuant provides all the protein identifications that a peptide might belong to. The protein identifications that MaxQuant provides along with the major protein identification differ for each experiment searched in different MaxQuant searches. Therefore, it is difficult to compare two experiments searched in different MaxQuant runs.

As one solution, running all of these files from different experiments in one MaxQuant run allows to overcome this problem. However, this approach compromises downstream statistical analysis. This results in the reduction of R^2 values (as shown for AUY922, Table 4.4), thus misrepresenting reproducibility.

To compare our SILAC based studies of Hsp90 inhibition to two recently published SILAC based studies of Hsp90 inhibition [56, 57], we attempted to cross reference our list of significant protein expression changes to those identified in these two studies. As discussed above, MaxQuant output provides multiple accession numbers to the proteins and genes, but this output for protein identity is not consistent, and does not exactly match across the different searches / studies. By using bio-informatics tools (courtesy of Tyler Warwick, Oklahoma State University) to combine protein lists form two different experiments we were only able to match 1/3rd of the total proteins from two different experiments. Thus, it was difficult to compare the results from the three studies, particularly in light of the large lists of protein expression changes identified. Instead, we compared results at the GO level.

Comparing GO analysis results from our study to those of Mann [56] and Kuster [57], we conclude that the effects of structurally diverse Hsp90 inhibitors are highly conserved across different cell lines and among the inhibitors. These conclusions are based on the observation that the processes affected in all the three studies were nearly indistinguishable despite the differences in the inhibitors, doses, cell lines, and experimental designs used (Tables 4.5 & 4.6). In contrast to these two SILAC studies, we did not observe a significant enrichment of GO terms associated with DNA repair and damage and proteasome core complex. We speculate that this might be due to the high micro-molar concentration of Hsp90 inhibitors used in those studies as opposed to the low nano-concentrations used in our study. We speculate that use of high doses of Hsp90 inhibitors results in apoptosis, thus leading to the up-regulation of proteasomal machinery. Down-

Table 4.4: Comparison of the R^2 values across the biological replicates in AUY922 data, by searching AUY922 data alone in MaxQuant versus searching AUY922 data along with 17-DMAG data in MaxQuant.

AUY922	R^2 values-When searched individually in MaxQuant	R^2 values-When searched along with 17-DMAG data in MaxQuant
BR1 vs. BR5	0.772	0.535
BR1 vs. BR4	0.771	0.614
BR1 vs. BR3	0.833	0.622
BR1 vs. BR2	0.834	0.653
BR2 vs. BR5	0.804	0.641
BR2 vs. BR4	0.844	0.651
BR2 vs. BR3	0.843	0.668
BR3 vs. BR5	0.806	0.646
BR3 vs. BR4	0.842	0.670
BR4 vs. BR5	0.828	0.661

regulation of DNA damage and DNA repair proteins might also be a cellular consequence of apoptosis.

We also observed that some of the GO terms from Kuster's lab data had very high p-values compared to p-values from our data and the data from Mann's lab (Table 4.6). We speculate that this might be because, we and Mann's lab used a 1.5 fold cut off whereas Kuster's lab did not. Using a 1.5 fold change criterion might result in the elimination of several proteins that are functionally related, thus resulting in the reduction of GO p-values.

Table 4.5: Comparison of the GO terms enriched in our study to the GO terms enriched in HeLa cells treated with 50 μM 17-DMAG.

GO term	Function	Hela cells treated with 50 μM 17-DMAG	Jurkat cells treated with AUY922	Jurkat cells treated with 17-DMAG
GO:0006259	DNA metabolic process	1E15	2.8E4	-
GO:0006986	Response to unfolded protein	8E12	2E9	1.38E11
GO:0016310	phosphorylation	3E9	4.9E7	2.2E5
GO:0006796	phosphate metabolic process	2E8	7.1E6	6.8E5
GO:0006793	phosphorus metabolic process	2E8	7.1E6	6.8E5
GO:0051789	response to protein stimulus	2E6	5.3E9	4.1E11
GO:0006468	protein amino acid autophosphorlylation	5E5	5.4E9	3.2E7
GO:0005694	chromosome	2E4	1.8E6	2E6
GO:0004672	protein kinase activity	5E13	5E12	2.2E10
GO:0003677	DNA binding	3E11	8.1E4	-
GO:0004674	protein serine-threonine kinase activity	1E9	4.3E9	3E6

Only GO terms common to both the studies were shown. The numbers represent the B-H corrected p-values for the selected GO terms.

Table 4.6: Comparison of the GO terms enriched in our study to the GO terms enriched in the SILAC study where four different cell lines were treated with 5-10 μM geldanamycin.

GO Term	Function	Jurkat cells treated with AUY922	Jurkat cells treated with 17-DMAG	Four different cancer cell lines treated with geldanamycin [57]			
				Cal27	Colo205	K562	MDAMB231
GO:0004672	Protein kinase activity	5.0E-12	2.2E-10	6.5E21	2E7	4.5E19	5E11
GO:0005524	ATP binding	3.6E-10	1.5E-07	2.4E38	1.1E28	1.2E29	1.8E21
GO:0032559	Adenyl ribonucleotide binding	6E-10	2.3E-07	2.5E38	1.7E28	1.6E29	2E21
GO:0004674	Protein serine/threonine kinase activity	4.3E-09	3E-06	1E13	0.002	9.5E15	7.1E8
GO:0030554	Adenyl nucleotide binding	9E-09	1.95E-06	1.4E35	1.4E28	8.2E29	1.3E21
GO:0001882	Nucleoside binding	8.2E9	7.5E7	5.9E35	3.1E28	1.1E28	1.3E21
GO:0001883	Purine nucleoside binding	2.3E8	1.9E6	7.9E35	1.6E28	4.2E28	1.7E21
GO:0032553	Ribonucleotide binding	8.2E8	1.1E5	1.5E39	1.3E28	3.9E32	3E20
GO:0032555	Purine ribonucleotide binding	8.2E8	1.1E5	1.5E39	1.3E28	3.9E32	3E20
GO:0006468	Protein amino acid phosphorylation	5.4E9	3.2E7	6.4E17	3.2E5	3.2E13	4.6E9
GO:0017076	Purine nucleotide binding	7.1E7	6E5	2.3E37	1E28	1.4E31	5.5E21
GO:0022403	Cell cycle phase	9.1E8	10E9	2.1E6	0.07	2E12	0.02
GO:0016310	Phosphorylation	4.9E7	2.1E5	1.4E16	1.9E5	8E14	2.6E8
GO:0004386	Helicase activity	4.2E5	5.71E4	4.2E4	0.0003	0.004	-

GO:0007049	Cell cycle	5.4E6	1.6E7	5.9E13	5.5E7	8.4E16	2.6E6
GO:0006796	Phosphate metabolic process	7.1E6	6.8E5	3.7E14	3.9E5	5.8E12	5.3E8
GO:0006793	Phosphorus metabolic process	7.1E6	6.8E5	3.7E14	3.9E5	5.8E12	5.3E8
GO:0005654	Nucleoplasm	1.9E5	1.4E5	8.4E7	0.0003	5.1E8	0.01
GO:0031981	Nuclear lumen	7E5	4.7E6	1.4E8	0.0001	4.3E8	0.03
GO:0000166	Nucleotide binding	2.3E4	-	1.9E38	1.3E32	4.4E36	1.5E19
GO:0022402	Cell cycle process	1.3E4	8.2E6	7.3E7	6.5E5	2E16	0.0003
GO:0000278	Mitotic cell cycle	1.4E4	6.6E5	4E7	4.8E5	1E16	0.002
GO:0005643	Nuclear pore	8E4	8.3E4	2E4	0.0008	0.0003	0.002

Only GO terms common to both the studies were shown. The numbers represent the B-H

corrected p-values for the selected GO terms. P values of the GO terms for the data from Wu et

al. were obtained from supplemental GO analysis excel sheet provided along with their

publication.

To validate the Hsp90 inhibitor-induced changes in protein expression identified in our

spectrum assays, we compared them to the protein expression changes identified in our SILAC

assays (Fig 4.8). The majority (87%) of the union of the sets of AUY-induced and 17-DMAG-

induced protein expression changes identified in our spectrum counting assays were also

identified in our SILAC assays (Fig 4.8). However, in our SILAC assays we identified 1148

additional changes that were not apparent in the spectrum counting assays (Fig 4.8). Because

these expression changes were conserved between both Hsp90 inhibitors used for the SILAC

assays, we are confident that they are real. Failure to detect them by spectrum counting reflects

the weakness of the spectrum counting technique. In the summary, high degree of similarity

between spectrum counting results vs. the SILAC results gives us confidence in both the assays.

However, in terms of the number of significant protein expression changes identified, SILAC is

superior to spectrum counting.
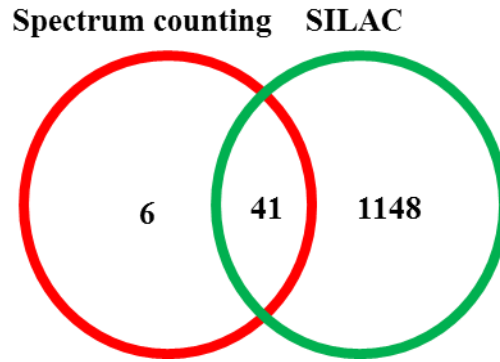
Figure 4.8: Comparison of the significant protein expression changes identified from spectrum counting assays to the significant protein expression changes identified from SILAC assays.

Proteins identified as significantly altered by both AUY922 and 17-DMAG (Student's T-test p values < 0.05) in spectrum counting assays were compared to the proteins identified as significantly altered by both AUY922 & 17-DMAG in SILAC assays (One sample T-test followed by Storey FDR correction). For this comparison, we selected the proteins with T-test p values < 0.05 in spectrum counting assays and the proteins with Storey corrected values < 0.05 in SILAC assays. Neither set was truncated by a fold change threshold.

CHAPTER V

Protein folding antagonist AZC potentiates the anti-proliferative effects of AUY922 in Jurkat leukemia cells.

Introduction

In our spectrum counting and SILAC assays, several chaperones were found to be up-regulated by Hsp90 inhibitor AUY922, with a magnitude greater than that of the down-regulated proteins. These results suggested that AUY922 causes protein folding burdens. Therefore, we speculated the protein folding burdens caused by AUY922 can be enhanced by combinatorial treatments with other protein folding antagonists.

Thus, we tested the anti-proliferative effects of AUY922 in Jurkat leukemia cells by combinatorial treatment with a protein folding antagonist L-azetadine-2-carboxylic acid (AZC). AZC is a proline analog that gets incorporated into newly synthesized proteins and leads to protein folding burdens by destabilizing proteins [107-110]. We also tested the anti-proliferative effects of AUY922 in the presence of another protein folding antagonist, namely tunicamycin. Tunicamycin inhibits N-glycosylation of proteins in the endoplasmic reticulum, and causes ER protein folding burdens. We further tested whether AUY922, AZC, and tunicamycin share conserved mechanisms, by comparing the proteomic fingerprints of cells treated with either of these drugs, or combination of AUY922 and AZC, using the Stable Isotope Labeling with Amino acids in Cell culture (SILAC) approach.

Materials and Methods

Materials used in this study were the same as described in Chapter II and chapter III. Conditions used to culture Jurkat cells were described in Chapter II.

AUY922 and AZC combinatorial drug treatments

For treatment with two different drugs, cells were seeded in 96 well plates at a density of 10,000 cells/100ul/well. After twenty four hours, cells were treated with indicated concentrations of the 1st drug or with DMSO. Following drug treatment, cells were incubated at 37°C in a CO_2 incubator. After ten hours of incubation, cells were treated with indicated concentrations of the second drug or DMSO. After 38 hours of incubation with 2nd drug, cell viability was determined using Cell Titer Aqueous One Solution Cell Proliferation Assay (MTS) reagent as described in Chapter II. All experiments were performed in three biological replicates.

SILAC labeling, drug treatments and preparation of samples for LC-MS/MS analysis

Jurkat cultures adapted to SILAC heavy media were treated with IC_{50} concentrations of either AUY922 (15 nM), or AZC (1 mM) or tunicamycin (130 ng/ml) for 48 hours. For control experiments Jurkat cultures adapted to SILAC light media were treated with DMSO. After 48 hours of treatment with drugs or DMSO, cultures were harvested, lysates from each drug treatment were mixed in 1:1 ratio (50 µg of treated and 50 µg of control) and samples were prepared for mass spectrometry using methods as described in Chapter III. For AZC and AUY922 combinatorial drug treatments, heavy labeled Jurkat cultures were pre-treated with IC_{50} concentration of AZC (1 mM), and after 10 hours of AZC treatment, cultures were treated with IC_{50} concentration of AUY922. For control experiments Jurkat cultures adapted to SILAC light media were treated with DMSO. After 38 hours of AUY922 treatment cultures were harvested and samples were prepared for mass spectrometry using methods as described in Chapter III.

MaxQuant searches and statistical analysis

Raw MS/MS files from low dose AUY922, AZC, AUY-AZC data were all searched in one MaxQuant run. Tunicamycin was searched alone in a separate MaxQuant run. Statistical analysis was performed on only the proteins that had intensities in both control and treated samples in all three biological replicates. Statistical tests and criteria used were the same as described in Chapter IV.

Results

The induction of chaperones and chaperonins (T-complex proteins) identified in our spectrum counting assays and SILAC assays suggested that part of the cytotoxic effects of Hsp90 inhibitors could be due to a global protein folding burden caused by these inhibitors. Thus, we hypothesized that the cytotoxicity of Hsp90 inhibitors could be enhanced by using them in combination with other protein folding antagonists.

L-Azetadine-2-carboxylic acid (AZC) is a four carbon ring analog of proline (Fig 5.1). Incorporation of AZC instead of proline into newly synthesized proteins compromises protein folding and induces the synthesis of Hsps in cytoplasm and ER [80, 111] . Thus, we tested the anti-proliferative effects of AUY922 in the presence and absence of AZC. The IC_{50} value for AZC for Jurkat cell proliferation was approximately 1 mM (not shown). Pre-treatment of Jurkat cells with AZC, followed by treatment with AUY922 reduced cell proliferation when compared to either drug alone (Fig 5.2). At high doses of AZC (1.6 mM and above), AZC dominated the response. At intermediate doses (0.71 to 1.1 mM), AZC potentiated the effects of AUY922. However, at low doses of AZC (0.2 mM – 0.47 mM) both drugs appeared to have synergistic effects. This conclusion was based on the observation that at low doses AZC by itself has no effects on cell proliferation, AUY922 inhibits proliferation of 20 % of the cells, whereas AZC and AUY together inhibit the proliferation of 40 % of the cells. If the drugs had additive effects then the percent of cells whose proliferation is inhibited should have been between 0 & 20 %.
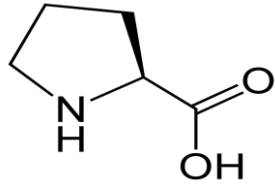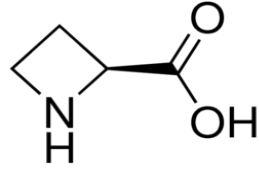
Proline   **L-Azetadine-2-carboxylic acid**

Figure 5.1 (Images from Wikipedia commons)

Figure 5.2-Pretreatment with AZC increases the anti-proliferative effects of AUY922 in Jurkat cells.

Jurkat cultures were pre-treated with indicated concentrations of AZC, followed by AUY922.

Cell proliferation was measured as described in Methods. One star, T-test p value ≤ 0.05; two stars, $p \leq 0.01$; three stars, $p \leq 0.001$.

This indicated that pre-treatment with AZC sensitized Jurkat cells to subsequent treatment with Hsp90 inhibitor. This suggests that AZC treatment results in decreased protein stability in the cell. As a result, AZC treated cells depend extensively on Hsp90 to support these compromised proteins. Inhibiting Hsp90 therefore compromises the proteostasis thus leading to reduced cellular proliferation.

However, reversing the order of addition of the two drugs (AUY922 treatment followed by AZC treatment) did not reduce cellular proliferation as compared to either drug alone (Fig 5.3). We speculate that pretreatment with AUY922 results in chaperone induction which offers protective response from subsequent unfolded protein burdens induced by AZC treatment.

We similarly tested the antiproliferative effects of AUY922 in the presence and absence of another protein folding antagonist, tunicamycin. Tunicamycin (Fig 5.4) inhibits glycosylation in the endoplasmic reticulum and results in the accumulation of under-glycosylated proteins. This leads to ER stress.

The IC_{50} value of tunicamycin for Jurkat cell proliferation was approximately 130 ng/ml (not shown). Tunicamycin exhibited a steeper dose curve when compared to AUY, and was similar to AUY922 by being cytostatic at higher doses. The percent of cells whose proliferation was inhibited by pretreatment of Jurkat cells with tunicamycin, followed by treatment with AUY were the same as the percent of cells whose proliferation was inhibited by either drug alone (Fig 5.5). Even though both drugs appeared to have slightly additive effects at low doses, these effects were not statistically significant. This suggests that tunicamycin compromises ER protein folding but not protein folding in the cytoplasm. Therefore pre-treatment with tunicamycin does not cause the cells to depend on cytoplasmic Hsp90 to fold these unfolded proteins. Therefore, subsequent compromise of Hsp90 function does not grossly reduce the cell proliferation.
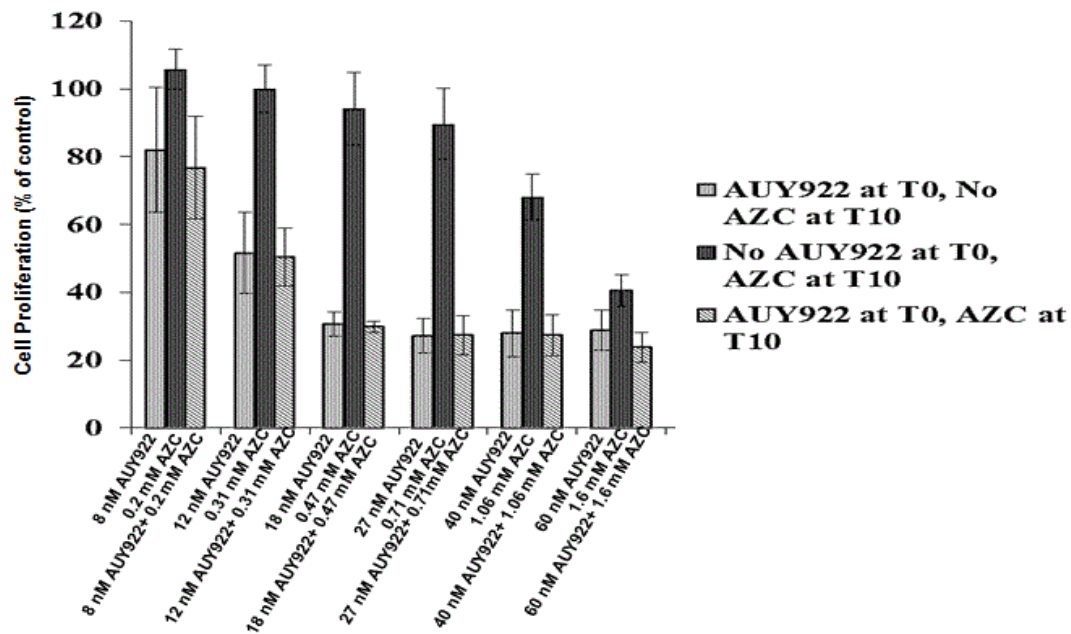
Figure 5.3: Pretreatment with AUY922 does not increase the anti-proliferative effects of AZC in Jurkat cells.

Jurkat cultures were pre-treated with indicated concentrations of AUY922, followed by AZC.

Cell proliferation was measured as described in Methods.
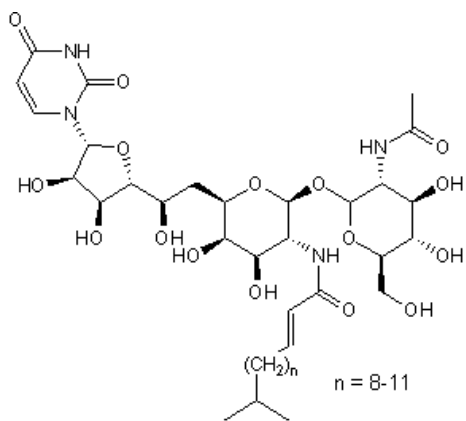
Figure 5.4. Tunicamycin (Image from Wikipedia commons)

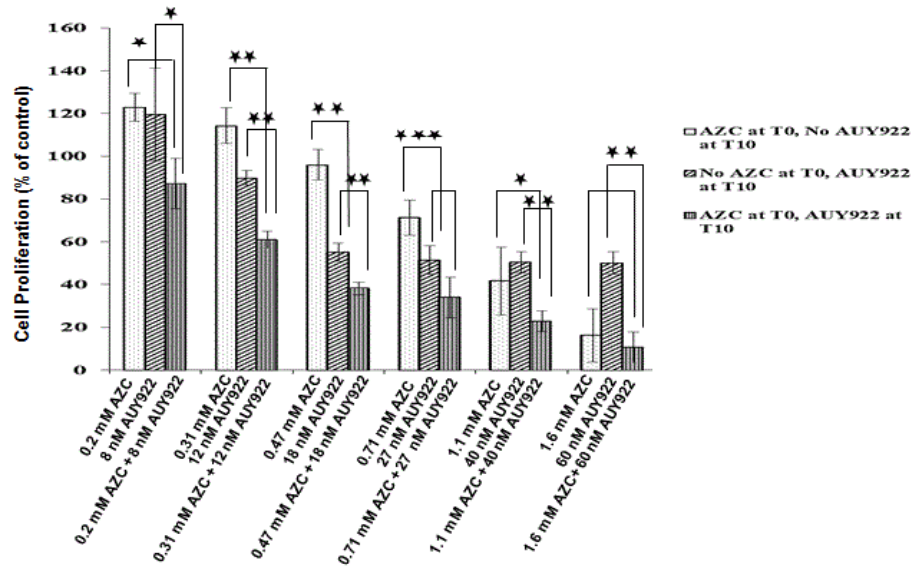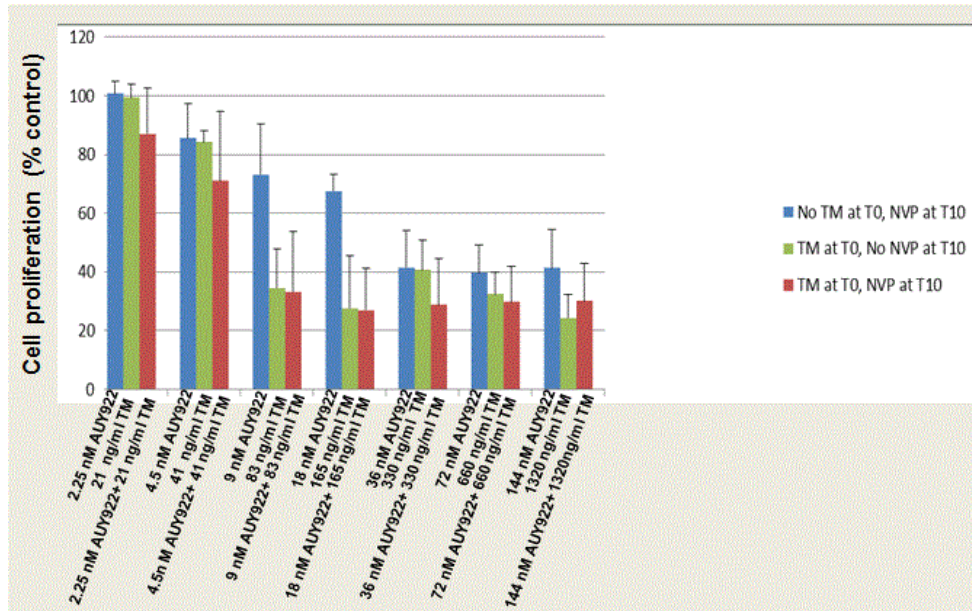***Figure 5.5: Pretreatment with TM does not increase the anti-proliferative effects of AUY922 in Jurkat cells.***

Jurkat cultures were pre-treated with indicated concentrations of TM, followed by AUY922. Cell proliferation was measured as described in Methods.

To compare the proteome-wide changes induced by AUY922, AZC, a combination of AUY922 and AZC, or tunicamycin, SILAC equilibrated Jurkat cultures were treated with IC_{50} doses of each drug (See methods). For AZC and AUY922 combinatorial treatments, Jurkat cultures were pre-treated with IC_{50} dose of AZC followed by treatment with IC_{50} dose of AUY922 after 10 hours of AZC pre-treatment.

To facilitate the bioinformatics comparison of the proteomic fingerprints of all four drug treatments, LC-MS/MS files from the AUY922, AZC, and AZC & AUY922 combination experiments were searched in a single MaxQuant search, as opposed to searching them in individual MaxQuant searches. However, LC-MS/MS raw files from tunicamycin experiment were searched individually. Our initial analysis indicated that tunicamycin induced very few protein expression changes and therefore, we decided to manually compare tunicamycin induced changes to the changes induced by the other three drugs.

Before analyzing the effects of the four drugs on Jurkat proteome, we assessed the quality of the raw data from all these drug treatments using the same approach as described in Chapter III. In all the drug treatments except tunicamycin, reproducibility across the three biological replicates was moderate (Table 5.1). The R^2 values for AUY922 across the three biological replicates ranged from 0.479 to 0.532 (Fig 5.6). The R^2 values for AZC across the three biological replicates ranged from 0.309 to 0.345 (Fig 5.7). The R^2 values for AZC and AUY922 combinatorial treatments across the three biological replicates ranged from 0.478 – 0.553 (Fig 5.8).

Table 5.1: Comparison of the R^2 values across the biological replicates in AZC data, by

searching AZC data alone in MaxQuant versus searching AZC data along with other data in

MaxQuant.

AZC	R^2 values-When searched individually in MaxQuant	R^2 values-When searched along with other experiments in MaxQuant
BR1 vs. BR2	0.592	0.345
BR1 vs. BR3	0.592	0.309
BR2 vs. BR3	0.667	0.391
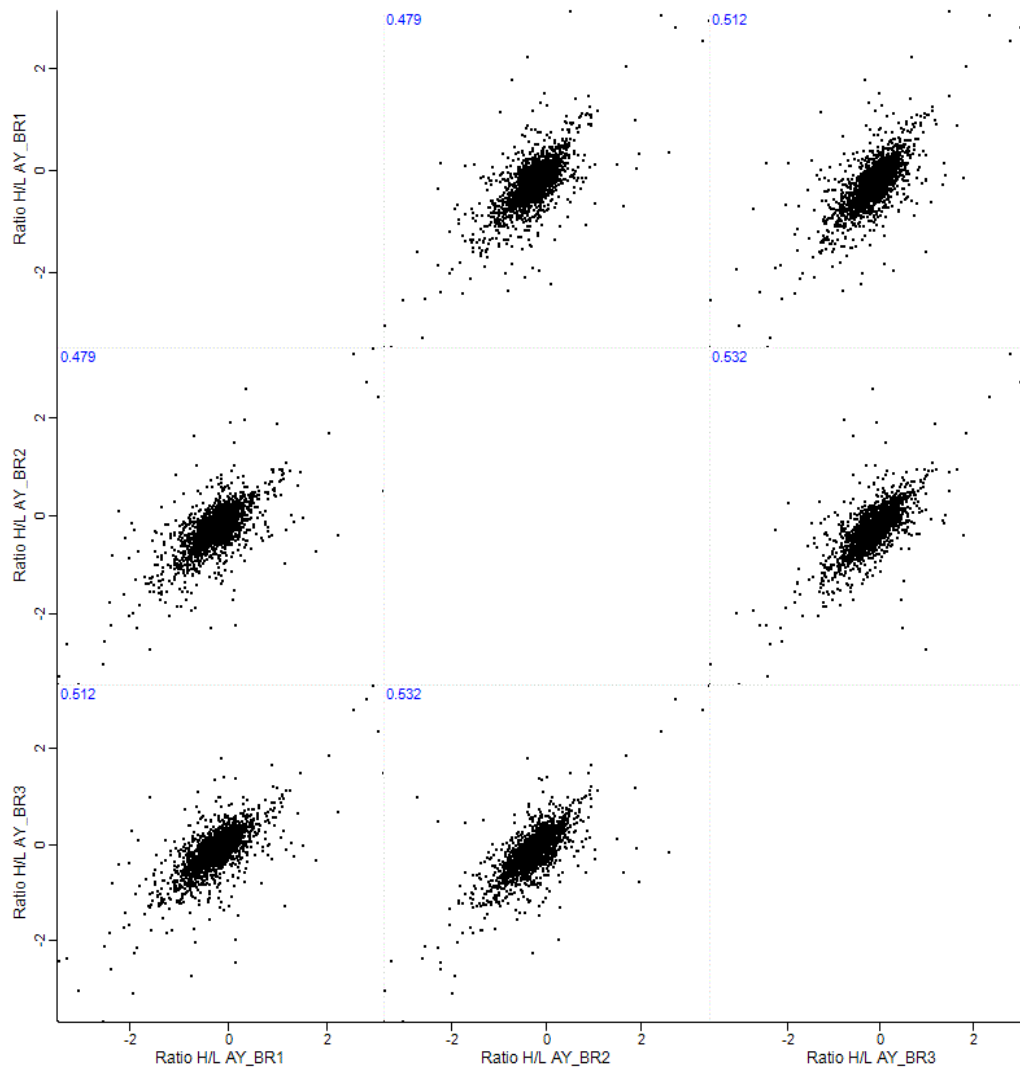
Figure 5.6: Reproducibility across the three biological replicates in Jurkat cultures treated with 15 nM AUY922.

Protein expression changes (Log$_2$ ratio H/L) were plotted across the three biological replicates. The X-axis and the Y-axis represent fold changes in protein expression. In this figure, AY denotes cells treated with AUY922, and BR denotes the individual biological replicate.
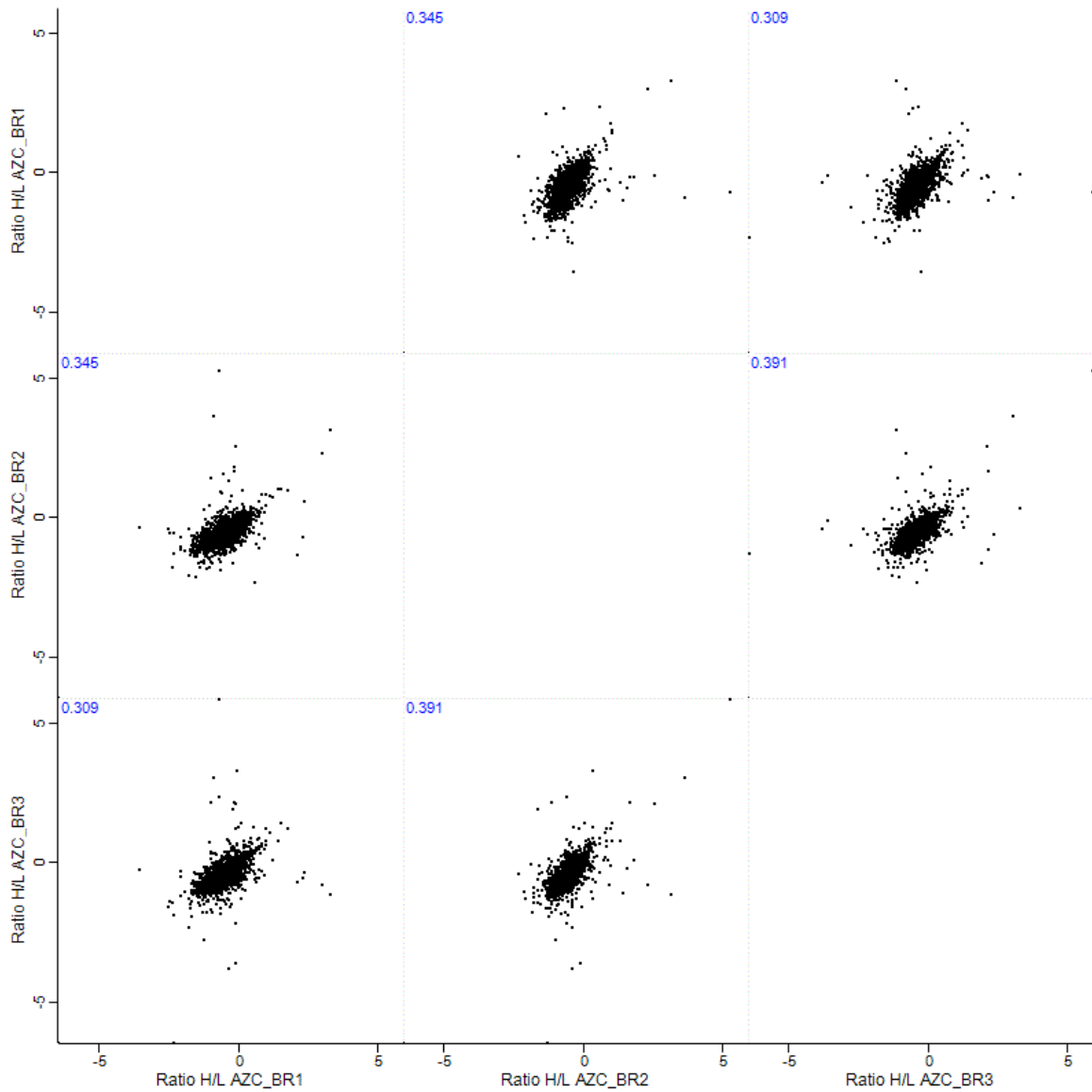
Figure 5.7: Reproducibility across the three biological replicates in Jurkat cultures treated with 1 mM AZC.

Protein expression changes (Log$_2$ ratio H/L) were plotted across the three biological replicates as described in Figure 5.6,
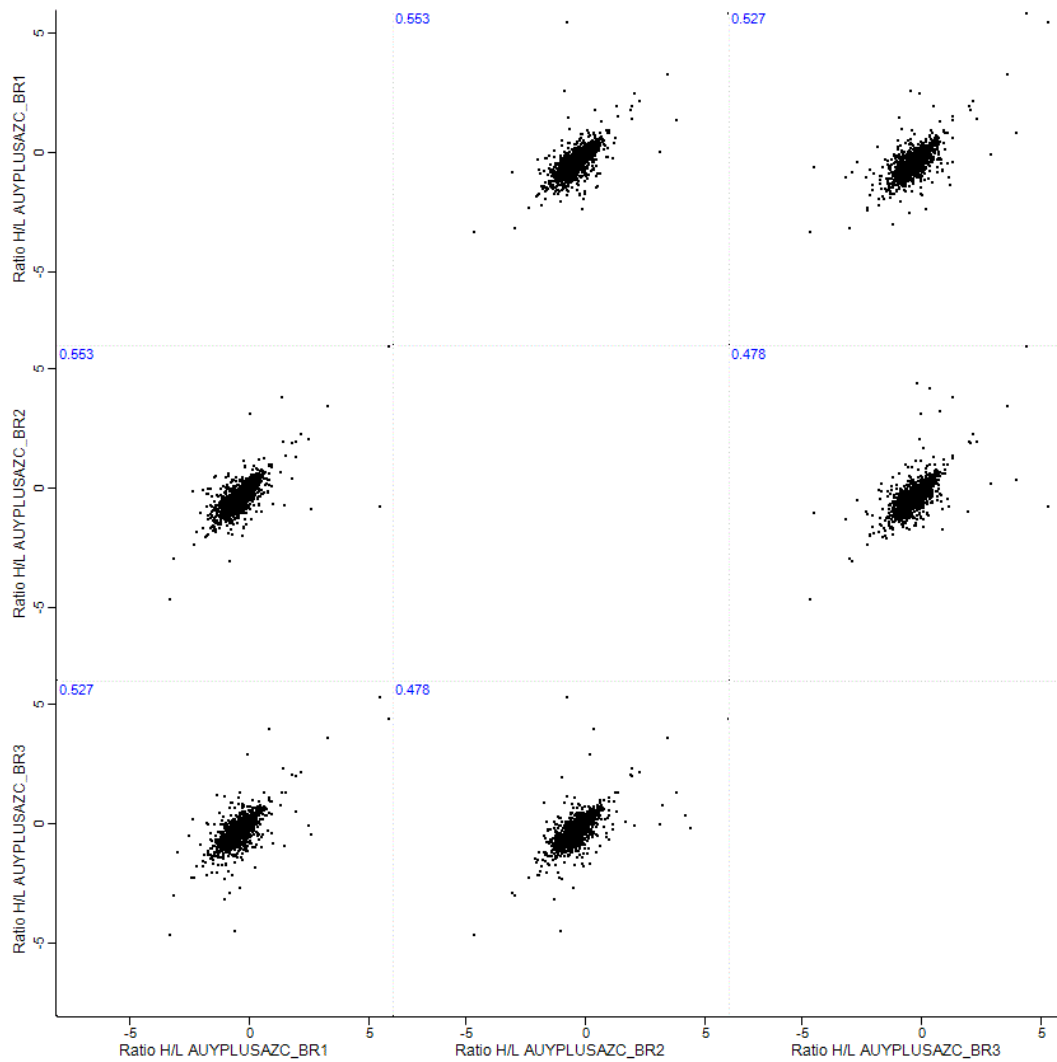
Figure 5.8: Reproducibility across the three biological replicates in Jurkat cultures treated with 1 mM AZC followed by 15 nM AUY922.

Protein expression changes (Log$_2$ ratio H/L) were plotted across the three biological replicates as described in Figure 5.6.

To examine the reasons for these moderate R^2 values observed across the biological replicates in AUY922, AZC, and AZC plus AUY922 combinatorial treatment experiments, the R^2 values in all three experiments obtained from individual MaxQuant searches of each drug treatment experiment we compared versus the R^2 values obtained by searching all three experiments in a single MaxQuant search. This revealed that searching the files from all three experiments in one MaxQuant search reduced the R^2 values (Example AZC -Table 5.1). Thus, we concluded that moderate R^2 values observed in AUY922, AZC and combinations of AUY and AZC were not due to problems with reproducibility, but because of searching all files in one MaxQuant search.

Reproducibility across the three biological replicates in tunicamycin dataset was also low, with R^2 values ranging from 0.215 to 0.278 (Fig 5.9), even though, the Tunicamycin files were searched as an individual set in MaxQuant. We speculated that these low R^2 values were due to the drug inducing relatively minor changes in the proteome.

Data from all the experiments was normalized using the normalization approach described in Chapter III. Normalization minimized variability across the biological replicates (not shown) in data from all the drugs, but without compromising the quality of the data (Fig 5.10-5.13).
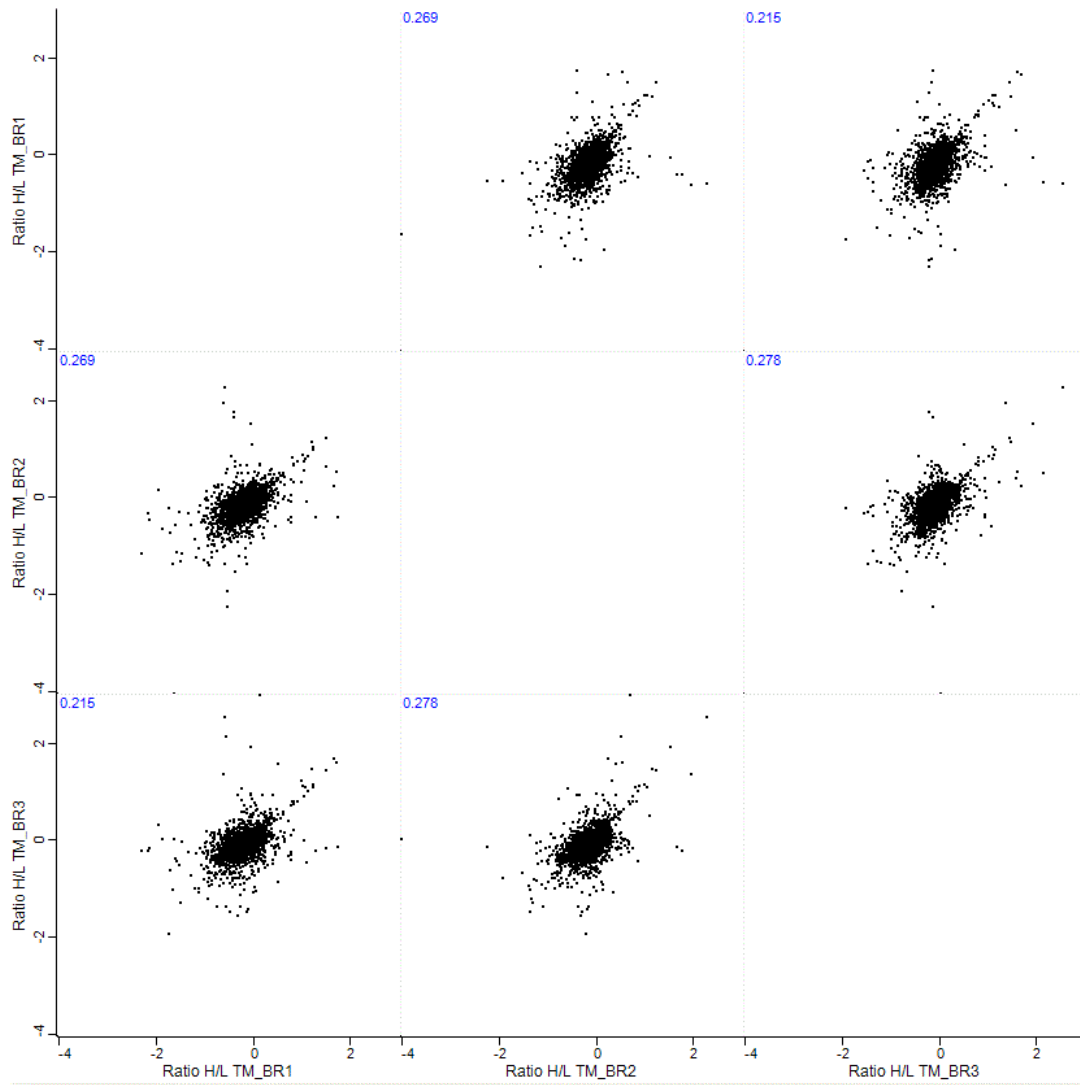
Figure 5.9: Reproducibility across the three biological replicates in Jurkat cultures treated with 130 ng/ml tunicamycin.

Protein expression changes (Log$_2$ ratio H/L) were plotted across the three biological replicates as described in Figure 5.6.

A.

B.
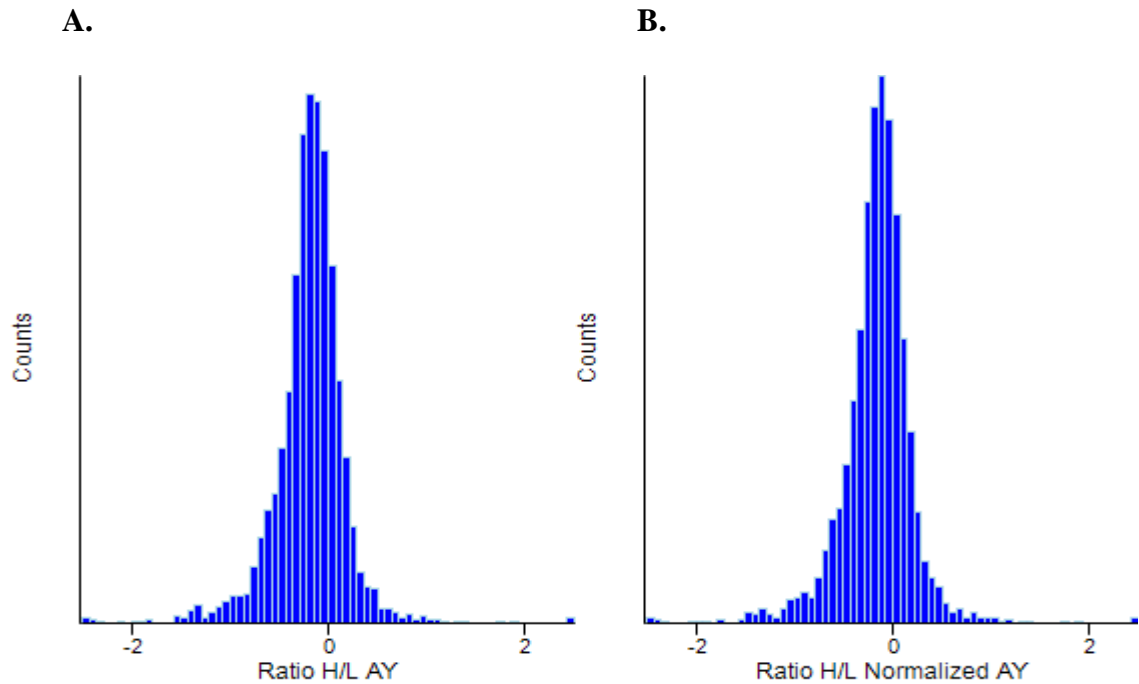
Figure 5.10: Histograms of average protein expression of all three biological replicates in cells treated with AUY922 before and after experiment-level normalization.

Ratios of H/L intensities from all the three biological replicates were averaged and plotted as histograms before (Panel A) and after (Panel B) normalization. The X-axis represents binning of proteins based on intensity. The Y-axis represents the number of proteins in each bin.
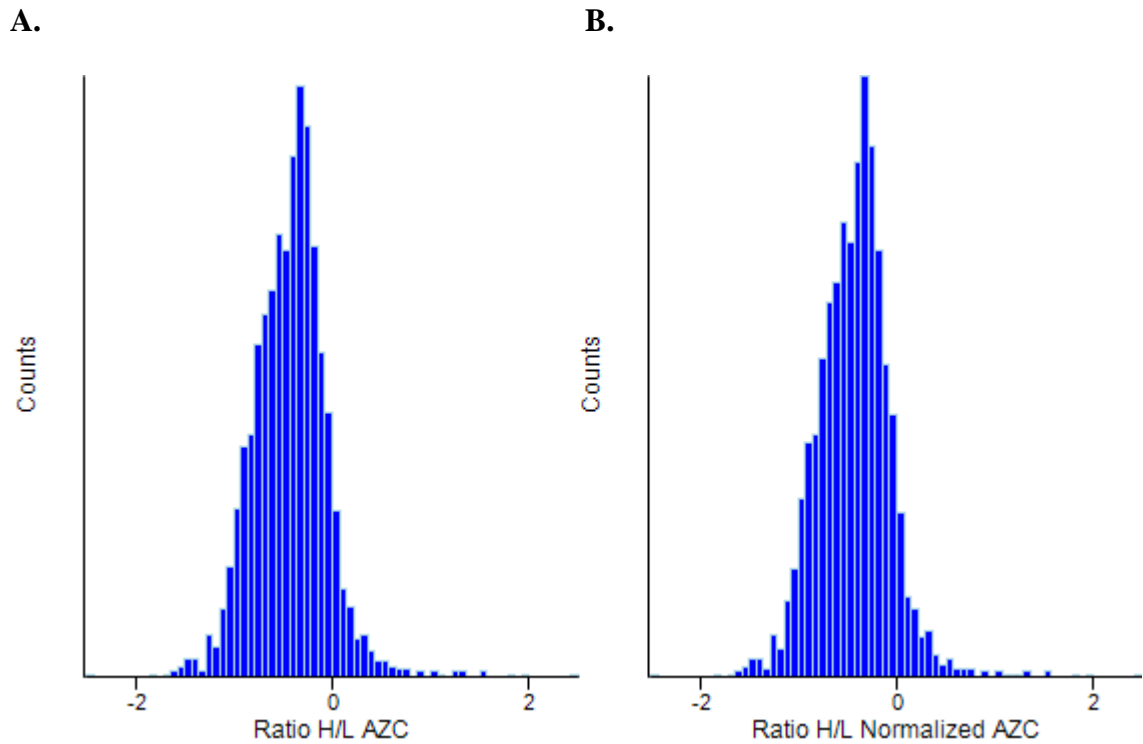
Figure 5.11: Histograms of average protein expression of all three biological replicates in cells treated with AZC before and after experiment-level normalization.

Ratios of H/L intensities from all the three biological replicates were averaged and plotted as histograms before (Panel A) and after (Panel B) normalization as described in Figure 5.10.

A.   **B.**
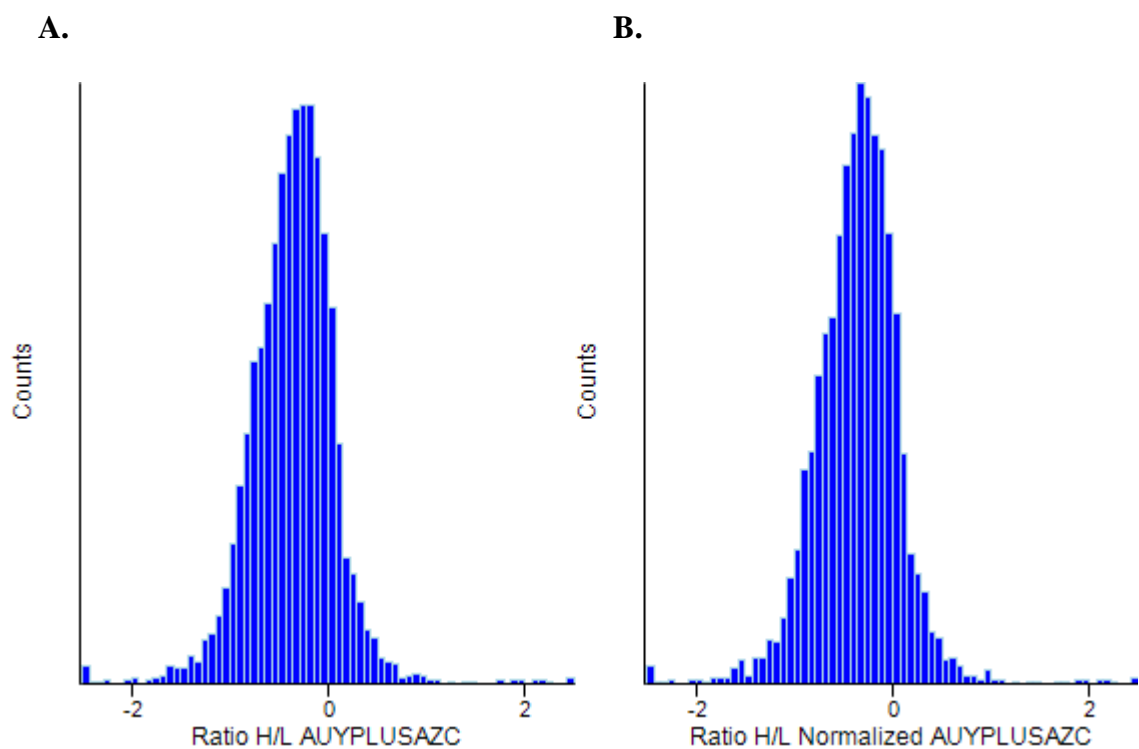
***Figure 5. 12: Histograms of average protein expression of all three biological
replicates in AUY 922 and AZC combinatorial treatments before and after experiment-
level normalization.***

Ratios of H/L intensities from all the three biological replicates were averaged and plotted as
histograms before (Panel A) and after (Panel B) normalization as described in Figure 5.10.

A.   **B.**
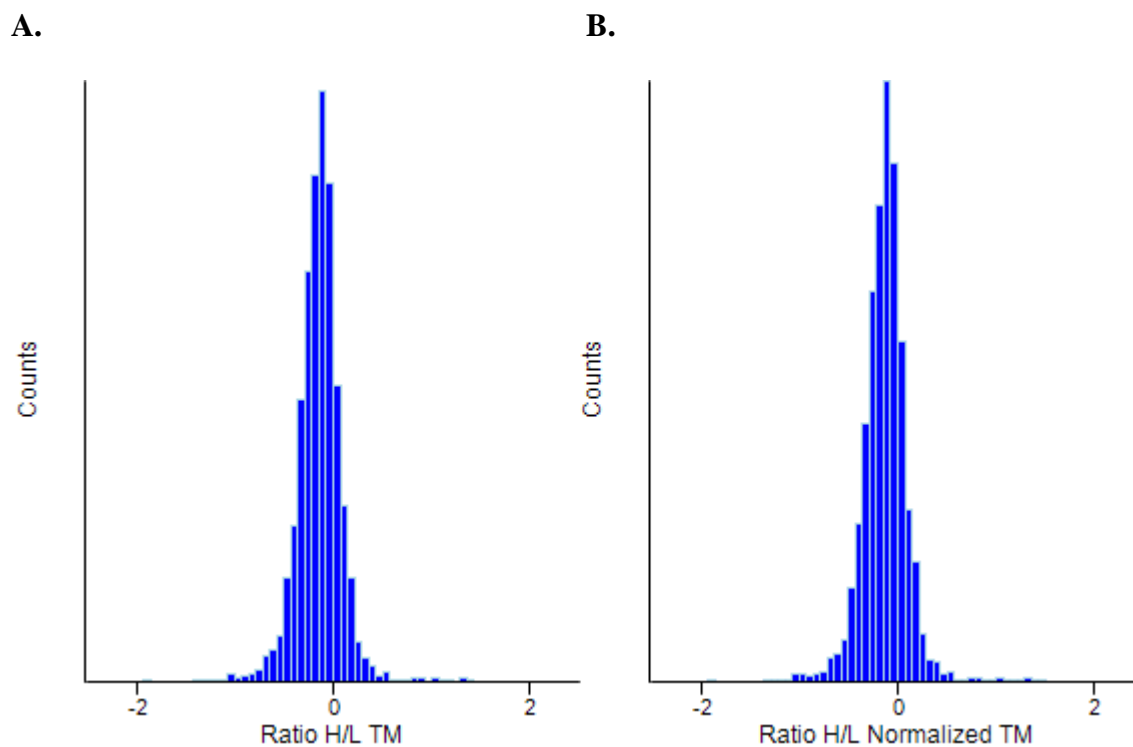
Figure 5.13: Histograms of average protein expression of all three biological replicates in tunicamycin dataset before and after experiment-level normalization.

Ratios of H/L intensities from all the three biological replicates were averaged and plotted as histograms before (Panel A) and after (Panel B) normalization as described in Figure 5.10.

By analyzing H/L ratio histograms from all the four experiments, our raw SILAC ratios implied down-regulation across all the proteome (e.g., Fig 5.10). Therefore, we wanted to ensure that the heavy and light lysates were mixed in a 1:1 ratio (50 µg of lysate from treated cells & 50 µg from control cells). To test this, we averaged all of the light protein intensities and all of the heavy protein intensities from each bio-replicate, and compared them (Table 5.2). Results showed that the average H/L ratios in AUY922 and tunicamycin experiments were close to 1.0 indicating there were no gross problems during the mixing of control and treated samples. Therefore, we concluded that the down-regulation bias in AUY922 and tunicamycin experiments was not due to improper mixing of heavy and light lysates, and instead reflected large real changes in the Jurkat proteome. We also confirmed that the down-regulation bias was not due to improper mixing by comparing H/L ratios for a selected list of house-keeping proteins in AUY922 and tunicamycin experiments (Table 5.3). The average housekeeping H/L ratios were close to 1.0 in both the AUY922 and tunicamycin experiments (Table 5.3). Thus, these results reinforced our conclusions that the down-regulation bias was not due to improper mixing.

However, the average H/L ratios in the AZC and in the AUY922-AZC combinatorial treatment experiments implied problems during the mixing of control and treated lysates (Table 5.2). This was also evident in the H/L ratios of the actin and several other house-keeping proteins (Table 5.3) in both experiments.

Table 5.2: Ratios of the average light and heavy protein intensities from AUY, AZC, AUY and AZC combinatorial treatment and tunicamycin experiments.

		Average of light (control) intensities	Average of heavy (treated) intensities	Ratio H/L intensities
AUY Low Dose	Biorep-1	1.8e9	1.8e9	0.99
	Biorep-2	1.5e9	1.5e9	0.97
	Biorep-3	3.1e9	3.3e9	1.06
Tunicamycin	Biorep-1	1.66e9	1.59e9	0.96
	Biorep-2	2.24e9	2.13e9	0.95
	Biorep-3	3.78e9	3.8e9	1.01
AZC	Biorep-1	1.2e9	1e9	0.85
	Biorep-2	1.5e9	1.2e9	0.79
	Biorep-3	1.1e9	9.8e8	0.87
AUYplusAZC	Biorep-1	1.97e9	1.78e9	0.90
	Biorep-2	1.94e9	1.78e9	0.90
	Biorep-3	1.53e9	1.5e9	0.97

Table 5.3: Comparison of H/L ratios of house-keeping proteins low dose AUY922, AZC, AUY & AZC combinatorial treatment and tunicamycin.

Protein name	AUY Low dose			Tunicamycin			AZC			AUYplusAZC		
	Ratio H/L BR1	Ratio H/L BR2	Ratio H/L BR3	Ratio H/L BR1	Ratio H/L BR2	Ratio H/L BR3	Ratio H/L BR1	Ratio H/L BR2	Ratio H/L BR3	Ratio H/L BR1	Ratio H/L BR2	Ratio H/L BR3
Actin, alpha	0.92	0.96	1.1	1.0	1.0	1.08	0.81	0.74	0.94	0.84	0.79	0.78
Actin, cytoplasmic 2	0.96	0.99	1.1	1.06	1.07	1.13	1.0	0.84	1.1	0.88	0.90	0.95
Tubulin alpha-1A chain	0.85	0.87	1.01	-	-	-	0.64	0.51	0.68	0.59	0.57	0.63
Tubulin alpha-1C chain	0.81	0.83	0.95	0.81	0.83	0.87	0.54	0.62	0.70	0.64	0.65	0.72
Tubulin beta chain	0.88	0.91	0.97	0.90	1.02	1.02	0.65	0.68	0.74	0.65	0.77	0.79
Tubulin beta-4A chain	0.76	0.85	0.87	0.81	0.88	0.94	0.69	0.63	0.70	0.68	0.75	0.65
Tubulin beta-4B chain	0.92	0.89	0.95	0.90	1.0	1.01	0.64	0.68	0.75	0.73	0.71	0.74
Average of all house-keeping proteins	0.87	0.90	0.99	0.91	0.97	1.0	0.71	0.67	0.80	0.72	0.73	0.75

H/L ratios of the house keeping proteins were shown. BR represents biological replicate.

To assess whether the down-regulation we observed is due to real changes or due to improper mixing of light and heavy lysates, we first speculated that the down-regulation bias observed in AZC and AUY and AZC combinatorial treatments might be due to: not identifying proteins with AZC containing peptides in the treated samples. To address this, we re-analyzed the protein expression ratios in AZC-treated cells using MaxQuant, but specifying proline to AZC as a variable modification (- 14.00 Da). Out of the total 58,494 peptides identified, only 1805 peptides had AZC as a modification and the AZC peptides were not specific to Heavy samples. However, the majority of the proteome was down-regulated. Subsequently, we speculated that MaxQuant might not be able to properly identify AZC-modified peptides. To address this question, we searched one LC-MS/MS file from the AZC experiment using a different search engine (Mascot), specifying AZC as a variable modification. We then validated the Mascot results using Scaffold. Of the total peptides that Mascot identified, 28 putative AZC peptides were identified. Close inspection of each peptide's MS/MS spectra showed that very few major ion fragments could be assigned to contiguous series (ladder) of hypothetical b & y ions. These results were consistent with the results obtained from MaxQuant, suggesting that AZC peptides were not being detected. Moreover the AZC peptides detected were not specific to treated samples. This strongly suggested that AZC peptides were not being identified. Thus, because AZC has been shown to be readily incorporated into proteins in cultured cells, we concluded that the AZC peptides were not identifiable on the basis of their MS/MS fragmentation patterns.

Since we were not able to identify AZC peptides by specifying AZC as a variable modification, we re-analyzed the protein expression ratios in AZC treated cells using MaxQuant, but by specifying proline to AZC as a fixed modification instead of variable modification to effectively

eliminate proline containing peptides from the database. Out of the 1818 peptides subsequently identified by MaxQuant, only 26 peptides contain proline (as an AZC modification). However, the ratios of H/L intensities still implied that the samples were not properly normalized. Thus, we concluded that problem is not just due to failure to identify AZC-peptides.

Because we could not correct the apparent H vs. L ratio defects by any of the methods above, we normalized the results from experiments using cells treated with AZC alone or with the AUY-AZC combination. To do this, the 3 light channels and the 3 heavy channels were first normalized using the experiment-level normalization approach described in Materials and Methods of Chapter III (Light intensities were normalized to average light intensities, heavy intensities were normalized to average heavy intensities). Following this experiment-level normalization, the light intensities and the heavy intensities were normalized to each other as shown below.

After performing this correction, the average of ratio of H/L intensities in each of the experiments involving AZC was 1.0. This was also evident in the histograms plotted before and after H/L ratio correction (Fig 5.14 & 5.15).

Correction factor $_{Light\ intensities}$ = Average $_{intensities\ (L-\ channel)}$ / Average $_{intensities\ (H+L-\ channel)}$

Correction factor $_{Heavy\ intensities}$ = Average $_{intensities\ (H-\ channel)}$ / Average $_{intensities\ (H+L-\ channel)}$

Corrected intensity of a protein $_{L-channel}$ = Intensity of a protein $_{L-channel}$ / Correction factor $_{Light\ intensities}$

Corrected intensity of a protein $_{H-channel}$ = Intensity of a protein $_{H-channel}$ / Correction factor $_{Heavy\ intensities}$

A.
B.
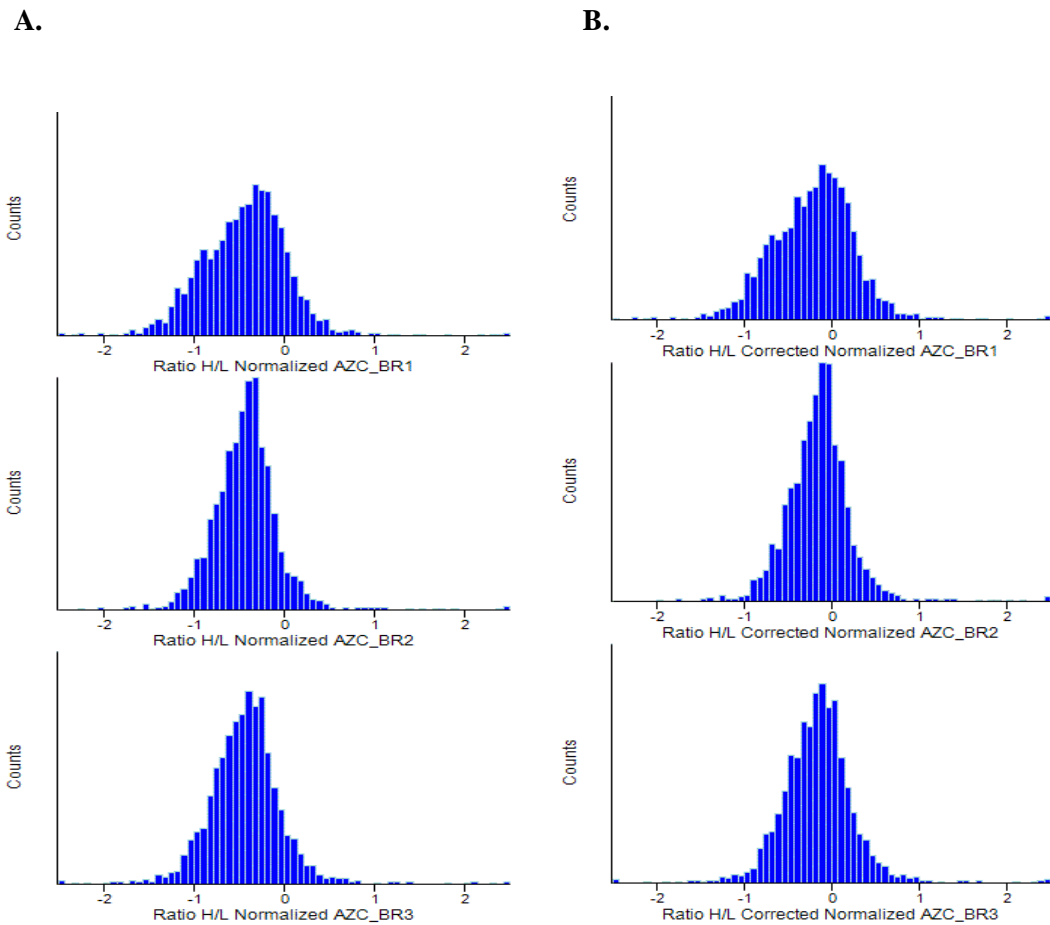
Figure 5.14: Ratio H/L intensity histograms of all three biological replicates in AZC before and after H/L ratio correction.

Ratios of H/L intensities from all the three bio-reps were plotted before (Panel A) and after (Panel B) correcting the H/L ratios .

A.

B.
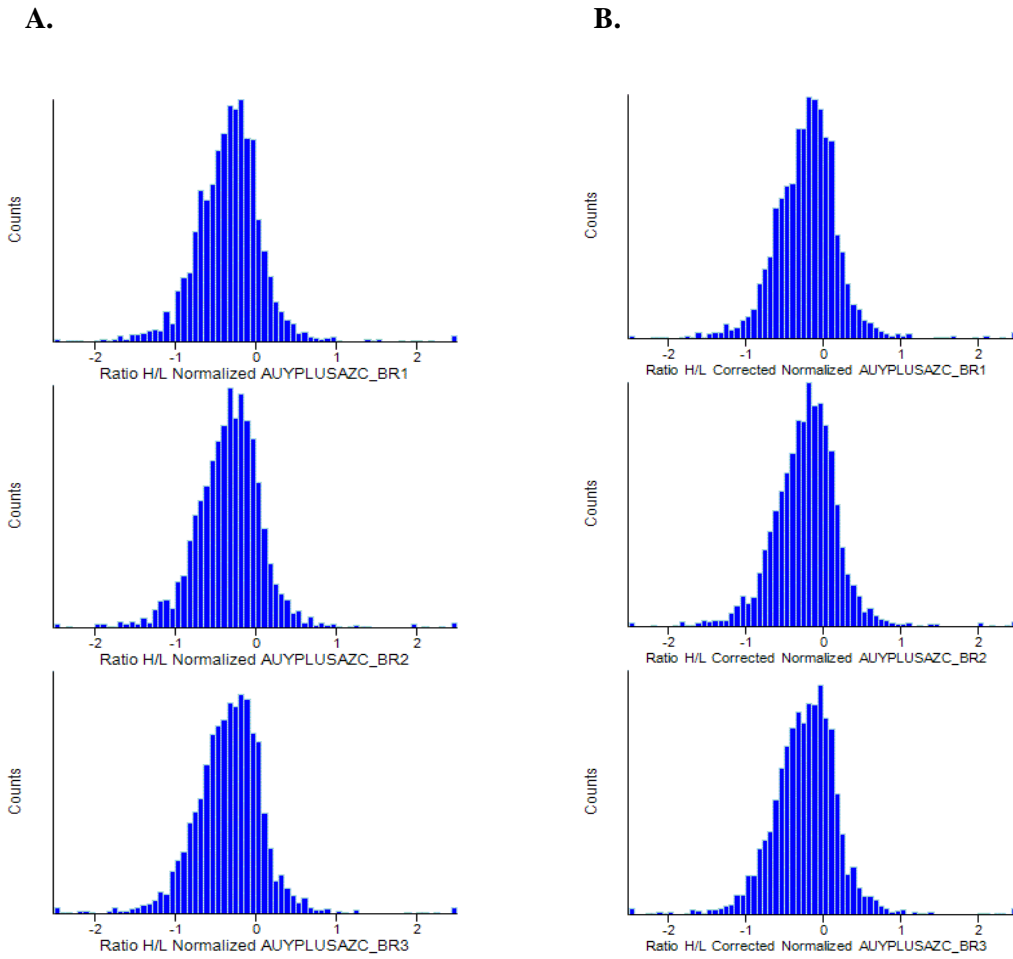
Figure 5.15: Ratio H/L intensity histograms of all three biological replicates in AUY & AZC combinatorial treatments before and after H/L ratio correction.

Ratios of H/L intensities from all the three bio-reps were plotted before (Panel A) and after (Panel B) correcting the H/L ratios .

In this work, our main objective was to determine the biological basis of the combinatorial effects of AUY922 and AZC. We also wanted to determine the biological basis for the absence of similar combinatorial effects between AUY922 and tunicamycin. To accomplish this, heavy label SILAC-equilibrated individual Jurkat cultures were treated with one of four conditions: (i) AUY922 IC_{50} dose (15 nM), hereafter referred to as "low dose AUY" or "LD AUY922", (ii) AZC at its IC_{50} dose (1 mM), hereafter referred to as "AZC", (iii) tunicamycin at its IC_{50} dose (130 ng/ml) hereafter referred to as "tunicamycin" and (iv) a combination of AUY922 at its IC_{50} dose (15 nM) plus AZC at its IC_{50} dose (1 mM) , hereafter referred to as "AUY-AZC". Combinatorial treatments of Jurkat cultures with AUY922 and tunicamycin were not assayed. Following drug treatments, proteins were harvested, subjected to LC-MS/MS, and analyzed by MaxQuant software.

We wanted to compare the protein expression changes induced by the drugs described above to each other, but it is difficult to compare data obtained from individual MaxQuant searches (see Discussion, Chapter IV). To faciliate drug vs. drug comparisons, the datasets above (the 4 drug treatments x 3 biological replicates each) were searched in a single MaxQuant build. As noted below, tunicamycin was omitted. Additionally, three LCMS/MS data files from cells treated with high doses of AUY922 (75 nM, representing 5-7X the IC_{50}, and hereafter referred to as "high dose AUY922" or "HD AUY922") were analyzed, as were three data files from cells treated with high doses of 17-DMAG (150 nM, representing the 5-7X the IC_{50}, hereafter referrred to as "high dose 17-DMAG or "HD 17-DMAG"). The later two treatments served as a benchmark for drugs sharing a common mechanism of action. Since our preliminary analysis indicated that tunicamycin-induced few protein expression changes, tunicamycin data files were searched as a separate MaxQuant build (because the small number of changes could be compared manually).

To determine if these data sets could be compared to each other, we analyzed the total number of protein expression changes identifed in each experiment. Results sohwed that the number of

152

proteins identified in each data set were nearly similar (Fig 5.16). Thus, we concluded that the data from the experiments could be compared.

Protein expression changes were validated using the statistical tests as described in Materials and Methods, using Storey FDR corrected p-value thresholds of < 0.05 and fold-change threshold of ≥ 1.5. Protein expression changes that passed both criteria were considered to be significant changes. These criteria identified 200-400 significant changes in cells treated with LD AUY, AZC, AUY-AZC , HD AUY and HD 17-DMAG (Table 5.4). In contrast, tunicamycin treated cells showed only 58 significant protein expression changes (Table 5.4).

To define the proteomics fingerprint characterestic of a common drug mechanism, we compared proteomes of cells treated with HD AUY922 vs. proteomes of cells treated with HD 17-DMAG. For this comparison, three out of five biological replicates from HD AUY and HD 17-DMAG were used. A total of 76 % of the changes identified in HD AUY922 treated cells were also observed in cells treated with HD 17-DMAG (Fig 5.17, Panel A). Similarly 63% of the changes identified in HD 17-DMAG treated cells were conserved in HD AUY treatments (Fig 5.17, Panel A). Moreover, the magnitude and direction (up-regulation or down-regulation) of their protein expression changes were also conserved (Fig 5.17, Panel B), generating an R^2 value of 0.814. The majority of the changes were represented in the upper right hand or lower left hand quadrants of the scatterplot, and there were few changes in lower right hand quadrant or the upper left hand quadrant of the plot comparing changes among both drugs. (Fig 5.17, Panel B). These observations defined the characterstics of a proteomics fingerprint for drugs sharing a common mechanism, using just three bio-replicates
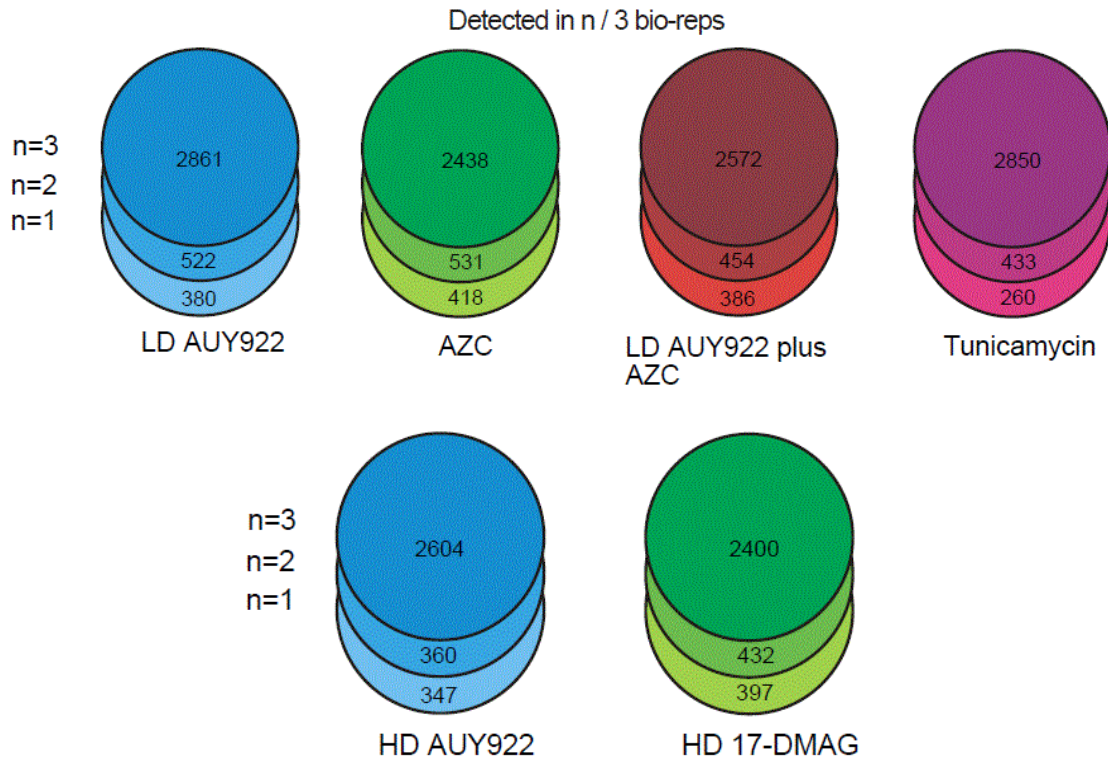
Figure 5.16: Total number of proteins detected across 3 biological replicates in the proteomes of drug-treated Jurkat cultures.

The number of biological replicates is denoted by "n". The n = 3 circle represents the number of proteins identified in 3/3 experiments. The n = 2 crescent represents the difference between the number of proteins identified in 3/3 experiments vs. the number of proteins identified in 2/3 experiments. The n = 1 crescent represents the difference between the number of proteins identified in 3/3 experiments vs. the number of proteins identified in 1/3 experiments.

Table 5.4: Effects of statistical tests and criteria for validating protein expression changes among 6 different drug treatments.

Test and/or criteria	LD AUY922	AZC	LD AUY plus & AZC	Tunicamycin	HD AUY922	HD DMAG
Proteins quantified (all 3 bio-reps)	2854	2429	2569	2807	2596	2397
One sample T-test (P < 0.05)	1115	839	1318	874	1235	1165
Storey FDR correction of one sample T-test p values (< 0.05)	1431	1013	1925	991	1775	1670
Fold change ≥ 1.5	287	338	414	97	299	304
Storey FDR corrected p-value thresholds of< 0.05 and fold change ≥ 1.5	250	265	402	58	288	291

A.

AUY922   17-DMAG

51   158   94

B.
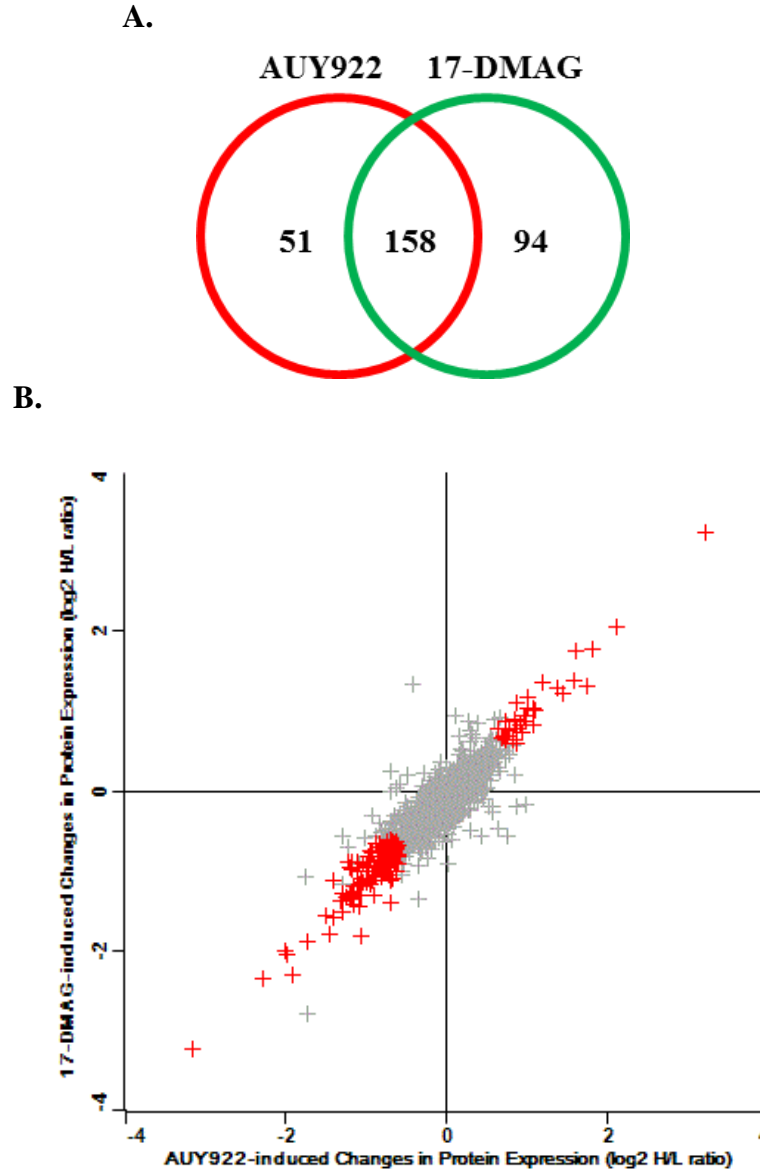
Figure 5.17: Comparison of the significant changes induced by HD AUY922 vs. HD 17-DMAG.

Panel A: Venn analysis of protein expression changes induced by HD AUY922 vs. HD 17-DMAG. Panel B: Comparison of magnitude of changes induced by both inhibitors. The X –axis represents log 2 treated/control (H/L) ratios of proteins in AUY, and the Y-axis represent log 2 H/L ratios of proteins in 17-DMAG. Red crosses represent significant changes caused by both inhibitors, while grey crosses represent insignificant changes in both the inhibitors.

156

Results from AUY922 and AZC combinatorial treatments indicated that inhibition of cellular

proliferation was higher in AUY-AZC treated cells compared to cells treated with each drug

alone. Thus, we predicted that both drugs have similar effects on the proteome. Therefore, we

compared the significant changes identified in each drug. Of the total changes identifed in cells

treated with LD AUY922, 34% of them were also observed in cells treated with AZC. Of the

changes identified in cells treated with AZC, 27% of the changes were also observed in cells

treated with LD AUY922 (Fig 5.18, Panel A). We also plotted the protein expression changes to

demonstrate their magnitude and direction (up or down-regulation) in both drugs (Fig 5.18, Panel

B). The R^2 value for this comparison was 0.298. Moreover, all the proteins showing significant

changes in both drugs were represented in the upper right hand quadrant or lower left hand

quadrant. None of the significant changes conserved to both drugs were represented in lower right

hand quadrant or the upper left hand quadrant. Since 30% of the protein expression changes were

conserved between both drugs, we concluded that the drugs shared similar but not identical

mechanisms.

Because the inhibition of cell proliferation was higher in Jurkat cells treated with a

combinations of AUY922 and AZC compared to either drug alone, we predicted that there would

be more protein expression changes in AUY922-AZC combinatorial treatments compared to

individual drug treatments. To test this, we compared the changes common to LD AUY- treated

cells to those observed in cells treated with AUY-AZC. We saw an increase in protein expression

changes (256 proteins) in cells treated with AUY-AZC compared to cells treated with each drug

alone. The total changes common to cells treated AUY922-AZC and cells treated with LD

AUY922 also increased (Fig 5.19, Panel A). We similarly compared changes common to AZC to

the changes induced by AUY-AZC . The total significant changes common to cells treated with

AUY-AZC and AZC were also higher (Fig 5.19, Panel B).

A.

LD AUY922   AZC

118   61   169
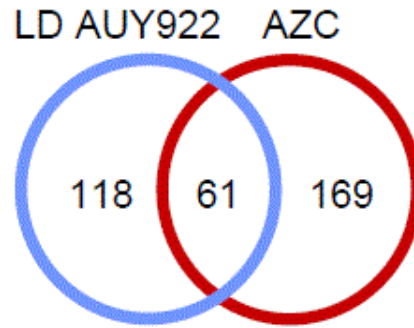
B.
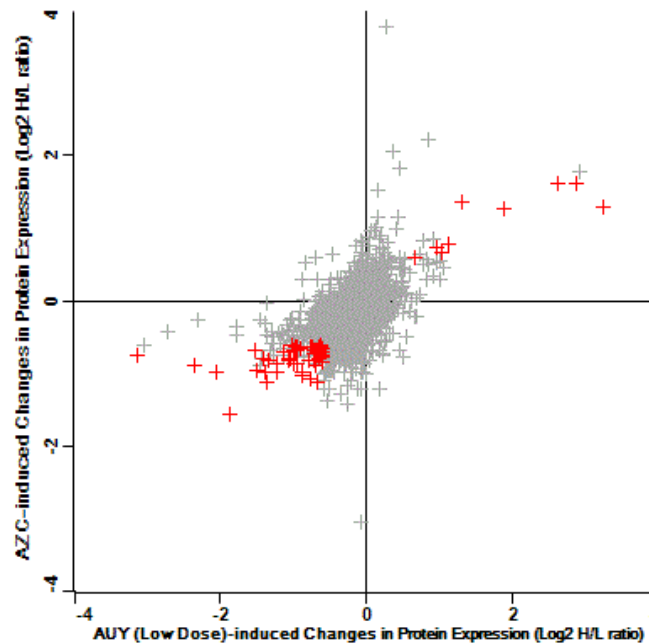
Figure 5.18: Comparison of the significant changes induced by LD AUY922 vs. AZC.

Panel A: Venn analysis of protein expression changes induced by LD AUY922 vs. AZC. Panel

B: Comparison of magnitude of changes induced by both inhibitors. The X –axis represents log 2

treated/control (H/L) ratios of proteins in LD AUY922, and the Y-axis represent log 2 H/L ratios

of proteins in AZC. Red crosses represent significant changes caused by both inhibitors, while

grey crosses represent insignificant changes in both the inhibitors.

A.

B.
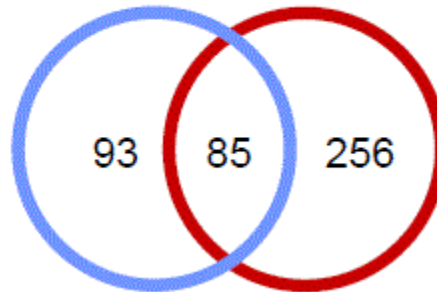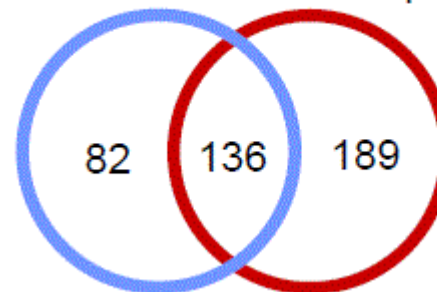
Figure 5.19: Comparison of the significant changes in LD AUY922 vs. LD AUY922 plus AZC, and AZC vs. LD AUY922 plus AZC.

Panel A: Venn analysis of the significant changes induced by LD AUY922 vs. AZC. Panel B: Venn analysis of the significant changes induced by LD AUY922 vs. LD AUY922 plus AZC.

Enrichment of protein expression changes in the combinatorial treatments suggested that some protein expression changes were similarly altered by both AUY922 and AZC (c.f. Fig 5.18, Panel A vs Fig 5.19, Panels A& B).

Since LD AUY922 and AZC appeared to have similar effects on some protein expression changes, we speculated that the down-regulated proteins will be more down-regulated in the combinatorial treatment compared to the individual drug treatments. Similarly, we speculated that the up-regulated chaperones will be more up-regulated in combinatorial treatments, than each drug treatment alone, since both the drugs cause protein folding burdens.

To test if our speculation was correct, we divided the significant protein expression changes into up-regulated and down-regulated. Then we averaged the H/L ratios of all these proteins in each drug treatment (LD AUY, AZC, and AUY- AZC combinatorial treatment). Results indicated that average H/L ratios for the down-regulated proteins from LD AUY and AUY-AZC were not significantly different from each other (Fig 5.20, Panel A). Similarly, the average H/L ratios for the up-regulated proteins from AUY922 and AUY- AZC were also not significantly different from each other (Fig 5.20, Panel B). Since the average H/L ratios of the down-regulated expression changes in LD AUY vs. AUY- AZC were not much different, we concluded that the magnitude of down-regulated protein expression changes was not higher in cells treated with combinations of AUY922 and AZC relative to those observed in cells treated with LD AUY alone.

Out of all the up-regulated proteins, four proteins showed statistically significant changes in LD AUY treated cells vs. AUY-AZC treated cells (Table 5.5). Among these four proteins, three of them were more up-regulated in cells treated with LD AUY compared to cells treated with AUY-AZC. In contrast, the magnitude of up-regulation of Serpin was higher in cells treated with LD AUY-AZC when compared to cells treated with LD AUY922. Surprisingly, these results

A.
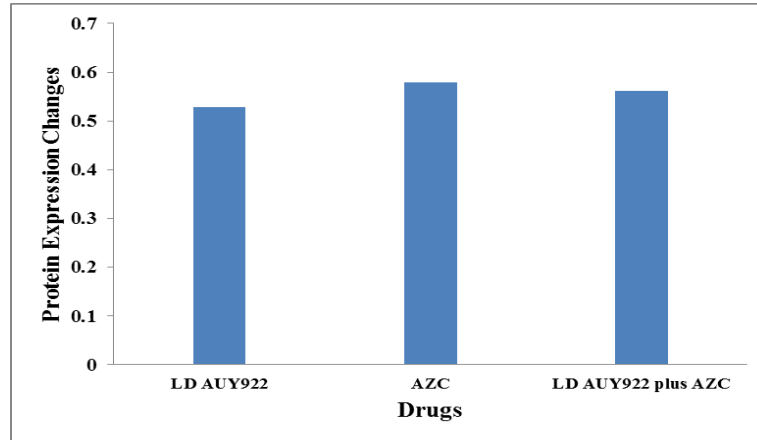
B.
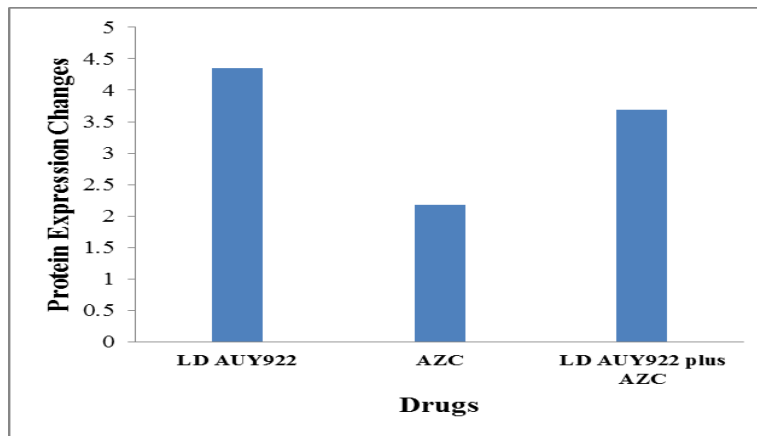
Figure 5.20: Comparison of the average H/L ratios of significant protein expression changes in LD AUY922 vs. LD AUY922 plus AZC.

H/L ratios of the significant protein expression changes in each drug treatment were averaged and compared to each other. Panel A: Comparison of the down-regulated expression changes. Panel B: Comparison of the up-regulated protein expression changes.

Table 5.5: Comparison of the H/L ratios of proteins up-regulated in LD AUY922 treated cells vs. AUY plus AZC treated cells.

Protein names	LD AUY922 H/L ratio				LD AUY922 plus AZC				T-test P-values
	BR1	BR2	BR3	Average	BR1	BR2	BR3	Average	
Bone marrow stromal antigen 2	1.96	2.04	2.22	2.07	1.09	1.47	1.51	1.36	0.017
Serpin H1	8.55	5.75	4.99	6.43	10.8	12	12.54	11.8	0.023
Heat shock 70 kDa protein 1A/1B	7.3	7.01	7.86	7.39	3.84	4.11	4.30	4.08	0.001
Docking protein 2	7.89	11.6	9.79	9.76	1.99	1.39	15.98	6.45	0.562
Heat shock protein HSP 90-beta	1.76	1.49	1.53	1.59	1.51	1.5	1.48	1.49	0.367
Tyrosine-protein kinase Blk	2.25	1.8	1.89	1.98	1.4	1.57	1.33	1.43	0.04
Heat shock protein HSP 90-alpha	2.49	2	2.1	2.2	1.69	1.7	1.67	1.69	0.075
DnaJ homolog subfamily B member 1	4.28	3.45	3.5	3.74	4.37	4.2	4.06	4.21	0.215
Average	4.56	4.39	4.24	4.4	3.34	3.49	5.36	4.06	

Statistical analysis was performed using Student's T-test, two tailed, unequal variance. P values < 0.05 were considered significant.

suggested a different model for the combinatorial effects of AUY922 and AZC (see Discussion).

Our assays of AUY922 and tunicamycin combinatorial treatments suggested that both drugs did not have additive effects on Jurkat cell proliferation (Fig 5.5, Chapter V). Thus, we predicted that the drugs might not share conserved effects on the proteome. To test our prediction, we compared the changes induced by LD AUY to the changes induced by tunicamycin to determine if the protein expression changes induced by both drugs were conserved. Of the significant changes induced by LD AUY, only 3.9% of the changes were observed in cells treated with tunicamycin. Among the tunicamycin induced changes, only 12% of the changes were observed in cells treated with LD AUY (Fig 5.21). Since only 7 out of total 223 protein expression changes were observed between both drugs, we concluded that both the drugs do not have common effects. Moreover, these changes might be false discoveries, based on our FDR threshold of 0.05 (7 out of 172 is 0.04). We did not compare the magnitude of expression changes between both drugs because they were searched separately in MaxQaunt, and thus could not be readily combined for generating scatterplots.

To validate tunicamycin-induced protein expression changes identified in our study, we compared them to tunicamycin-induced changes identified by Bull et al [76]. Only changes common to both studies were shown (Table 5.6). Up-regulation of ER chaperones in our study is consistent with the changes observed by Bull et al [76]. Thus, these results validate our mass spectrometry assays.
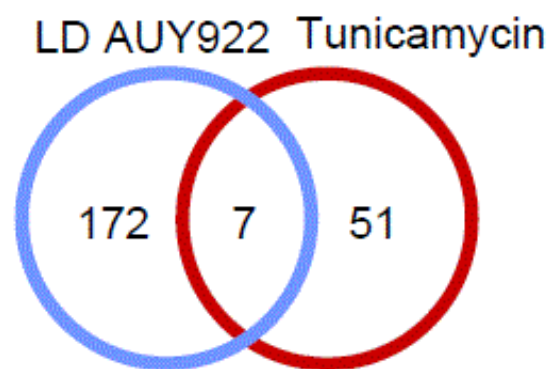
Figure 5.21: Comparison of the significant changes in LD AUY922 vs. tunicamycin.

Venn analysis of the significant changes induced by LD AUY922 vs. significant changes induced

by tunicamycin.

Table 5.6: Tunicamycin-induced protein expression changes common between our study and study from Bull et al.

Protein	Ratio of H/L intensities- Our study	Ratio of H/L intensities (Bull et al. 2012) **Note:** H is control and L is treated
78 kDa glucose-regulated protein	2.64	0.34
Endoplasmin	2.30	0.50
Protein disulfide-isomerase A3	1.73	0.85
Protein disulfide-isomerase A4	2.03	0.47
Protein disulfide-isomerase A6	1.79	0.86
Transferrin receptor protein 1	0.66	1.46
Thymidylate synthase	0.62	1.43
Protein transport protein Sec61 subunit beta	1.72	subunit alpha was up-regulated (0.78)
Lysosome-associated membrane glycoprotein 1	0.64	1.46
Integrin beta-1	0.48	1.56

Important Note: Bull et al. used light labeled cells for tunicamycin treatment and heavy labeled for control. Therefore H/L ratio > 1 means down-regulated and < 1 means up-regulated.

Bull et.al studied the changes induced by 10 μM tunicamycin in human neuroblastoma cells [76]. Values in the right hand column are from Bull et al., Table 1 and supplemental Table 1 and are represented for comparison only.

Discussion

In this study, AZC potentiates the anti-proliferative effects of AUY922 in cultured Jurkat leukemia cells (Fig 5.2). At higher doses, AUY922-AZC combinatorial treatments appear to have simple additive effects on cell proliferation. At lower doses, neither drug inhibits cell proliferation, but combinations of these doses of AZC and AUY922 inhibit the proliferation of cells (Fig 5.2). This hints of drug synergy at low doses. In contrast to AZC, tunicamycin does not potentiate AUY922's anti-proliferative effects (Fig 5.2).

AZC, AUY922, and tunicamycin compromise protein folding in different cellular compartments, and by different mechanisms. AZC is a proline analog. AZC causes global protein folding burdens by getting incorporated into the newly synthesized proteins and destabilizing them [107-109]. The Hsp90 inhibitor AUY922 destabilizes client proteins by compromising Hsp90 function. Although Hsp90 inhibitors GA , 17AAG and PU-H71 induce ER stress and up-regulate ER chaperones [73, 74], reports from fluorescence polarization assays indicate that AUY922 binds weakly to ER chaperone GRP94 when compared to cytosolic Hsp90 [22]. This suggests that AUY922 might be causing protein folding burdens in cytoplasm but not in endoplasmic reticulum (ER). Tunicamycin is a bacterial antibiotic that inhibits N-glycosylation of proteins in the ER and results in the accumulation of unfolded proteins in the ER.

We hypothesize a model for the combinatorial effects of AUY922 and AZC. Both AZC and Hsp90 inhibitors destabilize proteins. When cells are treated with both inhibitors, there is large destabilization of the cellular proteome. This results in additive or synergistic effects of both drugs.

We also hypothesize a model for the absence of combinatorial effects between AUY922 and tunicamycin. In this model, we hypothesize that the protein folding burdens caused by tunicamycin are largely confined to the ER. Whereas results from our SILAC assays and from the literature [22], indicate that AUY922 does not significantly induce ER chaperones. This suggests

166

that AUY922 does not cause ER protein folding burdens. Therefore, the absence for combinatorial effects of AUY922 and tunicamycin might largely be due to compartmentalization of their effects. AUY922 effects might largely be confined to cytoplasm. Whereas tunicamycin effects might largely be confined to ER.

Results from our SILAC assays were consistent with this model. AUY922 and AZC shared some protein targets that were common (Fig 5.18, Panel A). Among these common targets, proteins down-regulated by one drug were down-regulated by the other drug and proteins up-regulated by one drug were up-regulated by the other drug (Fig 5.18, Panel B), thus indicating similar effects. Moreover, we see an enrichment of protein expression changes in the combinatorial drug treatments, when compared to either drug alone (Fig 5.19 Panels A & B). These results are consistent with our model that both AUY922 and AZC compromise protein folding and both cause down-regulation of some common proteins. Also consistent with our model, tunicamycin and AUY922 do not have combinatorial effects, due to compartmentalization of their effects. Similarly, very few protein expression changes were common to AUY922 and tunicamycin (Fig 5.21).

Based on the model we hypothesized, we expected to see a higher magnitude of down-regulation of the protein targets common to AUY922 and AZC in cells treated with AUY-AZC compared to cells treated with each drug alone. Instead we observed that the magnitude of the down-regulation of the common targets was not higher in combinatorial treatments (Fig 5.20, Panel A).

We also expected to see a higher magnitude of chaperone induction in cells treated with AUY-AZC compared to cells treated with each drug alone. However, we did not see more chaperone induction in the cells treated with AUY-AZC like we expected (Fig 5.20, Panel B). Rather, we see that the magnitude of chaperone induction was lower in cells treated with combinations of AUY922 and AZC (Fig 5.20, Panel B & Table 5.4). Thus, these results suggested an alternate model for the combinatorial effects of AUY922 and AZC.

In this new model, combinatorial effects of AUY-AZC on Jurkat cell proliferation are largely due to suppression of chaperone induction, thus depriving cells of chaperone protection. This was evident in our assays where most chaperones are less upregulated (with the exception of Serpin H1) in the dual drug treatment. This suggests that AZC either destabilizes the chaperones or compromises the transcription of these chaperones by compromising the stability of Hsf1. Thus, we conclude that the reason for combinatorial effects of AUY922 and AZC are because of a compromise in the magnitude of chaperone induction.

However, one other possibility exists for the down-regulation of chaperones in AZC treated cells. It should be worth noting that in the AZC treated cells, the misfolded proteins (including chaperones) might be forming aggregates. These aggregated proteins might be lost in the insoluble fractions, thus resulting in low abundance of the aggregated protein in AZC treated samples compared to untreated samples. This speculation needs to be further tested to see if chaperone down-regulation is due to their destabilization and degradation caused by AZC or due to them being lost as insoluble aggregates in AZC treated samples.

However, as described above, the magnitude of up-regulation of one chaperone (Serpin H1), was higher in cells treated with AUY922 and AZC. SerpinH1 is collagen specific molecular chaperone. It is localized in the ER. It is regulated by Hsf1 [112]. Its expression is induced by heat shock [113] . It is also up-regulated upon Hsp90 inhibition. Up-regulation of Serpin H1 is implicated in the synthesis of collagens [114, 115]. We speculate that the upregulation of SerpinH1 in AUY&AZC dual treatments might be to fold the AZC-destabilized-collagen. However, this needs to be further explored.

Summarizing our results, AZC potentiates AUY922's effects by decreasing the magnitude of chaperone induction. This approach is similar to the use of Hsp90 inhibitors in combinations with other inhibitors that compromise chaperone induction. Reikvam et al. [116] showed that Hsp90 inhibitors in combination with Hsp70 inhibitors have increased anti-proliferative activity in acute myeloid leukemia cells [116]. Similarly Matokanovic et al. have shown that the effects of Hsp90

inhibitors can be enhanced by using them in combination with siRNA that silences Hsp70 [117]. Thus the results from our study suggest combinatorial approaches for enhancing AUY922's activity in combination with agents compromising chaperone induction.

Future Directions

By analyzing all the work and experimentation we did to study the proteomics of Hsp90 inhibition, we offer some thoughts on the experimental strategies we used, spectrum counting vs. SILAC, limitations of MaxQuant, experiments that should have been done and future directions.

After using spectrum counting and SILAC, we strongly recommend the use of SILAC, although it is expensive compared to spectrum counting. Spectrum counting is a relatively weaker technique and allows to identify only few hundred drug-induced changes. It is therefore difficult to predict the mechanisms of drug action based on these few changes. Whereas, SILAC offers better quantitation and allows identification of several thousands of proteins. Thus, by using SILAC we can gain insights into drug mechanisms.

We also strongly recommend the use of 5 biological replicates instead of three for SILAC experiments. Use of 5 biological replicates allows more protein identifications.

For comparing protein expression changes, we recommend using one sample T-test offered by Perseus, because it is more permissive than other tests and allows for identifying more protein expression changes. For multiple tests correction we recommend using BH test if there are no massive changes in the proteome. However, if the drug induces massive changes in the proteome, we recommend using Storey FDR test. We also suggest that using 1.5 fold change threshold for validating protein expression changes eliminates a lot of true protein expression changes and should only be used, when wanting to report only highly confident protein expression changes.

We also think that a bio-informatics program is needed to combine files generated from two different MaxQuant searches. This will be very helpful for comparing the proteomic fingerprints of different drugs. This will eliminate the need for searching all the files in a single MaxQuant

search, which otherwise compromises the quality of the data. Alternatively, MaxQuant programs might be written such that they generate a single protein ID for each protein, so that files from different MaxQuant searches can be easily combined.

We think that our work would have been better by including some experiments. Our studies should have included SILAC comparisons of low-dose 17-DMAG vs. low dose AUY922. Such low dose AUY922 vs. low dose 17-DMAG comparisons would have served as a better positive control for fingerprints of drugs sharing common mechanisms, rather than high dose AUY922 vs. high dose 17-DMAG comparisons. We should also have done proteomics of tunicamycin and AUY922 combinatorial treatments.

Supplemental Table 2.2 (Chapter II): Significant protein expression changes common to AUY922, 17-DMAG and radicicol based on spectrum counting assays.

S.No	IPI number	Gene name	Protein name	Up/Down
1	IPI00186290	EEF2	Elongation factor 2	D
2	IPI00218993	HSPH1	Isoform Beta of Heat shock protein 105 kDa	U
3	IPI00293464	DDB1	DNA damage-binding protein 1	D
4	IPI00304925	HSPA1A	Heat shock 70 kDa protein 1A/1B	U
5	IPI00027493	SLC3A2	Isoform 2 of 4F2 cell-surface antigen heavy chain	U
6	IPI00011200	PHGDH	D-3-phosphoglycerate dehydrogenase	U
7	IPI00031519	DNMT1	Isoform 1 of DNA (cytosine-5)-methyltransferase 1	D
8	IPI00023529	CDK6	Cyclin-dependent kinase 6	D
9	IPI00015947	DNAJB1	DnaJ homolog subfamily B member 1	U
10	IPI00026689	CDK1	Cyclin-dependent kinase 1	D
11	IPI00005614	SPTBN1	Isoform Long of Spectrin beta chain, brain 1	U
12	IPI00032140	SERPINH1	Serpin H1	U
13	IPI00377261	FUBP3	Isoform 1 of Far upstream element-binding protein 3	U
14	IPI00002214	KPNA2	Importin subunit alpha-2	D
15	IPI00382470	HSP90AA1	Isoform 2 of Heat shock protein HSP 90-alpha	U
16	IPI00017617	DDX5	Probable ATP-dependent RNA helicase DDX5	D
17	IPI00301263	CAD	CAD protein	D
18	IPI00010720	CCT5	T-complex protein 1 subunit epsilon	U
19	IPI00329789	ZAP70	Isoform 1 of Tyrosine-protein kinase ZAP-70	D
20	IPI00797279	UHRF1	E3 ubiquitin-protein ligase UHRF1 isoform 2	D
21	IPI00003865	HSPA8	Isoform 1 of Heat shock cognate 71 kDa protein	U
22	IPI00008524	PABPC1	Isoform 1 of Polyadenylate-binding protein 1	D
23	IPI00746165	WDR1	Isoform 1 of WD repeat-containing protein 1	U
24	IPI00550021	RPL3	60S ribosomal protein L3	D
25	IPI00219005	FKBP4	Peptidyl-prolyl cis-trans isomerase FKBP4	U
26	IPI00553185	CCT3	T-complex protein 1 subunit gamma	U
27	IPI00220362	HSPE1	10 kDa heat shock protein, mitochondrial	U
28	IPI00396370	EIF3B	Isoform 1 of Eukaryotic translation initiation factor 3 subunit B	D
29	IPI00020127	RPA1	Replication protein A 70 kDa DNA-binding subunit	D
30	IPI00217975	LMNB1	Lamin-B1	U
31	IPI00470891	CSDE1	Isoform Long of Cold shock domain-containing protein E1	D
32	IPI00008475	HMGCS1	Hydroxymethylglutaryl-CoA synthase, cytoplasmic	D

| 33 | IPI00007764 | HN1 | Isoform 1 of Hematological and neurological expressed 1 protein | D | |

Supplemental Table 2.3 (Chapter II): Significant protein expression changes common to any two inhibitors based on spectrum counting assays.

S.No	IPI number	Gene name	Protein name	Inhibitors	Up/Down
1	IPI00396435	DHX15	Putative pre-mRNA-splicing factor ATP-dependent RNA helicase DHX15	DMAG, Radicicol	D
2	IPI00290566	TCP1	T-complex protein 1 subunit alpha	AUY, Radicicol	U
3	IPI00001734	PSAT1	Phosphoserine aminotransferase	AUY, Radicicol	U
4	IPI00783097	GARS	Glycyl-tRNA synthetase	DMAG, Radicicol	U
5	IPI00013894	STIP1	Stress-induced-phosphoprotein 1	AUY, Radicicol	U
6	IPI00291097	PML	Isoform PML-13 of Protein PML	DMAG, Radicicol	U
7	IPI00456887	HNRNPUL2	Heterogeneous nuclear ribonucleoprotein U-like protein 2	DMAG, AUY	U
8	IPI00456969	DYNC1H1	Cytoplasmic dynein 1 heavy chain 1	DMAG, Radicicol	U
9	IPI00002459	ANXA6	Annexin A6	AUY, Radicicol	U
10	IPI00295857	COPA	Isoform 1 of Coatomer subunit alpha	DMAG, Radicicol	U
11	IPI00219446	PEBP1	Phosphatidylethanolamine-binding protein 1	DMAG, AUY	D
12	IPI00455134	HNRNPA3	Isoform 2 of Heterogeneous nuclear ribonucleoprotein A3	AUY, Radicicol	U
13	IPI00165949	ERAP1	Isoform 2 of Endoplasmic reticulum aminopeptidase 1	AUY, Radicicol	U
14	IPI00002966	HSPA4	Heat shock 70 kDa protein 4	DMAG, AUY	U
15	IPI00171903	HNRNPM	Isoform 1 of Heterogeneous nuclear ribonucleoprotein M	DMAG, AUY	U
16	IPI00465439	ALDOA	Fructose-bisphosphate aldolase A	DMAG, Radicicol	D
17	IPI00302927	CCT4	T-complex protein 1 subunit delta	DMAG, AUY	U
18	IPI00016910	EIF3C	Eukaryotic translation initiation factor 3 subunit C	DMAG, AUY	D
19	IPI00299524	NCAPD2	Condensin complex subunit 1	DMAG, Radicicol	D
20	IPI00019848	HCFC1	Isoform 1 of Host cell factor 1	DMAG, Radicicol	D
21	IPI00010471	LCP1	Plastin-2	AUY, Radicicol	U
22	IPI00000874	PRDX1	Peroxiredoxin-1	AUY,	U

				Radicicol	
23	IPI00025491	EIF4A1	Eukaryotic initiation factor 4A-I	AUY, Radicicol	D
24	IPI00642238	HP1BP3	Isoform 1 of Heterochromatin protein 1-binding protein 3	DMAG, Radicicol	U
25	IPI00219156	RPL30	60S ribosomal protein L30	DMAG, AUY	D
26	IPI00304612	RPL13A	60S ribosomal protein L13a	DMAG, Radicicol	D (DMAG) U (Radicicol
27	IPI00395568	PHF6	Isoform 1 of PHD finger protein 6	DMAG, Radicicol	U
28	IPI00009342	IQGAP1	Ras GTPase-activating-like protein IQGAP1	DMAG, AUY	U
29	IPI00012341		Isoform SRP40-1 of Serine/arginine-rich splicing factor 5	DMAG, AUY	U
30	IPI00411559	SMC4	Isoform 1 of Structural maintenance of chromosomes protein 4	DMAG, AUY	D
31	IPI00643041	RAN	GTP-binding nuclear protein Ran	AUY, Radicicol	D (Radicicol) U (AUY)
32	IPI00215637	DDX3X	ATP-dependent RNA helicase DDX3X	AUY, Radicicol	D
33	IPI00012066	PCBP2	poly(rC)-binding protein 2 isoform b (hnRNPE2)	AUY, Radicicol	D
34	IPI00790342	RPL6	60S ribosomal protein L6	AUY, Radicicol	D
35	IPI00221088	RPS9	40S ribosomal protein S9	AUY, Radicicol	D
36	IPI00013174	RBM14	Isoform 1 of RNA-binding protein 14	AUY, Radicicol	D
37	IPI00219913	BAP1	Ubiquitin carboxyl-terminal hydrolase 14	AUY, Radicicol	U
38	IPI00011274	HNRPDL	Isoform 1 of Heterogeneous nuclear ribonucleoprotein D-like	AUY, Radicicol	D (Radicicol) U (AUY)
39	IPI00011913	HNRNPA0	Heterogeneous nuclear ribonucleoprotein A0	AUY, Radicicol	U

Supplemental Table 2.4 (Chapter II): Significant protein expression changes in just one inhibitors based on spectrum counting assays.

S.No	IPI number	Gene name	Protein name	Inhibitors	Up/Down
1	IPI00027626	CCT6A	T-complex protein 1 subunit zeta	AUY	U
2	IPI00296337	PRKDC	Isoform 1 of DNA-dependent protein kinase catalytic subunit	AUY	D
3	IPI00026781	FASN	Fatty acid synthase	AUY	D
4	IPI00030706	AHSA1	Activator of 90 kDa heat shock protein ATPase homolog 1	AUY	U
5	IPI00023530	CDK5	Cyclin-dependent kinase 5	AUY	D
6	IPI00184533	USP11	Ubiquitin carboxyl-terminal hydrolase 11	Radicicol	U
7	IPI00000846	CHD4	Isoform 1 of Chromodomain-helicase-DNA-binding protein 4	AUY	D
8	IPI00007673	CHCHD2	Coiled-coil-helix-coiled-coil-helix domain-containing protein 2, mitochondrial	AUY	D
9	IPI00515097	LCK	Isoform 3 of Tyrosine-protein kinase Lck	AUY	D
10	IPI00305833	SMU1	WD40 repeat-containing protein SMU1	DMAG	D
11	IPI00376219	APBB1IP	Amyloid beta A4 precursor protein-binding family B member 1-interacting protein	DMAG	D
12	IPI00292894	TSR1	Pre-rRNA-processing protein TSR1 homolog	Radicicol	D
13	IPI00479262	EIF4G1	eukaryotic translation initiation factor 4 gamma 1 isoform 1	AUY	D
14	IPI00221108	TYMS	Thymidylate synthase	AUY	D
15	IPI00012462	EIF2A	Eukaryotic translation initiation factor 2A	AUY	D
16	IPI00218245	EVL	Isoform 1 of Ena/VASP-like protein	Radicicol	U
17	IPI00011696	VAV1	Proto-oncogene vav	Radicicol	U
18	IPI00465044	RCC2	Protein RCC2	AUY	D
19	IPI00007928	PRPF8	Pre-mRNA-processing-splicing factor 8	AUY	D
20	IPI00027834	HNRNPL	Heterogeneous nuclear ribonucleoprotein L	AUY	U
21	IPI00376317	EDC4	Isoform 1 of Enhancer of mRNA-decapping protein 4	AUY	D
22	IPI00007765	HSPA9	Stress-70 protein, mitochondrial	DMAG	U
23	IPI00013485	RPS2	40S ribosomal protein S2	DMAG	D
24	IPI00018465	CCT7	T-complex protein 1 subunit eta	DMAG	U
25	IPI00257508	DPYSL2	Dihydropyrimidinase-related protein 2	DMAG	U
26	IPI00007074	YARS	Tyrosyl-tRNA synthetase, cytoplasmic	DMAG	U
27	IPI00218342	MTHFD1	C-1-tetrahydrofolate synthase, cytoplasmic	Radicicol	D
28	IPI00022462	TFRC	Transferrin receptor protein 1	Radicicol	D
29	IPI00299904	MCM7	Isoform 1 of DNA replication licensing factor MCM7	Radicicol	D
30	IPI00784154	HSPD1	60 kDa heat shock protein,	AUY	U

			mitochondrial		
31	IPI00027230	HSP90B1	Endoplasmin	AUY	U
32	IPI00449049	PARP1	Poly [ADP-ribose] polymerase 1	AUY	U
33	IPI00221354	FUS	Isoform Short of RNA-binding protein FUS	DMAG	U
34	IPI00299573	RPL7A	60S ribosomal protein L7a	DMAG	D
35	IPI00104050	THRAP3	Thyroid hormone receptor-associated protein 3	DMAG	U
36	IPI00291755	NUP210	Isoform 1 of Nuclear pore membrane glycoprotein 210	DMAG	U
37	IPI00025874	DDOST	Dolichyl-diphosphooligosaccharide--protein glycosyltransferase subunit 1 precursor	AUY	U
38	IPI00215719	RPL18	60S ribosomal protein L18	AUY	D
39	IPI00007797	FABP5	Fatty acid-binding protein, epidermal	DMAG	D
40	IPI00514053	ARCN1	Coatomer subunit delta	DMAG	U
41	IPI00177728	CNDP2	Isoform 1 of Cytosolic non-specific dipeptidase	DMAG	D
42	IPI00002520	SHMT2	Serine hydroxymethyltransferase, mitochondrial	DMAG	D
43	IPI00376798	RPL11	Isoform 1 of 60S ribosomal protein L11	DMAG	D
44	IPI00182757	KIAA1967	Isoform 1 of Protein KIAA1967 (DBC)	AUY	D
45	IPI00329791	DDX46	Probable ATP-dependent RNA helicase DDX46	AUY	D
46	IPI00007927	SMC2	Isoform 1 of Structural maintenance of chromosomes protein 2	AUY	D
47	IPI00456359	ATXN2L	Isoform 1 of Ataxin-2-like protein	AUY	D
48	IPI00306043	YTHDF2	Isoform 1 of YTH domain family protein 2	AUY	D
49	IPI00013495	ABCF1	Isoform 2 of ATP-binding cassette sub-family F member 1	AUY	D
50	IPI00293434	SRP14	Signal recognition particle 14 kDa protein	DMAG	U
51	IPI00008986	SLC7A5	Large neutral amino acids transporter small subunit 1	DMAG	U
52	IPI00005198	ILF2	Interleukin enhancer-binding factor 2	DMAG	U
53	IPI00012772	RPL8	60S ribosomal protein L8	AUY	D
54	IPI00021290		ATP-citrate synthase	DMAG	D
55	IPI00010133	CORO1A	Coronin-1A	DMAG	U
56	IPI00299000	PA2G4	Proliferation-associated protein 2G4	DMAG	D
57	IPI00012535	DNAJA1	DnaJ homolog subfamily A member 1	Radicicol	U
58	IPI00375441	FUBP1	Isoform 1 of Far upstream element-binding protein 1	Radicicol	U
59	IPI00013788	HTATSF1	HIV Tat-specific factor 1	Radicicol	U
60	IPI00396378	HNRNPA2B1	Isoform B1 of Heterogeneous nuclear ribonucleoproteins A2/B1	AUY	U
61	IPI00010740	SFPQ	Isoform Long of Splicing factor, proline- and glutamine-rich	AUY	U

62	IPI00025091	RPS11	40S ribosomal protein S11	AUY	D
63	IPI00295851	COPB1	Coatomer subunit beta	AUY	U
64	IPI00030131		Isoform Beta of Lamina-associated polypeptide 2, isoforms beta/gamma	DMAG	U
65	IPI00294879	RANGAP1	Ran GTPase-activating protein 1	DMAG	U
66	IPI00022648	EIF5	Eukaryotic translation initiation factor 5	DMAG	U
67	IPI00012079	EIF4B	Eukaryotic translation initiation factor 4B	Radicicol	U
68	IPI00746004	RPS27L	40S ribosomal protein S27-like	Radicicol	D
69	IPI00022202		Isoform A of Phosphate carrier protein, mitochondrial	Radicicol	U
70	IPI00024364	TNPO1	Isoform 1 of Transportin-1	Radicicol	U
71	IPI00297579	CBX3	Chromobox protein homolog 3	Radicicol	U
72	IPI00020356		Uncharacterized protein	Radicicol	U
73	IPI00027107	TUFM	elongation factor Tu, mitochondrial precursor	AUY	U
74	IPI00012074	HNRNPR	Isoform 1 of Heterogeneous nuclear ribonucleoprotein R	AUY	U
75	IPI00008529	RPLP2	60S acidic ribosomal protein P2	AUY	U
76	IPI00301503	TRA2B	Isoform 1 of Transformer-2 protein homolog beta	AUY	U
77	IPI00554723		60S ribosomal protein L10	Radicicol	U

REFERENCES

1. Prodromou, C., et al., Identification and structural characterization of the ATP/ADP-binding site in the Hsp90 molecular chaperone. Cell, 1997. **90**(1): p. 65-75.
2. Stebbins, C.E., et al., Crystal structure of an Hsp90-geldanamycin complex: targeting of a protein chaperone by an antitumor agent. Cell, 1997. **89**(2): p. 239-50.
3. Meyer, P., et al., Structural and functional analysis of the middle segment of hsp90: implications for ATP hydrolysis and client protein and cochaperone interactions. Mol Cell, 2003. **11**(3): p. 647-58.
4. Marcu, M.G., T.W. Schulte, and L. Neckers, Novobiocin and related coumarins and depletion of heat shock protein 90-dependent signaling proteins. J Natl Cancer Inst, 2000. **92**(3): p. 242-8.
5. Matts, R.L., et al., Elucidation of the Hsp90 C-terminal inhibitor binding site. ACS Chem Biol, 2011. **6**(8): p. 800-7.
6. Walter, S. and J. Buchner, Molecular chaperones--cellular machines for protein folding. Angew Chem Int Ed Engl, 2002. **41**(7): p. 1098-113.
7. Taipale, M., D.F. Jarosz, and S. Lindquist, HSP90 at the hub of protein homeostasis: emerging mechanistic insights. Nat Rev Mol Cell Biol, 2010. **11**(7): p. 515-28.
8. Whitesell, L. and S.L. Lindquist, HSP90 and the chaperoning of cancer. Nat Rev Cancer, 2005. **5**(10): p. 761-72.
9. Joab, I., et al., Common non-hormone binding component in non-transformed chick oviduct receptors of four steroid hormones. Nature, 1984. **308**(5962): p. 850-3.
10. Sanchez, E.R., et al., Evidence that the 90-kDa phosphoprotein associated with the untransformed L-cell glucocorticoid receptor is a murine heat shock protein. J Biol Chem, 1985. **260**(23): p. 12398-401.
11. Lipsich, L.A., J.R. Cutt, and J.S. Brugge, Association of the transforming proteins of Rous, Fujinami, and Y73 avian sarcoma viruses with the same two cellular proteins. Mol Cell Biol, 1982. **2**(7): p. 875-80.
12. Stepanova, L., et al., Mammalian p50Cdc37 is a protein kinase-targeting subunit of Hsp90 that binds and stabilizes Cdk4. Genes Dev, 1996. **10**(12): p. 1491-502.
13. Prince, T., L. Sun, and R.L. Matts, Cdk2: a genuine protein kinase client of Hsp90 and Cdc37. Biochemistry, 2005. **44**(46): p. 15287-95.
14. Holt, S.E., et al., Functional requirement of p23 and Hsp90 in telomerase complexes. Genes Dev, 1999. **13**(7): p. 817-26.
15. Hartson, S.D. and R.L. Matts, Approaches for defining the Hsp90-dependent proteome. Biochim Biophys Acta, 2012. **1823**(3): p. 656-67.
16. Whitesell, L., et al., Inhibition of heat shock protein HSP90-pp60v-src heteroprotein complex formation by benzoquinone ansamycins: essential role for stress proteins in oncogenic transformation. Proc Natl Acad Sci U S A, 1994. **91**(18): p. 8324-8.

17.	Sharma, S.V., T. Agatsuma, and H. Nakano, Targeting of the protein chaperone, HSP90, by the transformation suppressing agent, radicicol. Oncogene, 1998. **16**(20): p. 2639-45.18.	Roe, S.M., et al., Structural basis for inhibition of the Hsp90 molecular chaperone by the antitumor antibiotics radicicol and geldanamycin. J Med Chem, 1999. **42**(2): p. 260-6.

19.	Jhaveri, K., et al., Advances in the clinical development of heat shock protein 90 (Hsp90) inhibitors in cancers. Biochim Biophys Acta, 2012. **1823**(3): p. 742-55.

20.	Roughley, S., et al., Hsp90 inhibitors and drugs from fragment and virtual screening. Top Curr Chem, 2012. **317**: p. 61-82.

21.	Jensen, M.R., et al., NVP-AUY922: a small molecule HSP90 inhibitor with potent antitumor activity in preclinical breast cancer models. Breast Cancer Res, 2008. **10**(2): p. R33.

22.	Eccles, S.A., et al., NVP-AUY922: a novel heat shock protein 90 inhibitor active against xenograft tumor growth, angiogenesis, and metastasis. Cancer Res, 2008. **68**(8): p. 2850-60.

23.	Stuhmer, T., et al., Signalling profile and antitumour activity of the novel Hsp90 inhibitor NVP-AUY922 in multiple myeloma. Leukemia, 2008. **22**(8): p. 1604-12.

24.	Gaspar, N., et al., Mechanistic evaluation of the novel HSP90 inhibitor NVP-AUY922 in adult and pediatric glioblastoma. Mol Cancer Ther, 2010. **9**(5): p. 1219-33.

25.	Lee, K.H., et al., Antitumor activity of NVP-AUY922, a novel heat shock protein 90 inhibitor, in human gastric cancer cells is mediated through proteasomal degradation of client proteins. Cancer Sci, 2011. **102**(7): p. 1388-95.

26.	Ueno, T., et al., Strong anti-tumor effect of NVP-AUY922, a novel Hsp90 inhibitor, on non-small cell lung cancer. Lung Cancer, 2012. **76**(1): p. 26-31.

27.	Itoh, H., et al., A novel chaperone-activity-reducing mechanism of the 90-kDa molecular chaperone HSP90. Biochem J, 1999. **343 Pt 3**: p. 697-703.

28.	Palermo, C.M., C.A. Westlake, and T.A. Gasiewicz, Epigallocatechin gallate inhibits aryl hydrocarbon receptor gene transcription through an indirect mechanism involving binding to a 90 kDa heat shock protein. Biochemistry, 2005. **44**(13): p. 5041-52.

29.	Donnelly, A. and B.S. Blagg, Novobiocin and additional inhibitors of the Hsp90 C-terminal nucleotide-binding pocket. Curr Med Chem, 2008. **15**(26): p. 2702-17.

30.	Shelton, S.N., et al., KU135, a novel novobiocin-derived C-terminal inhibitor of the 90-kDa heat shock protein, exerts potent antiproliferative effects in human leukemic cells. Mol Pharmacol, 2009. **76**(6): p. 1314-22.

31.	Samadi, A.K., et al., A novel C-terminal HSP90 inhibitor KU135 induces apoptosis and cell cycle arrest in melanoma cells. Cancer Lett, 2011. **312**(2): p. 158-67.

32.	Blagosklonny, M.V., et al., Mutant conformation of p53 translated in vitro or in vivo requires functional HSP90. Proc Natl Acad Sci U S A, 1996. **93**(16): p. 8379-83.

33.	Neckers, L., Hsp90 inhibitors as novel cancer chemotherapeutic agents. Trends Mol Med, 2002. **8**(4 Suppl): p. S55-61.

34.	Sawai, A., et al., Inhibition of Hsp90 down-regulates mutant epidermal growth factor receptor (EGFR) expression and sensitizes EGFR mutant tumors to paclitaxel. Cancer Res, 2008. **68**(2): p. 589-96.

35.	Isaacs, J.S., et al., Hsp90 regulates a von Hippel Lindau-independent hypoxia-inducible factor-1 alpha-degradative pathway. J Biol Chem, 2002. **277**(33): p. 29936-44.

36.	Eustace, B.K., et al., Functional proteomic screens reveal an essential extracellular role for hsp90 alpha in cancer cell invasiveness. Nat Cell Biol, 2004. **6**(6): p. 507-14.

37. Supko, J.G., et al., Preclinical pharmacologic evaluation of geldanamycin as an antitumor agent. Cancer Chemother Pharmacol, 1995. **36**(4): p. 305-15.

38. Jones, D.T., et al., Geldanamycin and herbimycin A induce apoptotic killing of B chronic lymphocytic leukemia cells and augment the cells' sensitivity to cytotoxic drugs. Blood, 2004. **103**(5): p. 1855-61.

39. Soga, S., et al., Radicicol leads to selective depletion of Raf kinase and disrupts K-Ras-activated aberrant signaling pathway. J Biol Chem, 1998. **273**(2): p. 822-8.

40. Ki, S.W., et al., Radicicol binds and inhibits mammalian ATP citrate lyase. J Biol Chem, 2000. **275**(50): p. 39231-6.

41. Workman, P., et al., Drugging the cancer chaperone HSP90: combinatorial therapeutic exploitation of oncogene addiction and tumor stress. Ann N Y Acad Sci, 2007. **1113**: p. 202-16.

42. Kamal, A., et al., A high-affinity conformation of Hsp90 confers tumour selectivity on Hsp90 inhibitors. Nature, 2003. **425**(6956): p. 407-10.

43. Workman, P., Altered states: selectively drugging the Hsp90 cancer chaperone. Trends Mol Med, 2004. **10**(2): p. 47-51.

44. Barrott, J.J. and T.A. Haystead, Hsp90, an unlikely ally in the war on cancer. FEBS J, 2013. **280**(6): p. 1381-96.

45. Workman, P., Combinatorial attack on multistep oncogenesis by inhibiting the Hsp90 molecular chaperone. Cancer Lett, 2004. **206**(2): p. 149-57.

46. Luo, W., et al., Heat shock protein 90 in neurodegenerative diseases. Mol Neurodegener, 2010. **5**: p. 24.

47. Xu, W., et al., Chaperone-dependent E3 ubiquitin ligase CHIP mediates a degradative pathway for c-ErbB2/Neu. Proc Natl Acad Sci U S A, 2002. **99**(20): p. 12847-52.

48. Zou, J., et al., Repression of heat shock transcription factor HSF1 activation by HSP90 (HSP90 complex) that forms a stress-sensitive complex with HSF1. Cell, 1998. **94**(4): p. 471-80.

49. Shamovsky, I., et al., RNA-mediated response to heat shock in mammalian cells. Nature, 2006. **440**(7083): p. 556-60.

50. Bagatell, R., et al., Induction of a heat shock factor 1-dependent stress response alters the cytotoxic activity of hsp90-binding agents. Clin Cancer Res, 2000. **6**(8): p. 3312-8.

51. Lee, J.H., et al., Heat shock protein 90 (HSP90) inhibitors activate the heat shock factor 1 (HSF1) stress response pathway and improve glucose regulation in diabetic mice. Biochem Biophys Res Commun, 2013. **430**(3): p. 1109-13.

52. Maloney, A., et al., Gene and protein expression profiling of human ovarian cancer cells treated with the heat shock protein 90 inhibitor 17-allylamino-17-demethoxygeldanamycin. Cancer Res, 2007. **67**(7): p. 3239-53.

53. Schumacher, J.A., et al., Proteome-wide changes induced by the Hsp90 inhibitor, geldanamycin in anaplastic large cell lymphoma cells. Proteomics, 2007. **7**(15): p. 2603-16.

54. Falsone, S.F., et al., A proteomic approach towards the Hsp90-dependent ubiquitinylated proteome. Proteomics, 2007. **7**(14): p. 2375-83.

55. Song, D., et al., Antitumor activity and molecular effects of the novel heat shock protein 90 inhibitor, IPI-504, in pancreatic cancer. Mol Cancer Ther, 2008. **7**(10): p. 3275-84.

56. Sharma, K., et al., Quantitative proteomics reveals that Hsp90 inhibition preferentially targets kinases and the DNA damage response. Mol Cell Proteomics, 2012. **11**(3): p. M111 014654.

57. Wu, Z., A. Moghaddas Gholami, and B. Kuster, Systematic identification of the HSP90 candidate regulated proteome. Mol Cell Proteomics, 2012. **11**(6): p. M111 016675.

58. Bouchecareilh, M. and W.E. Balch, Proteostasis: a new therapeutic paradigm for pulmonary disease. Proc Am Thorac Soc, 2011. **8**(2): p. 189-95.

59. Hartl, F.U., A. Bracher, and M. Hayer-Hartl, Molecular chaperones in protein folding and proteostasis. Nature, 2011. **475**(7356): p. 324-32.

60. Ali, A., et al., HSP90 interacts with and regulates the activity of heat shock factor 1 in Xenopus oocytes. Mol Cell Biol, 1998. **18**(9): p. 4949-60.

61. Straus, D., W. Walter, and C.A. Gross, DnaK, DnaJ, and GrpE heat shock proteins negatively regulate heat shock gene expression by controlling the synthesis and stability of sigma 32. Genes Dev, 1990. **4**(12A): p. 2202-9.

62. Craig, E.A. and C.A. Gross, Is hsp70 the cellular thermometer? Trends Biochem Sci, 1991. **16**(4): p. 135-40.

63. Voellmy, R. and F. Boellmann, Chaperone regulation of the heat shock protein response. Adv Exp Med Biol, 2007. **594**: p. 89-99.

64. Chakrabarti, A., A.W. Chen, and J.D. Varner, A review of the mammalian unfolded protein response. Biotechnol Bioeng, 2011. **108**(12): p. 2777-93.

65. McDowell, W., et al., Glucose trimming and mannose trimming affect different phases of the maturation of Sindbis virus in infected BHK cells. Virology, 1987. **161**(1): p. 37-44.

66. Bernassola, F., A. Ciechanover, and G. Melino, The ubiquitin proteasome system and its involvement in cell death pathways. Cell Death Differ, 2010. **17**(1): p. 1-3.

67. Voges, D., P. Zwickl, and W. Baumeister, The 26S proteasome: a molecular machine designed for controlled proteolysis. Annu Rev Biochem, 1999. **68**: p. 1015-68.

68. Wiedmann, B., et al., A protein complex required for signal-sequence-specific sorting and translocation. Nature, 1994. **370**(6489): p. 434-40.

69. Kirstein-Miles, J., et al., The nascent polypeptide-associated complex is a key regulator of proteostasis. EMBO J, 2013. **32**(10): p. 1451-68.

70. Marcu, M.G., et al., Heat shock protein 90 modulates the unfolded protein response by stabilizing IRE1alpha. Mol Cell Biol, 2002. **22**(24): p. 8506-13.

71. Davenport, E.L., et al., Heat shock protein inhibition is associated with activation of the unfolded protein response pathway in myeloma plasma cells. Blood, 2007. **110**(7): p. 2641-9.

72. Siegelin, M.D., et al., Exploiting the mitochondrial unfolded protein response for cancer therapy in mice and human cells. J Clin Invest, 2011. **121**(4): p. 1349-60.

73. Taiyab, A., A.S. Sreedhar, and M. Rao Ch, Hsp90 inhibitors, GA and 17AAG, lead to ER stress-induced apoptosis in rat histiocytoma. Biochem Pharmacol, 2009. **78**(2): p. 142-52.

74. Gallerne, C., A. Prola, and C. Lemaire, Hsp90 inhibition by PU-H71 induces apoptosis through endoplasmic reticulum stress and mitochondrial pathway in cancer cells and overcomes the resistance conferred by Bcl-2. Biochim Biophys Acta, 2013. **1833**(6): p. 1356-66.

75. Prachasilchai, W., et al., The protective effect of a newly developed molecular chaperone-inducer against mouse ischemic acute kidney injury. J Pharmacol Sci, 2009. **109**(2): p. 311-4.

76. Bull, V.H. and B. Thiede, Proteome analysis of tunicamycin-induced ER stress. Electrophoresis, 2012. **33**(12): p. 1814-23.

77. Bush, K.T., et al., Pretreatment with inducers of ER molecular chaperones protects epithelial cells subjected to ATP depletion. Am J Physiol, 1999. **277**(2 Pt 2): p. F211-8.

78. Prachasilchai, W., et al., A protective role of unfolded protein response in mouse ischemic acute kidney injury. Eur J Pharmacol, 2008. **592**(1-3): p. 138-45.

79. Rubenstein, E., et al., Azetidine-2-carboxylic acid in garden beets (Beta vulgaris). Phytochemistry, 2006. **67**(9): p. 898-903.

80. Trotter, E.W., et al., Misfolded proteins are competent to mediate a subset of the responses to heat shock in Saccharomyces cerevisiae. J Biol Chem, 2002. **277**(47): p. 44817-25.

81. Barbosa-Tessmann, I.P., et al., Activation of the unfolded protein response pathway induces human asparagine synthetase gene expression. J Biol Chem, 1999. **274**(44): p. 31139-44.

82. Nguyen, D.T., et al., Nck-dependent activation of extracellular signal-regulated kinase-1 and regulation of cell survival during endoplasmic reticulum stress. Mol Biol Cell, 2004. **15**(9): p. 4248-60.

83. Fenn, J.B., et al., Electrospray ionization for mass spectrometry of large biomolecules. Science, 1989. **246**(4926): p. 64-71.

84. Hillenkamp, F. and M. Karas, Mass spectrometry of peptides and proteins by matrix-assisted ultraviolet laser desorption/ionization. Methods Enzymol, 1990. **193**: p. 280-95.

85. Hu, Q., et al., The Orbitrap: a new mass spectrometer. J Mass Spectrom, 2005. **40**(4): p. 430-43.

86. Jones, A.W. and H.J. Cooper, Dissociation techniques in mass spectrometry-based proteomics. Analyst, 2011. **136**(17): p. 3419-29.

87. Gygi, S.P., et al., Quantitative analysis of complex protein mixtures using isotope-coded affinity tags. Nat Biotechnol, 1999. **17**(10): p. 994-9.

88. Ross, P.L., et al., Multiplexed protein quantitation in Saccharomyces cerevisiae using amine-reactive isobaric tagging reagents. Mol Cell Proteomics, 2004. **3**(12): p. 1154-69.

89. Ong, S.E., et al., Stable isotope labeling by amino acids in cell culture, SILAC, as a simple and accurate approach to expression proteomics. Mol Cell Proteomics, 2002. **1**(5): p. 376-86.

90. Lau, K.W., et al., Capture and analysis of quantitative proteomic data. Proteomics, 2007. **7**(16): p. 2787-99.

91. Perkins, D.N., et al., Probability-based protein identification by searching sequence databases using mass spectrometry data. Electrophoresis, 1999. **20**(18): p. 3551-67.

92. Craig, R. and R.C. Beavis, TANDEM: matching proteins with tandem mass spectra. Bioinformatics, 2004. **20**(9): p. 1466-7.

93. Cox, J., et al., Andromeda: a peptide search engine integrated into the MaxQuant environment. J Proteome Res, 2011. **10**(4): p. 1794-805.

94. Searle, B.C., Scaffold: a bioinformatic tool for validating MS/MS-based proteomic studies. Proteomics, 2010. **10**(6): p. 1265-9.

95. Cox, J. and M. Mann, MaxQuant enables high peptide identification rates, individualized p.p.b.-range mass accuracies and proteome-wide protein quantification. Nat Biotechnol, 2008. **26**(12): p. 1367-72.

96. Niewidok, N., et al., Hsp90 Inhibitors NVP-AUY922 and NVP-BEP800 May Exert a Significant Radiosensitization on Tumor Cells along with a Cell Type-Specific Cytotoxicity. Transl Oncol, 2012. **5**(5): p. 356-69.

97. Walsby, E., et al., The Hsp90 inhibitor NVP-AUY922-AG inhibits NF-kappaB signaling, overcomes microenvironmental cytoprotection and is highly synergistic with fludarabine in primary CLL cells. Oncotarget, 2012. **3**(5): p. 525-34.

98. Srethapakdi, M., et al., Inhibition of Hsp90 function by ansamycins causes retinoblastoma gene product-dependent G1 arrest. Cancer Res, 2000. **60**(14): p. 3940-6.

99. Premkumar, D.R., et al., Synergistic interaction between 17-AAG and phosphatidylinositol 3-kinase inhibition in human malignant glioma cells. Mol Carcinog, 2006. **45**(1): p. 47-59.

100. Lazebnik, Y.A., et al., Cleavage of poly(ADP-ribose) polymerase by a proteinase with properties like ICE. Nature, 1994. **371**(6495): p. 346-7.

101. Oliver, F.J., et al., Importance of poly(ADP-ribose) polymerase and its cleavage in apoptosis. Lesson from an uncleavable mutant. J Biol Chem, 1998. **273**(50): p. 33533-9.

102. Voruganti, S., et al., The anticancer drug AUY922 generates a proteomics fingerprint that is highly conserved among structurally diverse Hsp90 inhibitors. J Proteome Res, 2013. **12**(8): p. 3697-706.

103. Hochberg, Y. and Y. Benjamini, More powerful procedures for multiple significance testing. Stat Med, 1990. **9**(7): p. 811-8.

104. Kall, L., et al., Posterior error probabilities and false discovery rates: two sides of the same coin. J Proteome Res, 2008. **7**(1): p. 40-4.

105. Huang da, W., B.T. Sherman, and R.A. Lempicki, Systematic and integrative analysis of large gene lists using DAVID bioinformatics resources. Nat Protoc, 2009. **4**(1): p. 44-57.

106. Supek, F., et al., REVIGO summarizes and visualizes long lists of gene ontology terms. PLoS One, 2011. **6**(7): p. e21800.

107. Takeuchi, T. and D.J. Prockop, Biosynthesis of abnormal collagens with amino acid analogues. I. Incorporation of L-azetidine-2-carboxylic acid and cis-4-fluoro-L-proline into protocollagen and collagen. Biochim Biophys Acta, 1969. **175**(1): p. 142-55.

108. Baum, B.J., et al., Incorporation of L-azetidine-2-carboxylic acid into hemoglobin in rabbit reticulocytes. Biochem Biophys Res Commun, 1973. **53**(4): p. 1350-6.

109. Trasko, C.S., C. Franzblau, and R.F. Troxler, Incorporation of L-azetidine-2-carboxylic acid into hemoglobin S in sickle erythrocytes in vitro. Biochim Biophys Acta, 1976. **447**(4): p. 425-35.

110. Knowles, S.E. and F.J. Ballard, Effects of amino acid analogues on protein synthesis and degradation in isolated cells. Br J Nutr, 1978. **40**(2): p. 275-87.

111. Li, W.W., et al., Induction of the mammalian GRP78/BiP gene by Ca2+ depletion and formation of aberrant proteins: activation of the conserved stress-inducible grp core promoter element by the human nuclear factor YY1. Mol Cell Biol, 1997. **17**(1): p. 54-60.

112. Sasaki, H., et al., Induction of heat shock protein 47 synthesis by TGF-beta and IL-1 beta via enhancement of the heat shock element binding activity of heat shock transcription factor 1. J Immunol, 2002. **168**(10): p. 5178-83.

113. Hirayoshi, K., et al., HSP47: a tissue-specific, transformation-sensitive, collagen-binding heat shock protein of chicken embryo fibroblasts. Mol Cell Biol, 1991. **11**(8): p. 4036-44.

114. Razzaque, M.S. and T. Taguchi, The possible role of colligin/HSP47, a collagen-binding protein, in the pathogenesis of human and experimental fibrotic diseases. Histol Histopathol, 1999. **14**(4): p. 1199-212.

115. Gettins, P.G., Serpin structure, mechanism, and function. Chem Rev, 2002. **102**(12): p. 4751-804.

116. Reikvam, H., et al., Increased antileukemic effects in human acute myeloid leukemia by combining HSP70 and HSP90 inhibitors. Expert Opin Investig Drugs, 2013. **22**(5): p. 551-63.

117. Matokanovic, M., et al., Hsp70 silencing with siRNA in nanocarriers enhances cancer cell death induced by the inhibitor of Hsp90. Eur J Pharm Sci, 2013. **50**(1): p. 149-58.

APENDIX A

Abbreviations

GA-	Geldanamycin
Hsp-	Heat shock protein
17-DMAG-	17-Dimethylaminoethylamino-17-demethoxygeldanamycin
MCM-	Mini chromosome maintenance proteins
UPR-	Unfolded protein response
HSR-	Heat shock response
ERAD-	Endoplasmic reticulum associated protein degradation
CID-	Collision induced dissociation
ECD-	Electron capture dissociation
ETD-	Electron capture dissociation
ICAT-	Isotope coded affinity tags
IAA-	Iodoacetamide
TCEP-	(tris (2-carboxyethyl) phosphine)
DTT-	Dithiothreotol
ACN-	Acetonitrile
TFA-	Trifluoro acetic acid
DMSO-	Dimethyl sulfoxide
Cdk6-	Cyclin dependent kinase 6
IC50-	50% inhibitory concentration
SC-	Spectrum counting
SILAC-	Stable isotope labeling with amino acids in cell culture
H-	Heavy or treated samples
L-	Light or control (DMSO) samples
MQ-	MaxQuant
FDR-	False discovery rate
B-H-	Benjamini Hochberg
AZC-	L-azetadine-2-carboxylic acid
TM-	Tunicamycin
FWHM-	Full width at half maximum height
GO-	Gene Ontology
Biorep-	Biological replicate

APPENDIX B

Supplemental excel sheets
Supplemental excel sheet 1 - Raw intensities of all drugs in separate tabs of the excel sheet.
Supplemental excel sheet 2 - Treated/ control ratios of normalized intensities, one sample T-test p-values, and Storey FDR corrected values of T-test p-values for all drugs in separate tabs of the excel sheet.

VITA

SUDHAKAR VORUGANTI

Candidate for the Degree of

Doctor of Philosophy

Thesis: THE PROTEOMICS FINGERPRINTS OF AUY922 AND 17-DMAG INDICATE COMMON MECHANISMS OF ACTION FOR HSP90 INHIBITORS.

Major Field: Biochemistry and Molecular Biology

Biographical:

Education: Masters of Science in Biochemistry

Completed the requirements for the Doctor of Philosophy in Biochemistry and Molecular Biology at Oklahoma State University, Stillwater, Oklahoma in December 2013

Completed the requirements for the Master of Science in Biochemistry at Nagarjuna University, Guntur, Andhra Pradesh, India in 2001.

Completed the requirements for the Bachelor of Science in Biochemistry at Andhra University, Vishakhapatnam, Andhra Pradesh, India in 1998.

Experience: 6 years of biotech industry experience before joining PhD.

Professional Memberships: ASMS